ASSESSMENT OF DEGRADATION MECHANISM AND STABILITY OF A CUT SLOPE IN JOINTED AND SHEARED LIMESTONE ALONG ANKARA-ESKİŞEHİR E90 HIGHWAY

A THESIS SUBMITTED TO
THE GRADUATE SCHOOL OF NATURAL AND APPLIED SCIENCES
OF
MIDDLE EAST TECHNICAL UNIVERSITY

BY

BURAK ÖZTEKİN

IN PARTIAL FULFILLMENT OF THE REQUIREMENTS
FOR
THE DEGREE OF MASTER OF SCIENCE
IN
GEOLOGICAL ENGINEERING

DECEMBER 2004

Approval of the Graduate School of Natural and Applied Sciences

_____

Prof. Dr. Canan Özgen
Director

I certify that this thesis satisfies all the requirements as a thesis for the degree of Master of Science.

_____

Prof. Dr. Asuman G. Türkmenoğlu
Head of Department

This is to certify that we have read this thesis and that in our opinion it is fully adequate, in scope and quality, as a thesis for the degree of Master of Science.

_____

Assoc. Prof. Dr. Tamer Topal
Supervisor

Examining Committee Members

Prof. Dr. Vedat Doyuran	(METU, GEOE)	_____
Assoc. Prof. Dr. Tamer Topal	(METU, GEOE)	_____
Prof. Dr. Reşat Ulusay	(HACETTEPE UNI.)	_____
Prof. Dr. Vedat Toprak	(METU, GEOE)	_____
Assist. Prof. Dr. M. Lütfi Süzen	(METU, GEOE)	_____

I hereby declare that all information in this document has been obtained and presented in accordance with academic rules and ethical conduct. I also declare that, as required by these rules and conduct, I have fully cited and referenced all material and results that are not original to this work.

Name, Last name: Burak Öztekin

Signature :

ABSTRACT

ASSESSMENT OF DEGRADATION MECHANISM AND STABILITY OF A CUT SLOPE IN JOINTED AND SHEARED LIMESTONE ALONG ANKARA-ESKİŞEHİR E90 HIGHWAY

Öztekin, Burak

M.S., Department of Geological Engineering

Supervisor: Assoc. Prof. Dr. Tamer Topal

December 2004, 128 pages

Due to rapidly growing population of Ankara city (Turkey) and traffic load, it is required to widen some of the existing highways. One of them is Ankara-Eskişehir (E-90) highway that connects highly populated areas to the city center. During widening, several cut slopes were formed along the highway route. However, some instability problems such as small-sized rock falls and rock detachments have occurred along a cut slope in highly jointed, folded and sheared limestone. They caused local degradation of the cut slope. The cut slope has a slope angle varying from 71° to 84° and contains several shear zones.

In this study, the relationships between the existing detachment zones and various parameters (e.g. block size, point load strength index, weathering, shear zone, daylight zone) considered to be important for slope instability were investigated using GIS-based statistical landslide susceptibility analyses in order to predict the further aerial extension of the detachment zones with time. During the overlay analyses, statistical index and weighting factor methods were used by means of TNT-MIPS software. The outcomes of the analyses using both methods are compared and

evaluated together with the field observations to check the reliability of the methods and to assess the detachment zones that may develop in the future. Additionally, limit equilibrium analyses were also carried out for the determination of the possible large scale mass failures.

The overlay analyses indicate some risky zones where detachments are likely to occur in the future. On the other hand, the limit equilibrium analysis of the rock mass using Bishop simplified method shows that except one section no mass failure is expected in the cut slope.

Suitable remediation measures which include the use of wire mesh, shotcrete, toe support, and concrete barrier blocks or catch/barrier fences are recommended for these zones.

Keywords: Slope stability, degradation, GIS, limestone, Ankara.

ÖZ

ANKARA-ESKİŞEHİR E90 KARAYOLU ÜZERİNDEKİ ÇATLAKLI VE MAKASLANMIŞ KİREÇTAŞINDA AÇILAN ŞEVİN DURAYLILIK VE DEGRADASYON MEKANİZMASININ BELİRLENMESİ

Öztekin, Burak
Yüksek Lisans, Jeoloji Mühendisliği Bölümü
Tez Yöneticisi : Doç. Dr. Tamer Topal

Aralık 2004, 128 sayfa

Ankara'nın hızlı büyüyen nüfusu ve trafik yoğunluğu nedeniyle, var olan bazı karayollarının genişletilmesi gerekmektedir. Bu yollardan biri olan Ankara-Eskişehir (E-90) karayolu yüksek nüfuslu yerleşim yerlerini şehir merkezine bağlar. Yol genişletme sırasında, karayolu güzergahı boyunca çok sayıda yol yarması oluşturulmuştur. Bununla beraber çok çatlaklı, kıvrımlı ve makaslanmış kireçtaşı içinde açılan yol yarması boyunca küçük boyutlu kaya düşmesi ve kaya dökülmesi gibi şev duraysızlığı problemleri oluşmuştur. Bu durum, şevde yer yer şev degradasyona (gerilemesine) neden olmuştur. Şevin açısı 71^{o} ile 84^{o} arasında değişmekte olup, şevde çok sayıda makaslama zonu yer almaktadır

Bu çalışmada, dökülme bölgeleri ve önemli olduğu düşünülen çeşitli parametrelerin (blok boyutu, nokta yükleme dayanım indeksi, bozunma, makaslama zonu ve günlenme zonu) ilişkisi, gelecekte zamanla gelişebilecek dökülme bölgelerinin alansal dağılımını tahmin edebilmek için, GIS tabanlı istatistiksel analizlerle incelenmiştir. Çakıştırma analizleri sırasında, TNT-MIPS bilgisayar programı yardımıyla istatistiksel indeks ve ağırlık faktörü yöntemleri kullanılmıştır. Her iki yöntem sonucunda elde edilen veriler,

yöntemlerin güvenilirliklerinin kontrolü ve gelecekte oluşabilecek olası dökülme bölgelerinin belirlenmesine yönelik olarak arazi gözlemleri ile karşılaştırılmış ve değerlendirilmiştir. Bunlara ek olarak, kütle yenilmesi türündeki muhtemel duraysızlıkları belirleyebilmek için limit denge analizleri yapılmıştır.

Yapılan çakıştırma analizleri ile gelecekte bazı dökülmelerin olabileceği riskli bölgeler belirlenmiştir. Öte yandan, Basitleştirilmiş Bishop yöntemi kullanılarak kaya kütlesinde yapılan limit denge analizinde, bir zon dışında incelenen yol yarması için herhangi bir kütle yenilmesi beklenmemektedir.

Bu bölgeler için çelik hasır, şatkrit, topuk desteği ve beton bariyer bloklardan yada bariyer çitlerden oluşan koruma yöntemleri önerilmiştir.

Anahtar kelimeler: Şev duraylılığı, degradasyon, GIS, kireçtaşı, Ankara.

To My Family and Itır

ACKNOWLEDGMENTS

I would like to express my indebted appreciation to my supervisor Assoc. Prof. Dr. Tamer Topal for his guidance, supervision and encouragements from the very beginning of this thesis.

I would also like to express my gratitude Assist. Prof. Dr. Mehmet Lütfi Süzen for his caring, comments and suggestions in the critical parts of the study.

I am grateful to my friends Çağıl Kolat and Başak Şener for their care and valuable helps in the analysis.

I am also indebted to my friend Ahmet Utku Özden for his assistance during the field and laboratory tests.

I would like to thank Müge Akın as well for her valuable assistance.

This thesis would never be completed without the help, support and brotherhood of Murat Uğur, my cousin.

Finally, I would like to thank my family and Itır for their courage, patience and support during the preparation of this thesis.

TABLE OF CONTENTS

LIST OF TABLES

TABLE

LIST OF FIGURES

FIGURE

CHAPTER I

INTRODUCTION

1.1. Purpose and Scope

As a result of rapidly growing population of Ankara city, new settlement areas have been arisen. One of these areas is Çayyolu that has become popular recently. Its connection with the city center has long been established by Ankara-Eskişehir (E-90) highway. But a few years ago, due to increasing traffic load and as a precaution to decrease traffic intensity for the coming years, the E-90 highway has gone into improvement. It was widened and new lanes were added. During widening, several cut slopes were formed along the highway route. However, some instability problems occurred along the cut slope located near “Koru Sitesi”. The cut slope was formed in highly jointed, sheared and nearly horizontal but locally folded limestone. The instabilities are generally in the mode of sloughing failures that is characterized by occasional rock falls in the form of raveling or localized slumping/sliding of rocks degraded by weathering (U.S. Army Corps of Engineers, 1994). Therefore, current conditions which locally threaten traffic safety also caused local degradation of the cut slope having a slope angle ranging between 71° to 84°. The cut slope is 470 m long and has a height ranging from a few meters to 18.5 m.

The aim of this study is to assess the degradation mechanism of the cut slope by examining the relationships between the existing detachment zones and related geotechnical parameters, to assess the stability of the cut slope, and to suggest remedial measures based on the extent and the type of the instabilities for the purpose of slope protection.

In order to accomplish this task, the study was started with literature review based on previous works concerning the study area and slope stability practices. It was followed by the field study. At this stage, scan-line surveys were carried out and photographs were taken all along the slope. In the next step, field and laboratory tests were performed. From both field survey and testing stage, input data for the overlay and limit equilibrium analyses were obtained. Finally, the results of all the analyses were combined with engineering judgment and some remediations were recommended for unstable zones of the cut slope.

1.2. Location and Accessibility

The study area is located along the Eskişehir-Ankara E90 highway about 14 km away from the city center, near the Migros shopping center and “Koru Sitesi”. The site is accessible throughout the year by asphalt paved Eskişehir-Ankara E90 highway (Figures 1.1. and 1.2.)

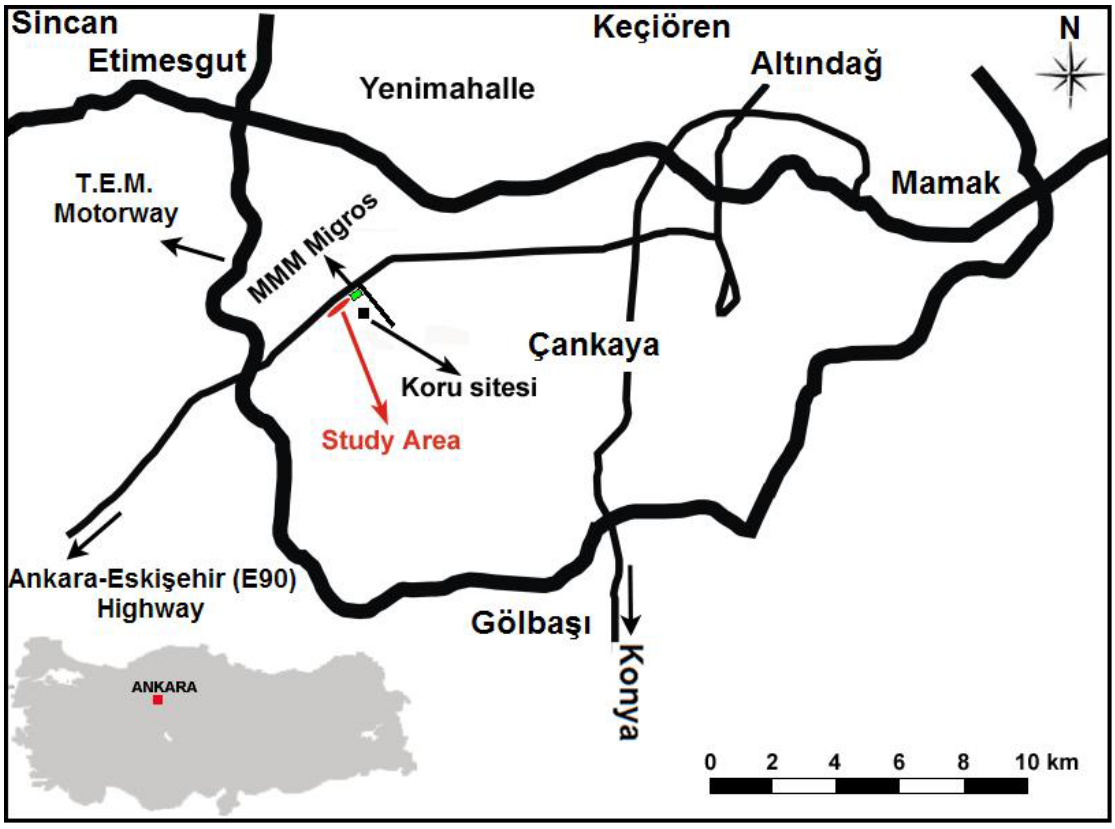

Figure 1.1. Location map of the study area.

Figure 1.2. Photograph showing panaromic view of the studied cut slope (x2 vertical exaggeration).

1.3. Climate

The study area is located in Central Anatolia where continental climate prevails, that is; the summers are hot and dry with cool nights, the winters are cold with rain and snow. Monthly average temperature and precipitation values for Ankara between the years 1925 and 1996 are given in Table 1.1. The average temperature is the highest in August (29°C) whereas the coldest (-6°C) in January through the year. The average precipitation is the highest in December (58mm/month) and the lowest in July and August (13mm/month). The average values for humidity and the days with frost are 60.4% and 84 days, respectively (DMİ, 2004).

Table 1.1. Monthly average temperature and precipitation data for Ankara between 1925 and 1996 (DMİ, 2002).

	MONTHS											
	Jan.	**Feb.**	**Mar.**	**Apr.**	**May**	**Jun.**	**Jul.**	**Aug.**	**Sep.**	**Oct.**	**Nov.**	**Dec.**
Average Temperature (High,°C)	3	5	11	16	21	25	28	29	25	19	12	5
Average Temperature (Low, °C)	-6	-4	-1	3	7	9	12	12	8	4	0	-3
Average Precipitation (mm)	53	43	38	43	53	33	13	13	23	28	33	58

1.4. Geology

Based on the studies by Akyürek et al.(1996) and Sarıaslan et al.(1998), Limestone block (Permian), Elmadağ formation (Triassic), Akbayır formation (Jurassic), Hançili formation (Tertiary), Bozdağ basalt (Tertiary), Gölbaşı formation (Tertiary) and alluvium (Quaternary) are exposed in the close vicinity of the study area. However, the cut-slope lies in the Akbayır formation (Figure 1.3). For this reason, only this unit will be described in this section.

The Akbayır formation consists of clayey or/and biomicritic limestone which is white, cream, beige, and locally red in color, thin to medium bedded and contains chert nodules or bands. The bottom part of the formation begins with marl (yellow to brownish green in color), siltstone and clayey limestone interbedding. Above that part, hemiplagic limestone is found. In this hemipelagic limestone, tectonic deformations observed in the form of fracturing, folding and primary sedimentary structures such as slump and breccia can also be seen. In addition, micritic limestones, oolite bearing limestone, and turbiditic-calcarenitic levels locally exist.

Thicknesses of the beds vary between 5-40 cm for the limestone. The typical feature of this limestone is chert lenses and bands. Also fossils like *Radiolaria*, *Spongia*, *Echinodermata* and *Calpionellide* can be observed. The deposits that form the upper part of the formation include greenish marl and olistostromal lenses in between marl. The olistostrome which consists of the micritic limestone and chert has a thickness ranging between 2 and 15 cm .

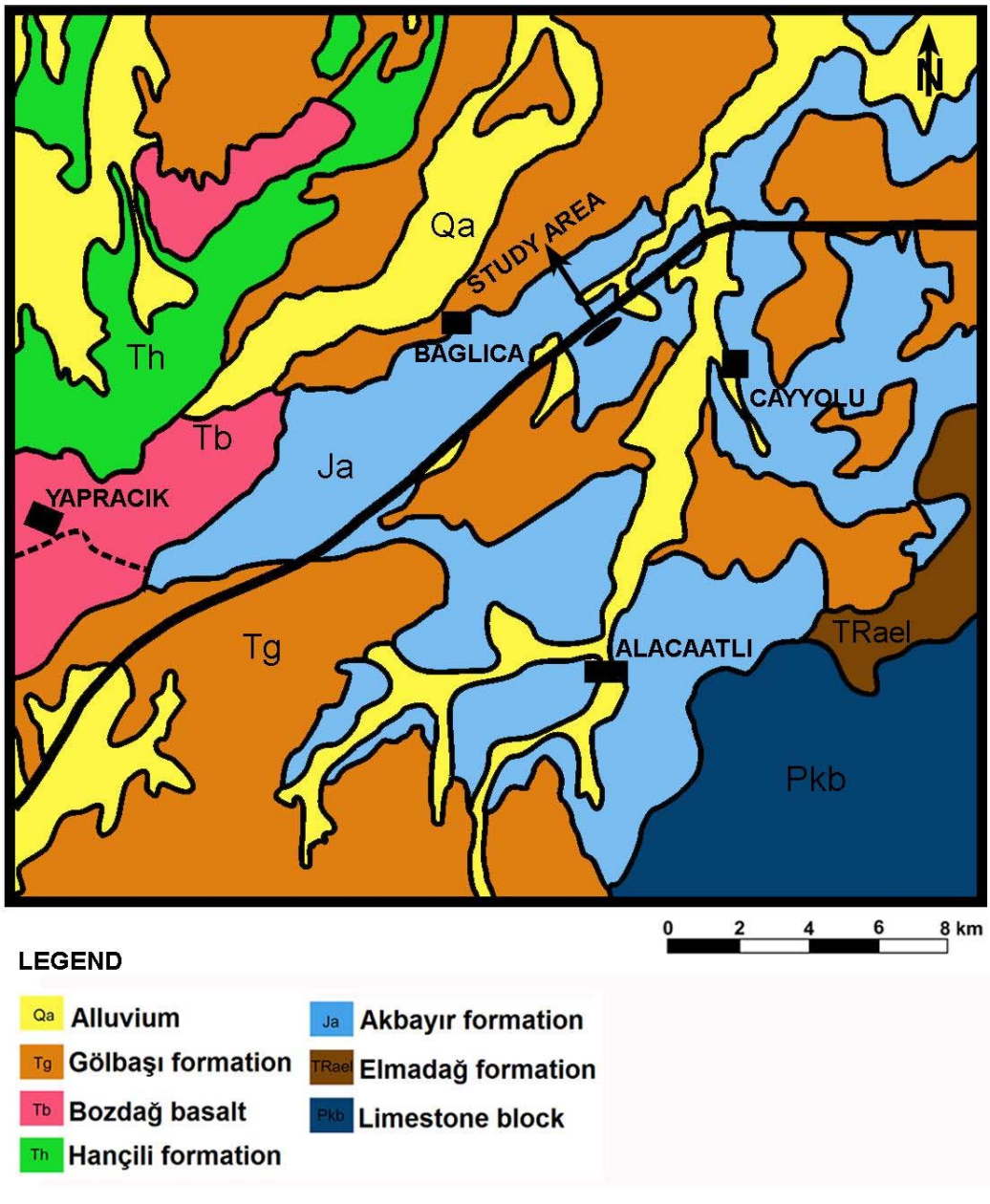

Figure 1.3. Geologic map of the close vicinity of the study area (Modified from Sarıaslan et al., 1998).

1.5. Seismicity of the Study Area

The study area is located in the 4th degree earthquake zone which corresponds to peak horizontal ground acceleration ranging from 0.1g to 0.2g (Kandilli observatory, 2004). The epicenters of the earthquakes that are greater than 4 in magnitude since 1900, are illustrated in the seismicity map (Figure 1.4). Only a few earthquake epicenters with a magnitude less than 5 located in Ankara.

The most important fault which may adversely affect the study area is the North Anatolian Fault Zone. It is about 100 km away from the site and has a capability to produce an earthquake magnitude of 7.5. Several attenuation relationships available in the literature are used in this study. They are given in Table 1.2.

Table 1.2. Peak horizontal ground acceleration values of the study area based on various attenuation relationships

Attenuation relationship by	Peak horizontal ground acceleration (g)
Sabetta and Pugliese (1987)	0,050
Campbell (1988)	0,100
Joyner and Boore (1988)	0,030
Fukushima and Tanaka (1990)	0,079
Abrahamson and Silva (1997)	0,076
Boore et al. (1997)	0,107
Sadigh, et al. (1997)	0,060
Ulusay, et al. (2004)	0,057

The acceleration values based on the attenuation relationships for the study area vary from 0.03g to 0.11g. The peak horizontal ground accelerations for the study area are given by Gülkan et al. (1993) as 0.085g, 0.11g and 0.13g for 100, 225 and 475 years return periods, respectively. A value of 0.10 g for an area very close to the study area was used by Teoman et al. (2004).

Considering the above mentioned acceleration values, 0.10g which roughly corresponds to the upper bound of the calculated accelerations is accepted as peak horizontal ground acceleration for the study area.

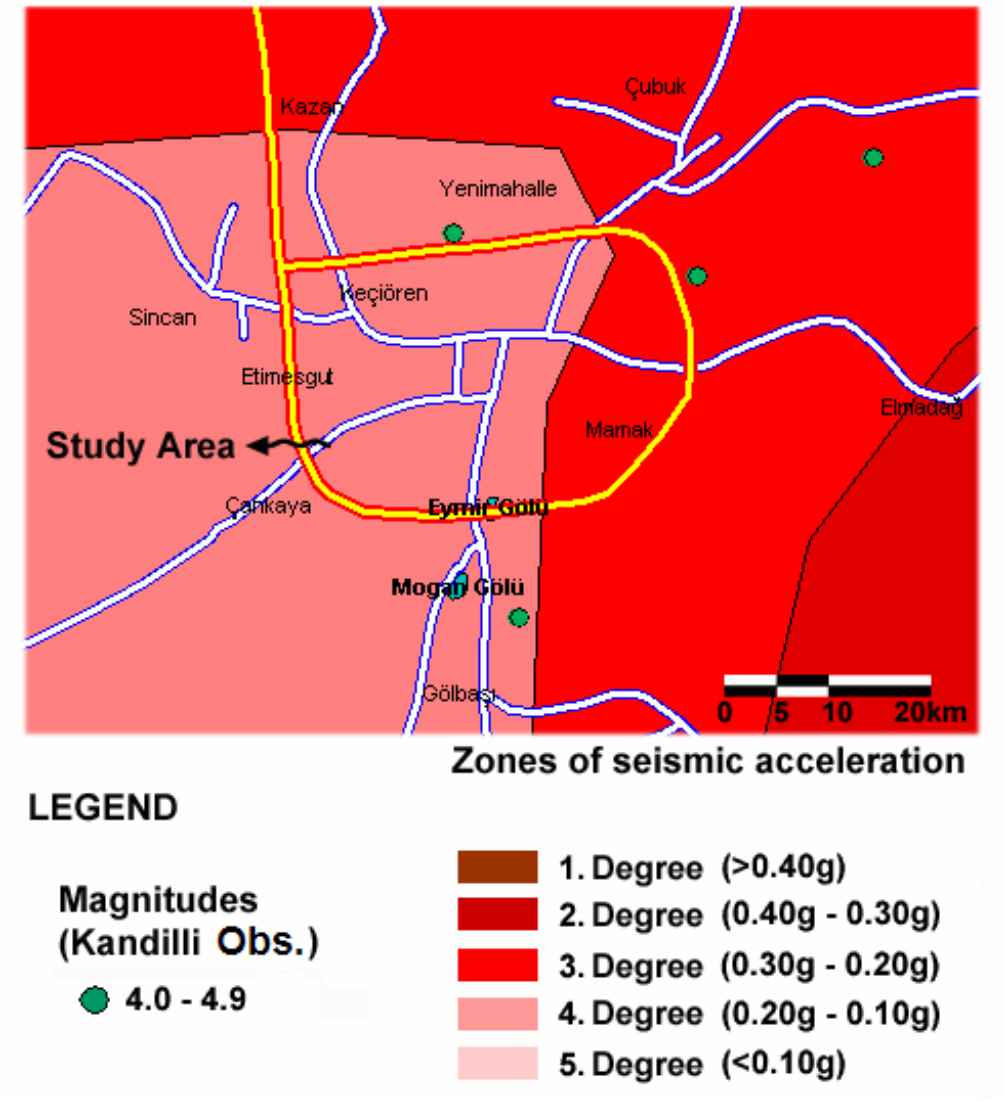

Figure 1.4. Seismicity map including part of Ankara and the close vicinity of the study area for the period 1900-2004 (Kandilli Observatory, 2004).

1.6. Method of Study

The studies are conducted in 3 main stages. These are briefly data acquisition, analysis and recommendations based on the analysis. The data acquisition stage can further be subdivided into preliminary studies, field studies and laboratory studies. On the other hand, analysis stage can be separated into overlay and limit equilibrium analysis subsections.

The first section of the data acquisition stage is mainly based on collecting the preliminary information about the study area. This is achieved through literature review on geology of the area, slope stability practice, collecting information on the seismicity and the climatic conditions of the close vicinity of the study area. The second section of the data acquisition stage is the field studies that include visual inspection and taking photographs. Furthermore, information on discontinuity, rock mass and intact rock material characteristics were gathered through scan-line survey, and field testing (point load strength and Schmidt rebound hardness) were also conducted to determine material properties of the limestone. During the third section, laboratory studies were carried out in which material properties like unit weight, porosity, uniaxial compressive strength, slake durability and sonic velocity were determined through the tests. In addition to these tests, scan-line data gathered during field studies were evaluated by utilizing Dips software of Rocscience (1999) to assess the discontinuity orientations of the limestone besides scan-line data with field observations and laboratory testing lead the way to the determination of cohesion (c) and internal friction angle (Φ) of the rock mass by utilizing Rocklab software (Rocscience 2002a). The geotechnical layers utilized throughout the overlay analysis were prepared in this section with the help of photoanalysis and the field observations.

First part of the analysis stage is the GIS-based overlay analysis, which was carried out by utilizing the five parameter maps (block size, point load

strength index, weathering, shear zone, and daylight zone) and an inventory map (detachment zones) prepared in this study. During the overlay analysis, statistical index (W_i) (Van Westen, 1997) and weighting factor (Wf) (Çevik, 2002) methods were used through TNT-Mips software by Microimages (2000). The outcomes of the analysis using both methods were compared and evaluated together with the field observations to check the reliability of the methods and to assess the detachment zones that may develop in the future. In the second part of analysis, possibilities of the potential mass failures were studied via Simplified Bishop limit equilibrium method through Slide software of Rocscience (2002b).

And finally in the third stage, based on the extent and the type of the possible failures, recommendations were made for unstable zones of the cut slope.

CHAPTER II

ENGINEERING GEOLOGICAL PROPERTIES OF LIMESTONE

This section is based on the determination of the engineering geological properties of the limestone (except for the shear strength parameters which will be discussed in Chapter IV) exposed in the study area by means of the field and laboratory studies.

The field studies briefly include scan-line survey, mapping of block size, weathering grades, detachment, shear and daylight zones (which will be discussed in detail in Chapter III), taking photographs along the cut slope, sample collection and field testing (point load strength and Schmidt rebound hardness). Concise laboratory studies involve the evaluation of the scan-line and field testing data, determination of both dry and saturated unit weights, porosity, slake durability, sonic velocity, uniaxial compressive strength of rock material and determination of the shear strength parameters of the rock mass. The details concerning each of these properties will be given in the following sections.

2.1. Material Properties of the Limestone

Because of the vast range in properties of rocks, which reflect varieties of structures, fabrics, and components, engineers rely on a number of basic measurements to describe rocks quantitatively. Certain properties that are relatively easy to measure are valuable in this regard and may be designated index properties (Goodman, 1989). Apart from quantitative description of the

limestone, the values obtained from these measurements are directly used in the analysis.

2.1.1. Porosity and Unit Weight

From an engineering standpoint, pores are by far the most important property in a rock because they are the weakest. They govern physical attributes such as strength, deformability, and hydraulic conductivity (Franklin and Dusseault, 1989). In general, porosity and unit weight are interrelated. Moreover, the determination of the unit weight values is critical for the calculation of factor of safety during the limit equilibrium analyses for slopes. This makes determination of the unit weight vital as an input data in slope stability analysis apart from being an index test.

A total of 36 samples were collected during field studies and tested as irregular lumps. Porosity, dry and saturated unit weights of the limestone were calculated from these samples according to the methods suggested by ISRM (1981). The average values with standard deviations were determined as 8.1% $\pm$ 2.07% for porosity, 24.4 kN/m^3 $\pm$ 0.56 kN/m^3 and 25.2 kN/m^3 $\pm$ 0.37 kN/m^3 for the dry and saturated unit weights, respectively. These values reveal that, the limestone has moderate unit weight and medium porosity according to the classifications by Anon (1979). Details of the test results for each sampling location are tabulated in Appendix A.

2.1.2. Uniaxial Compressive Strength

For many years the uniaxial compressive strength (UCS) test was the main quantitative method for characterizing the strength of rock materials (Hawkes and Mellor, 1970). The test is still the basis of many rock

classifications (Franklin and Dusseault, 1989). The main drawback of the uniaxial compressive strength test is the time and effort consuming process of sample preparation for the testing. Also, the major problem in this study concerning uniaxial compressive strength test is the sample preparation. Since the limestone in the cut slope is highly jointed and sheared, it is very difficult to acquire suitable size rock material (cylindrical or cubic) as suggested by the method of ISRM (1981). The collected blocks disintegrate into smaller particles due to heavy jointing, sample disturbance and the effect of weathering at some locations. In this case, it is impractical to extend the uniaxial compressive strength test to characterize the limestone all along the cut slope. As a result, fifteen cubic samples (with side lengths of nearly 5 cm) obtained from a single location were tested. Based on the test results, the average value of the uniaxial compressive strength with standard deviation of the limestone is determined as 39.4 MPa $\pm$ 13.98 MPa. According to ISRM (1981) classification, it is moderately strong rock.

2.1.3. Point Load Strength Index

The point load strength test is intended as an index test for the strength classification of rock materials. It may also be used to predict other strength parameters with which it is correlated, for example uniaxial tensile and compressive strengths (ISRM, 1981).

The point load strength index test was carried out according to the procedures proposed by ISRM (1985) at 28 locations in the field by using portable point load strength index apparatus. Briefly, 280 specimens, that are irregular lumps collected directly from the exposed slope surface, were tested from which uncorrected point load strength (I_s) of the limestone was determined. Size-corrected point load strength ($I_{s(50)}$) was determined according to the

procedures suggested by ISRM (1985). From the tests, the average corrected point load strength ($I_{s(50)}$) with standard deviation along the study area was determined as 3.5 MPa $\pm$ 0.87 MPa. Detailed test result at each location can be found in the Appendix B. Based on the test results, the correlation factor (k) between the uniaxial compressive strength and the point load strength index is found to be 12. According to Norbury (1986) and Topal (2000), such a low value may be obtained for weak rocks. Considering the fact that the limestone is moderately strong rock, low value of the correlation factor may be attributed to the small scale cracks (which will also be discussed in sonic velocity test), and the disturbance of the samples used in the uniaxial compressive strength test.

2.1.4. Schmidt Rebound Hardness

Schmidt rebound hardness test is quicker, simpler but a less reliable alternative to the point load strength index test for the estimation of the rock strength (ISRM, 1981). The test was performed according to ISRM (1981), using L-type Schmidt hammer at 36 locations in the field. 20 rebound measurements were taken at each location (total of 720). The lowest ten recordings were discarded and average Schmidt hammer values were determined from the remaining 10 measurements at each location. The test results are tabulated in Appendix C. The average value of the Schmidt hammer rebound hardness of the limestone is found to be 31. For the estimation of the uniaxial compressive strength of the limestone, the chart given in Figure 2.1 considering the Schmidt rebound hardness value and the dry unit weight is used. Based on this evaluation, the average uniaxial compressive strength with standard deviation of the limestone is estimated as 44.8 MPa $\pm$ 25.27 MPa. Although this average value is quite close to the actual UCS of the limestone, it shows great deviations in some locations. The reason for this deviation is highly jointed and loose character of the limestone in the study area. According to Ulusay and Sönmez (2002), this test is not recommended for closely spaced loose rock masses. As a

result, using the UCS values correlated from the point load strength tests through out this study seems to be more logical.

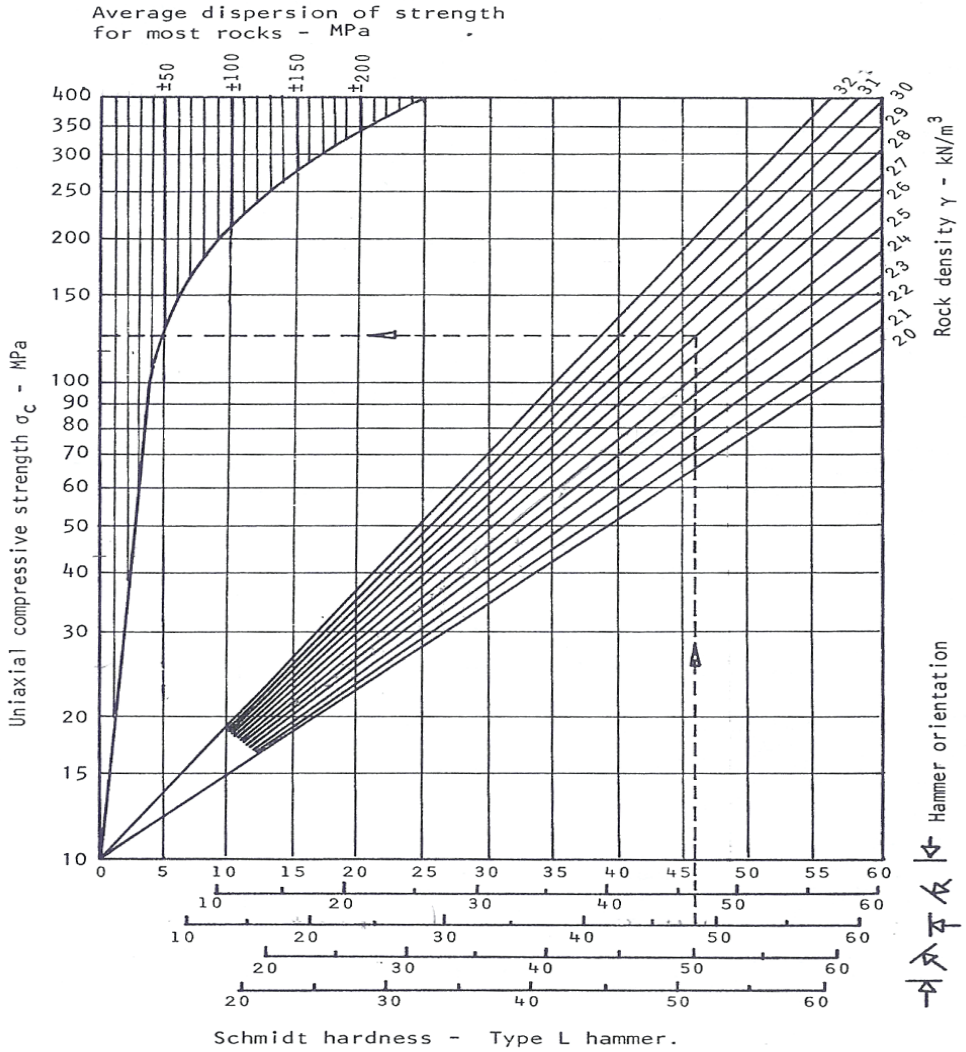

Figure 2.1. Relationship between Schmidt rebound value and the uniaxial compressive strength of rock (Hoek and Bray, 1977).

2.1.5. Sonic velocity

This test is intended as a method to determine the velocity of propagation of elastic waves in laboratory rock testing (ISRM, 1981). Theoretically, the velocity with which stress waves are transmitted through rock depends

exclusively upon their elastic properties and density. In practice, a network of fissures in the specimen superimposes an overriding effect. This being the case, the sonic velocity can serve to index the degree of fissuring within rock specimens (Goodman, 1989).

For this test, fifteen dry cubic limestone samples (5x5cm size) were tested using pulse transmission technique through Pundit-Plus. During the test, 54 KHz transducers were utilized for the P-wave measurements.

As a result of the test, average P-wave velocity with standard deviation of the limestone is determined as 3662.7 $\pm$ 470.87 m/sec which corresponds to moderate velocity according to the classification proposed by Anon (1979). This is a low value for limestone, it may be attributed to small scale cracks or fissures in the limestone.

2.1.6. Slake Durability

Slake durability test is intended to assess the resistance offered by a rock sample to weakening and disintegration when subjected to two standard cycles of drying and wetting (ISRM, 1981).

The test was carried out according to the procedure proposed by ISRM (1981). The test samples were taken from two locations that represent slightly and moderately weathered parts of the limestone. After two cycles of testing, 98.9% of the samples from slightly weathered zone retained and for the moderately weathered zone 98.2% of the samples preserved.

Based on these results, the limestone can be classified as very high to high durability based on Gamble's classification (Goodman, 1989).

2.2. Mass Properties of the Limestone

The limestone cut face in the study area was divided into 21 sections in order to carry out scanline survey (Figure 2.2). Detailed photograph of each section was also taken for further investigations.

During scan-line survey, over 1600 measurements concerning orientation, spacing, aperture, persistence, infilling, roughness and weathering state of the discontinuities were taken. In the light of these measurements and observations made in the field, the study area was divided into three main sectors as; A, B and C (Figure 2.2.).

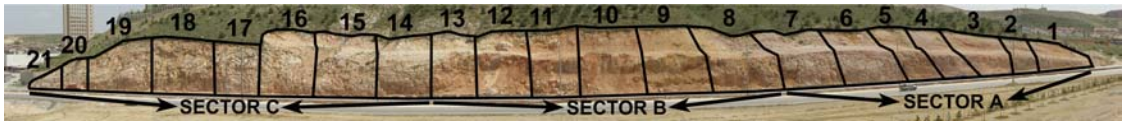

Figure 2.2. Study area with 21 scan-line sections, and sectors A, B and C.

In the limestone bedding, joints and shear zones constitute the main discontinuity types. The limestone in the study area was folded and highly jointed (Figures 2.3. and 2.4.). Therefore, the dip direction and dip amount of the discontinuities vary considerably from one scan-line section to another and also in some parts of a single scan-line section.

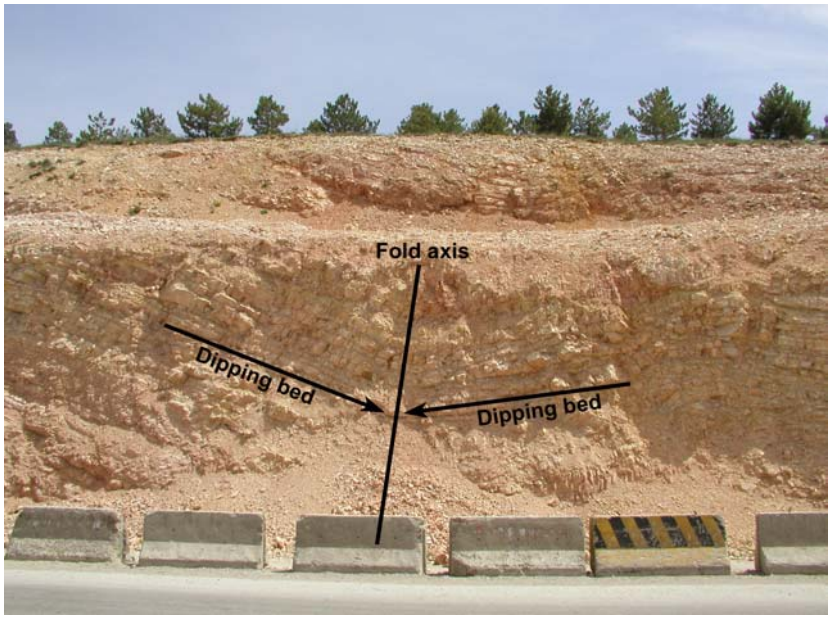

Figure 2.3. Photograph showing the folded limestone in the study area.

Figure 2.4. Photograph showing a highly jointed section of the limestone.

Dip direction and dip amount data for the discontinuities collected from the study area were evaluated for each scan-line section by using a computer software called Dips (version 5.04, Rocscience, 1999) in the light of the observations that were made in the field. As a result of these evaluations, the dominant joint sets were found. Since the limestone in the study area is folded

and has variable character, the dominant direction for bedding were also needed to be determined. The discontinuity data belonging to each of the three main sectors (A, B and C) were used to obtain scatter plot and contour plot (Figures 2.5 to 2.10). Based on these evalutions; dominant dip direction and dip amount in Sector A for bedding plane is 200/24°; for Joint Set 1 and Joint Set 2 are 244/61° and 340/79°, respectively (Figures 2.5 and 2.6). There is also significant amount of concentration observed in Figure 2.6 which has a dominant dip direction and dip amount of 94/60°. However, this concentration is a result of the variations in the orientation of joint set 2, therefore it is not treated as an additional joint set to the current ones.

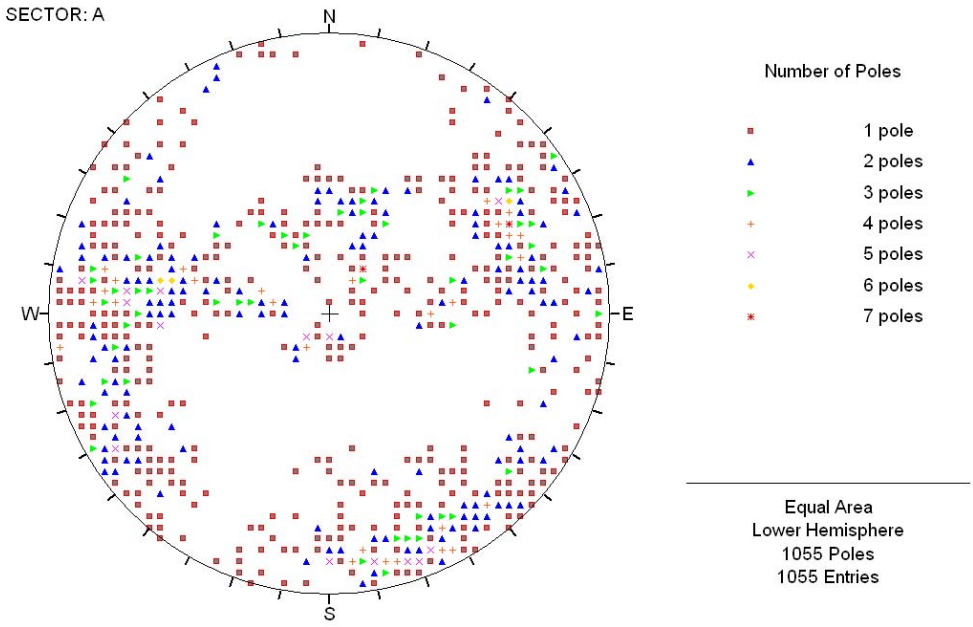

Figure 2.5. Scatter plot of the poles of the discontinuities at Sector A.

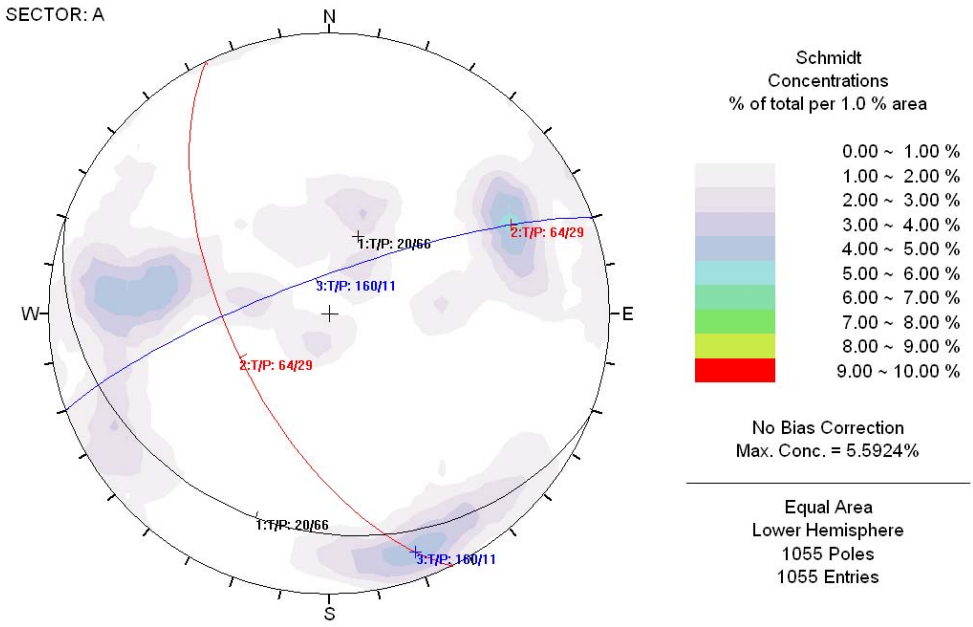

Figure 2.6. Contour plot of the poles of the discontinuities at Sector A with dominant discontinuity orientations.

For Sector B, 130/14° is the dominant dip direction and dip amount for the bedding plane; 062/67° and 317/79° are the dominant dip direction and dip amount for Joint Set 1 and 2, respectively (Figures 2.7 and 2.8).

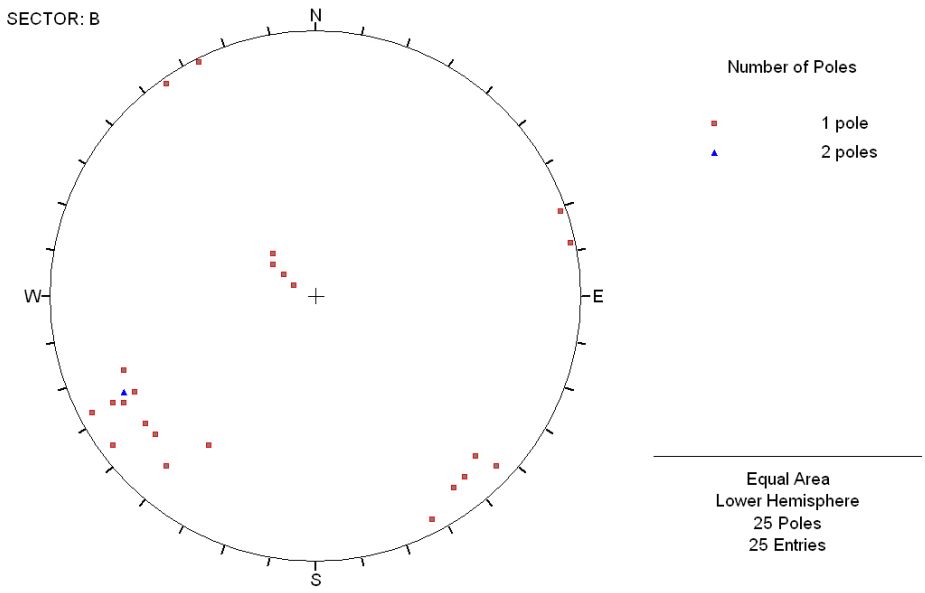

Figure 2.7. Scatter plot of the poles of the discontinuities at Sector B.

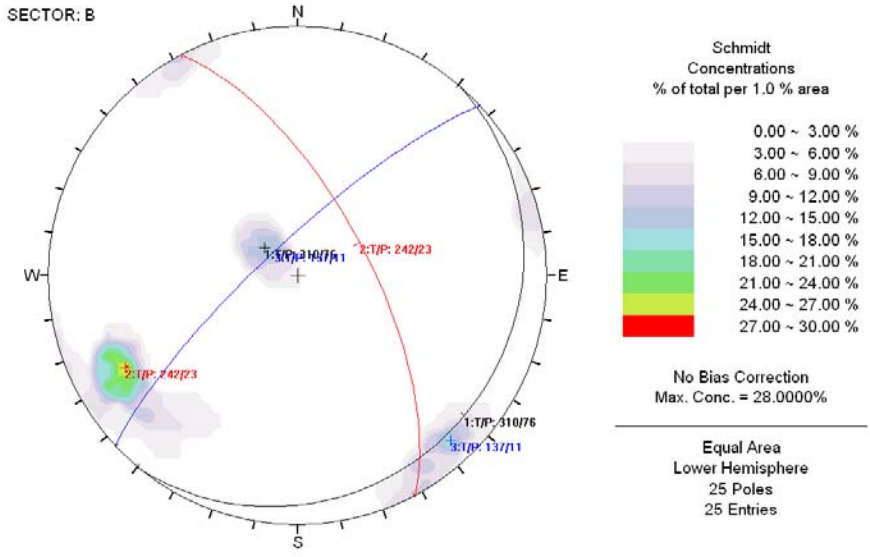

Figure 2.8. Contour plot of the poles of the discontinuities at Sector B with dominant discontinuity orientations.

The dominant dip direction and dip amount for bedding plane in Sector C is 113/19°. However, for Joint Sets 1 and 2, the dominant dip direction and dip amount are 276/86° and 342/61°, respectively (Figures 2.9 and 2.10). For the shear zones in the study area, there are two dominant directions given as 64/77° and 191/67° (Figure 2.11 and 2.12).

The spacing of the discontinuities developed within the limestone generally ranges from close (60-200mm) to very closely spacing (20-60mm) (ISRM, 1981). The discontinuity spacing distribution histograms for each sector (A, B and C) are shown in Figures 2.9., 2.10. and 2.11. Although there are some fluctuations in the histograms, they generally fit negative exponential distribution function as suggested by Priest (1993). The coefficient of correlation (r) for sectors A and C are about 0.90 and 0.88, respectively. However, r for sector B is 0.73 which is a low value compared to the other two values. This may be attributed to scattering of limited number of data collected in sector B due to the sampling bias.

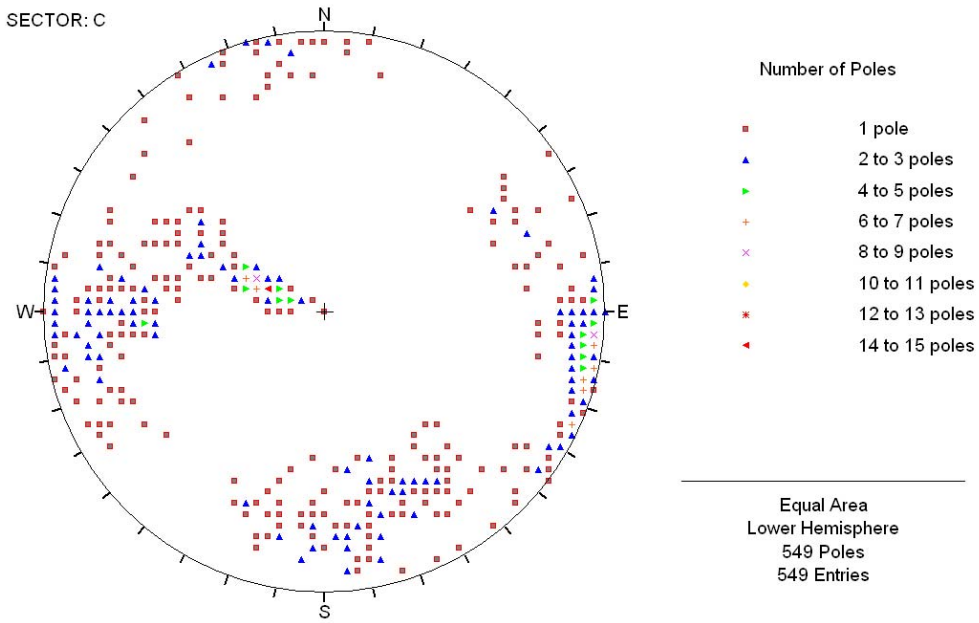

Figure 2.9. Scatter plot of the poles of the discontinuities at Sector C.

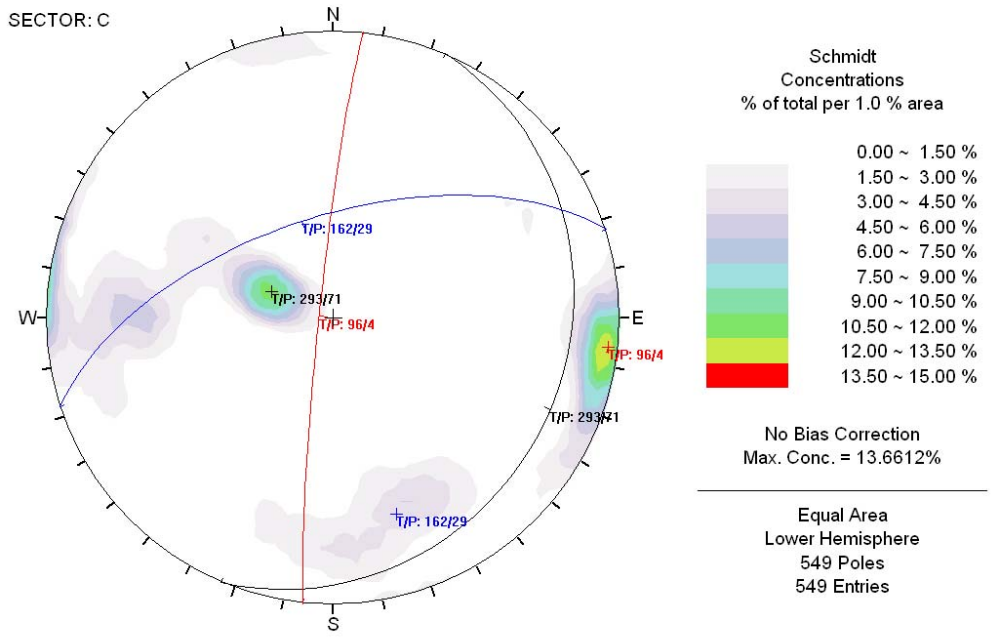

Figure 2.10. Contour plot of the poles of the discontinuities at Sector C with dominant discontinuity orientations.

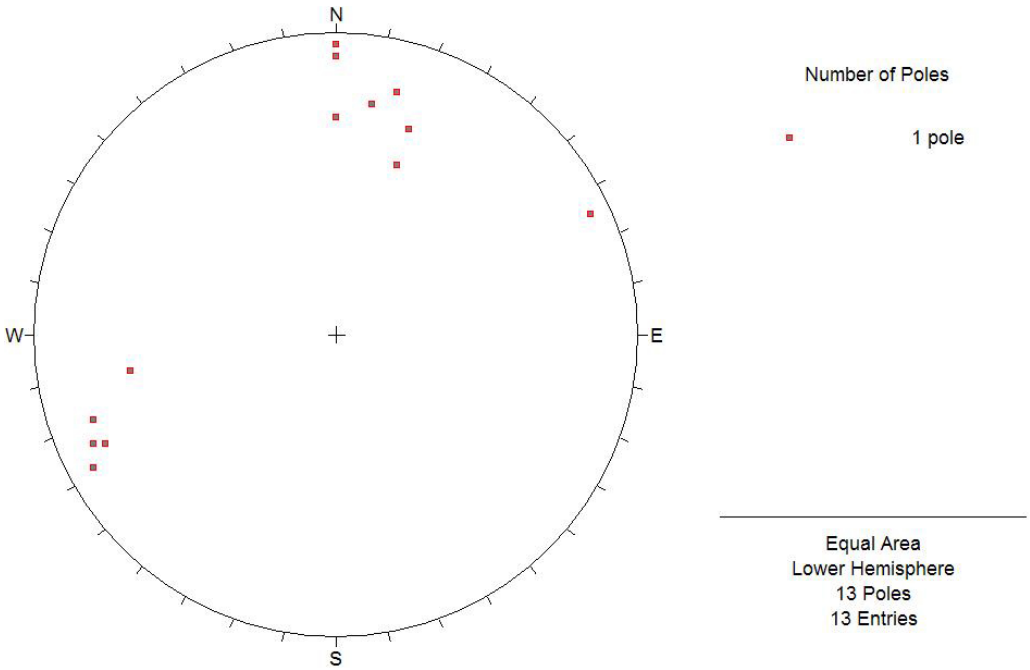

Figure 2.11. Scatter plot of the poles of the shear zones in the study area.

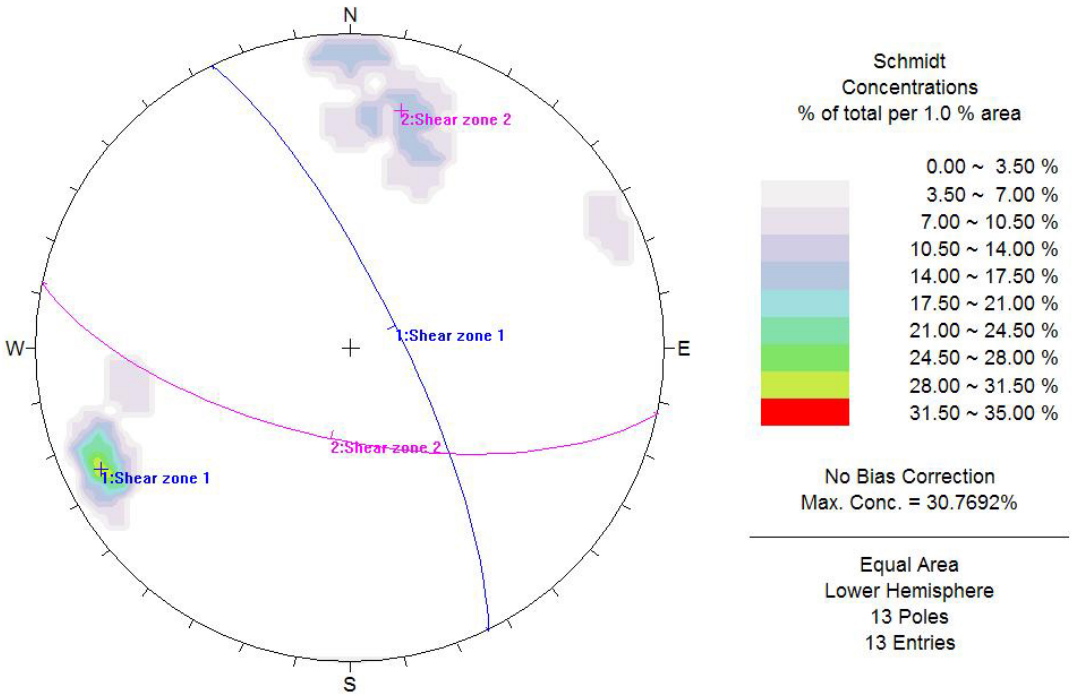

Figure 2.12. Contour plot of the poles of the shear zones in the study area with dominant discontinuity orientations

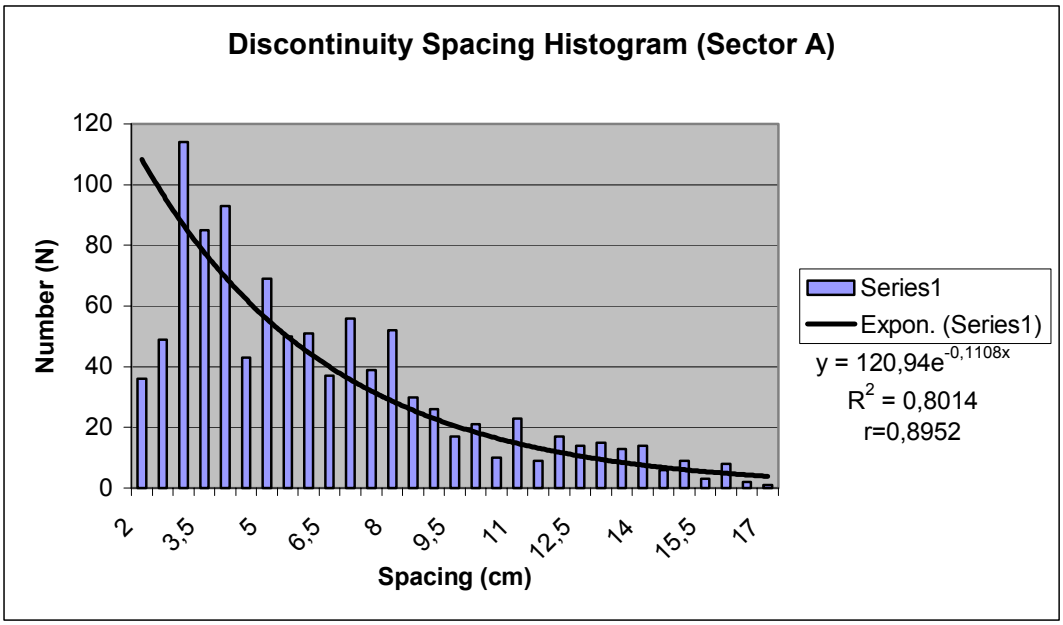

Figure 2.13. Discontinuity spacing histogram with negative exponential distribution function fitted for Sector A.

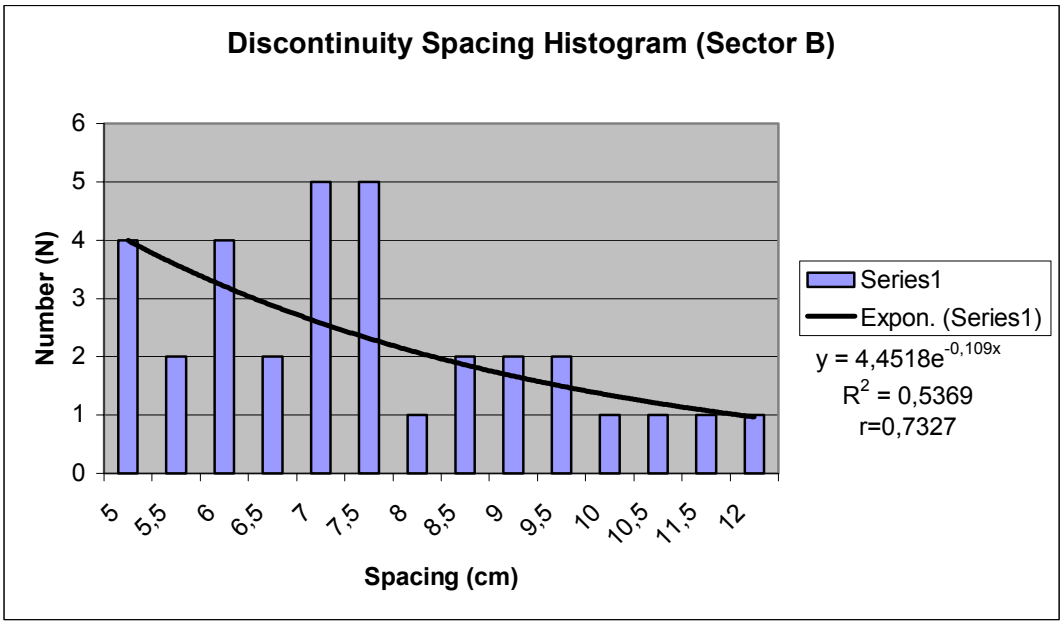

Figure 2.14. Discontinuity spacing histogram with negative exponential distribution function fitted for Sector B.

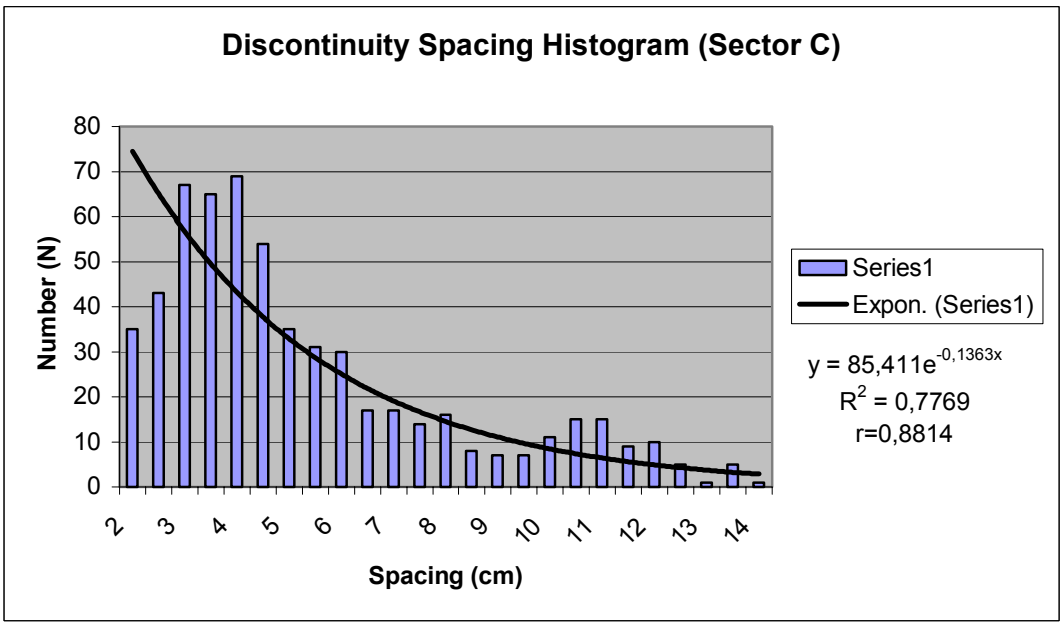

Figure 2.15. Discontinuity spacing histogram with negative exponential distribution function fitted for Sector C.

For all sectors, both joint sets exhibit very low persistence (<1 m) (ISRM, 1981). On the other hand, the bedding plane has high persistence (>10 m) (ISRM, 1981).

For Sector A; the aperture of the bedding plane ranges between tight to open (0.1-2.5 mm) (ISRM, 1981) whereas for the joint sets, aperture ranges between partly open to open (0.25-2.5 mm) (ISRM, 1981). For Sector B, aperture for the bedding plane ranges between open and moderately wide (0.5-10 mm) (ISRM, 1981), and it is also the case for the joint sets. Aperture values for the bedding plane and joint sets in Sector C range from tight to moderately wide (0.1-10 mm) (ISRM, 1981) and from tight to open (0.1-2.5 mm), respectively . In all sectors, the discontinuities are mostly free of infilling material but locally some clayey infilling can also be observed. The surface roughnes for the bedding plane is generally slightly rough to rough and undulating in some sections; for the joint surfaces slightly rough with local undulations in some parts and stepped near the surface.

The rock mass in the study area displays slightly weathered, moderately weathered and highly weathered grades according to the classification proposed by BSI (1981). More detailed description about these grades and their distributions in the study area will be discussed in Chapter III.

CHAPTER III

GIS BASED OVERLAY ANALYSIS FOR THE DETACHMENT ZONES

The factors affecting the landslide hazard can be classified in two categories: the intrinsic variables that contribute to landslide susceptibility, such as geology, slope gradient, aspect, elevation, geotechnical properties of the slope forming material, vegetation cover, and drainage patterns; and the extrinsic variables that tend to trigger landslides in an area of given susceptibility, such as heavy rainfall, earthquakes, and volcanoes (Wu and Siddle, 1995; Atkinson and Massari, 1998; Dai et al., 2001). Although the probability of landslide occurrence depends on both intrinsic and extrinsic variables, the extrinsic variables may change over a very short time span, and are thus very difficult to estimate. If extrinsic variables are not taken into account, the term ‘‘susceptibility’’ could be employed to define the likelihood of occurrence of a landslide event. The spatial distribution of the intrinsic variables within a given area determines the spatial distribution of the landslide susceptibility in that region (Carrara et al., 1995; Dai et al., 2001). Landslide susceptibility may be assessed through heuristic, statistical and deterministic approaches (Yin and Yan, 1988; Soeters and Van Westen, 1996; Van Westen and Terlien, 1996; Dai et al., 2001; Çevik and Topal, 2003).

In this study, the stability of the study area is investigated through factor of safety calculations by means of limit equilibrium analysis. However, the limestone in the study area is highly jointed, folded and also sheared in some places which make it to display rather complex character. So being another dimension, overlay analysis was carried out through statistical analysis by utilizing TNT-Mips software of Microimages (Version 6.2) for the prediction of the

areas that are likely to detach in the future. By carrying out overlay analysis, it is expected to delineate sloughing failures that are generally characterized by occasional rock falls or localized slumping/sliding of rocks degraded by weathering.

The main difference of this study from the conventional GIS applications is; rather than studying on map view, analysis is carried out directly on the photographs of the slope face (section view). The main idea in this analysis is to predict future instabilities, which may occur as local detachments rather than deep seated mass failures, from the ones occurred in the past. The methodology used in this thesis is briefly defined by Luzi and Pergalani (1996) as indirect approach, which evaluates the importance of the combination of different landslide triggering factors, mostly using statistical techniques. The results can be extrapolated to landslide free areas having similar combinations of triggering factors. This method also named as indirect method (Van Westen, 1993; Rowbotham and Dudycha, 1998). So, firstly the factors or parameters that were thought to contribute instability were selected by employing engineering judgment gained through the field observations. From these parameters/factors, various layers containing nearly homogeneous engineering geological mapping zones were produced, and they were rasterized using TNT-Mips software. Resolution of 10x10 cm pixel size is selected. These layers are point load strength, weathering, block size, daylight and shear zones. Apart from these layers, detachment zones were also mapped as an inventory layer. In the analysis part, two methodologies are utilized, namely statistical index method (W_i) of Van Westen (1997) and weighting factor (Wf) method (Çevik, 2002; Çevik and Topal, 2003) which will be briefly discussed in the following sections. In addition, in order to check the contribution and the effect of each layer, sensitivity analyses were carried out by removing each one of the layers at a time.

3.1. Input Data and Data Production

In this section, the production of input data and the basis for creating each individual parameter class are briefly discussed. Also further information on the percentages of the detachments in each parameter class out of total detachments and the density of the detachments in each parameter class (given in percentages) will be tabulated. For the following sections, they will be referred as percent detachment and detachment density. They can be formulated as:

$$\%\ \text{detachment} = \frac{Npix(Si)}{\sum Npix(Si)}$$

$$Densclas = \frac{Npix(Si)}{Npix(Ni)}$$

where,

% detachment : The percentage of the detachment in a certain parameter class out of total detachments

Densclas : The detachment density within the parameter class.

Npix(Si) : Number of pixels, which contain detachments, in a certain parameter class.

Npix(Ni) : Total number of pixels in a certain parameter class.

∑Npix(Si) : Total number of pixels, which contain detachments, in the study area

3.1.1. Detachment Layer

Detachment zones illustrate instabilities that has taken place until now, dominantly in the form of raveling and sloughing. Detachment layer for overlay analysis was produced through the field surveys and photograph interpretation. In the detachment layer, there are two classes or zones; zones with detachments and zones without detachments (Figure 3.2). Detachment zones comprise about 23% of the total study area (Figure 3.1).

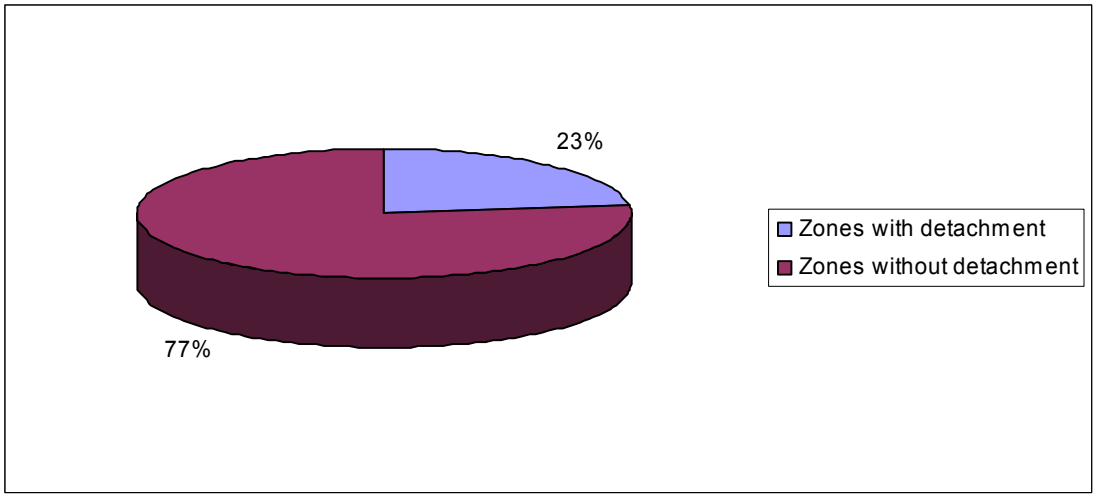

Figure 3.1. Percentage of the detachments in the cut slope

Figure 3.2. Zonation map of the cut slope for the detachment layer.

3.1.2. Point Load Strength Layer

Point load strength layer was produced on the basis of the results obtained from point load strength index tests which were carried out throughout the cut slope. The categories given in Rock Mass Rating System (Bieniawski, 1989) are utilized for the preparation of the point load strength layer. As a result, the cut slope was divided into four categories or zones for the point load strength layer (Table 3.1 and Figure 3.3). The point load strength layer is shown in Figure 3.5. For this layer; about 46% of total detachments occurred in Class II, 34% in Class III, 16% in Class IV and 4% in Class I (Figure 3.3). On the other hand, 72% of Class I, 50% of Class II, 9% of Class III and 4% of Class IV are dominated by detachments (Figure 3.4).

Table 3.1. Range of point load strength values for each category according to RMR classification.

Category No.	**I**	**II**	**III**	**IV**
Range of point load strength index values (MPa)	4-10	2-4	1-2	<1

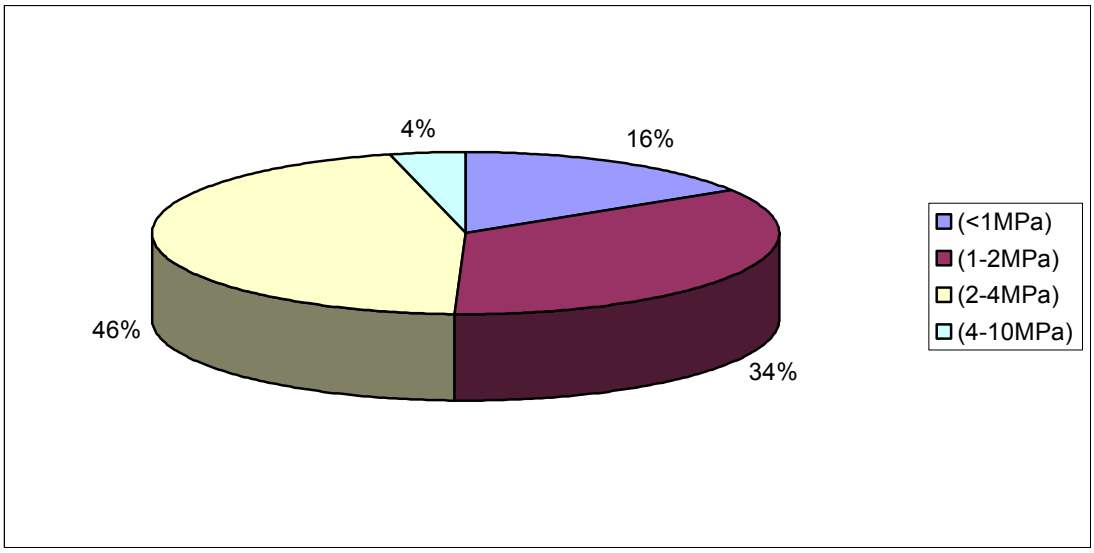

Figure 3.3. Percent detachment in each point load strength category.

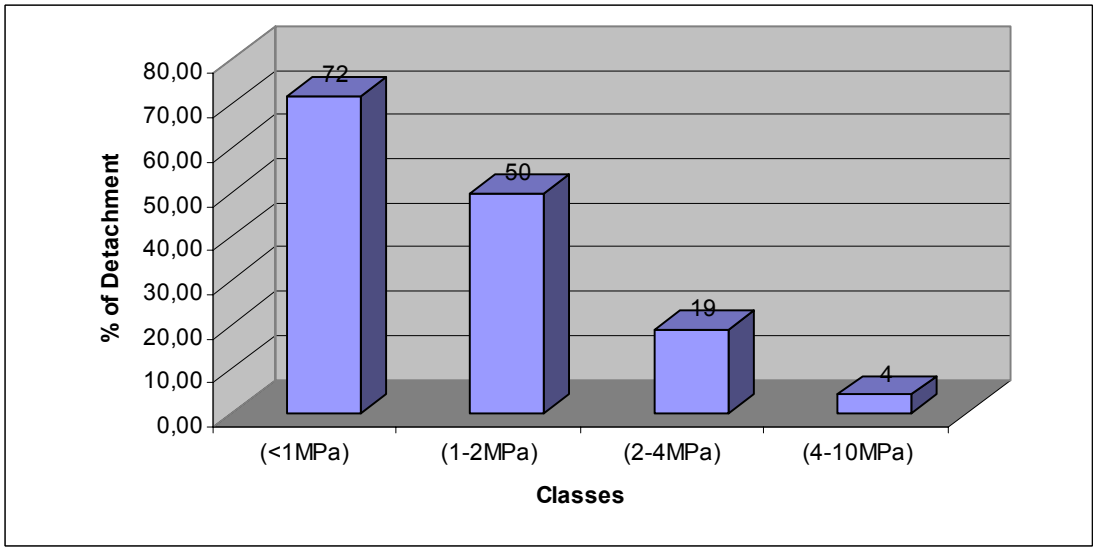

Figure 3.4. Detachment density in each point load strength class.

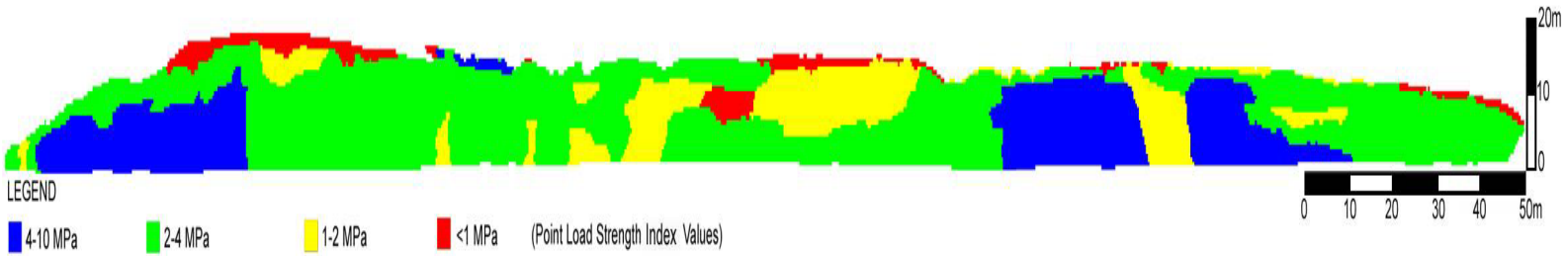

Figure 3.5. Zonation map of the cut slope for the point load strength index layer.

3.1.3. Weathering Layer

Although there are various weathering classifications, most of them refer to weathering of silicate rocks. Solution for chemical weathering and disintegration for physical weathering may be much more significant than other weathering processes for limestone (Fookes and Hawkins, 1988). Therefore, the classifications based on weathering of silicate rocks may not be so suitable for the carbonate rocks. However, the field observations in the cut slope reveal that the effect of discontinuities on weathering and argillaceous character of the limestone control the development of the weathering. Dissolution is not found to be the major weathering process in the study area. Therefore, the weathering classification (Table 3.2) proposed by BSI (1981) was adapted in this study.

Table 3.2. Scale of weathering grades of rock mass (modified from BSI, 1981)

Term	Description	Grade
Fresh	No visible sign of rock material weathering; perhaps slight discoloration on major discontinuity surfaces.	I
Slightly Weathered	Discoloration indicates weathering of rock material and discontinuity surfaces. All the rock material may be discolored by weathering	II
Moderately Weathered	Less than half of the rock material is decomposed or disintegrated to a soil. Fresh or discolored rock is present either as continuous framework or as cornerstones.	III
Highly Weathered	More than half of the rock material is decomposed or disintegrated to a soil. Fresh or discolored rock is present either as continuous framework or as cornerstones.	IV
Completely Weathered	All rock material is decomposed and/or disintegrated to soil. The original mass structure is still largely intact.	V
Residual Soil	All rock material is converted to soil. The mass structure and material fabric are destroyed. There is a large change in volume, but the soil has not been significantly transported.	VI

Weathering layer was prepared through field observations and photograph interpretation based on the selected weathering classification. Although there are 6 grades present in this classification, the limestone in the

study area, displays grades II, III and IV (Figures 3.6-3.8). For each of these grades, detachment percentages are given as: 73% of total detachment is in moderately weathered zone, 24% of total detachment is in highly weathered zones and 3% of total detachment is in slightly weathered zone (Figure 3.6). Alternatively, detachments are present in about 73% of highly weathered zone, 25% of moderately weathered zone and 3% of slightly weathered zone (Figure 3.7).

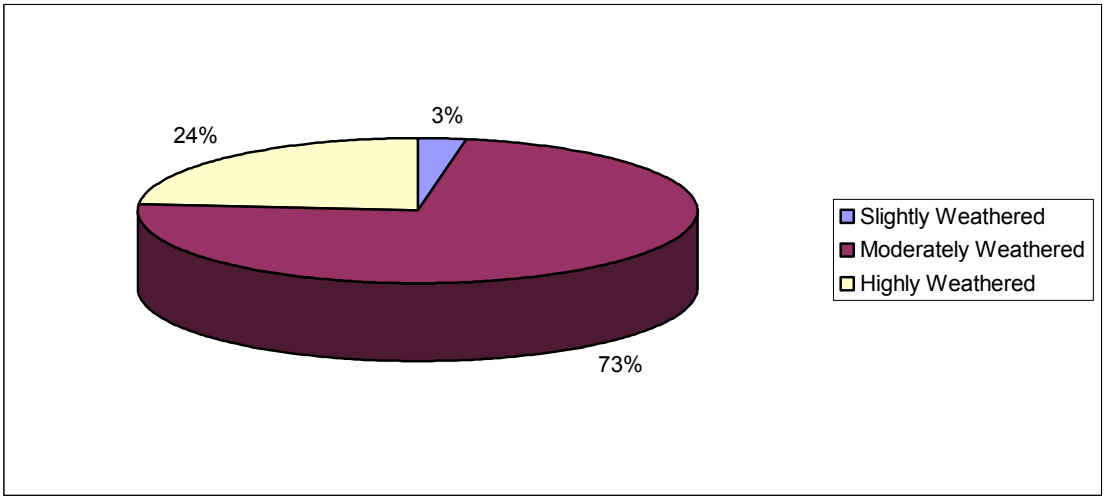

Figure 3.6. Percent detachment in each weathering grade.

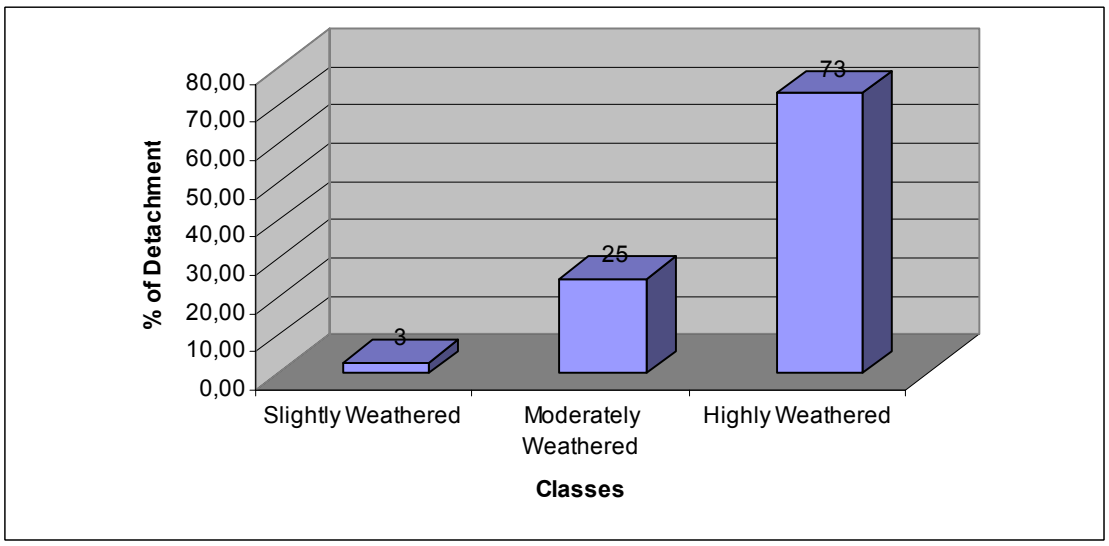

Figure 3.7. Detachment density in each weathering class.

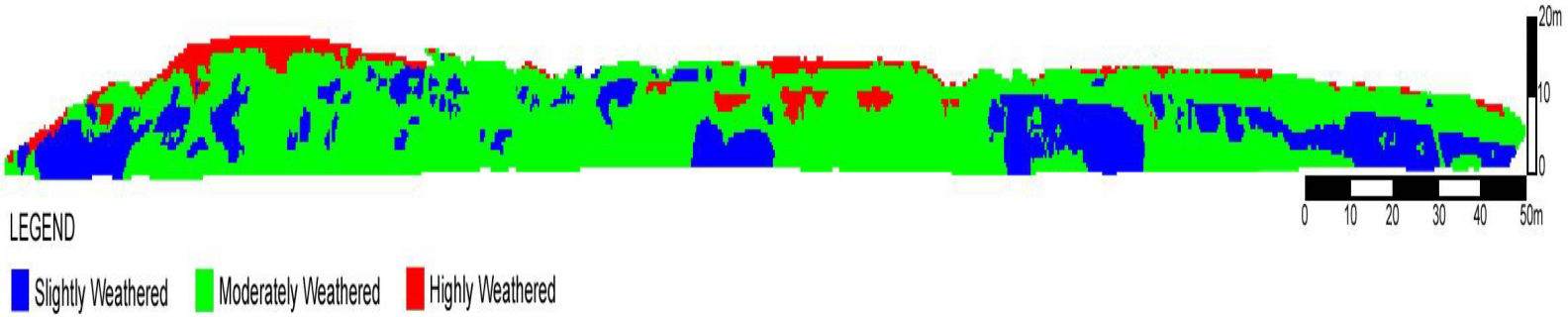

Figure 3.8. Zonation map of the cut slope for the weathering layer.

3.1.4. Block Size Layer

The spacing values used in the preparation of this layer were obtained via scanline surveys along the study area. In this study, the range of block size classes (Table 3.3) given in ISRM (1981) was adopted. On the basis of the calculated J_v (volumetric joint count of ISRM, 1981), three block size categories exist in the cut slope (Figures 3.9 and 3.10). The distribution of the block size categories is shown in Figure 3.11. For this layer; about 90% of total detachments occurred in J_v>30 and 10% in J_v=10-30 block size class (Figure 3.9). On the other hand, 24.15% of J_v>30 size class, 19.59% of J_v=10-30 size class, and 0.15% of J_v=3-10 size class are dominated by the detachments (Figure 3.10).

Table 3.3. Block size classes for the range of values (modified from ISRM, 1981)

Description	**J_v (Joint/m^3)**
Very large blocks	<1
Large blocks	1-3
Medium-sized blocks	3-10
Small blocks	10-30
Very small blocks	>30

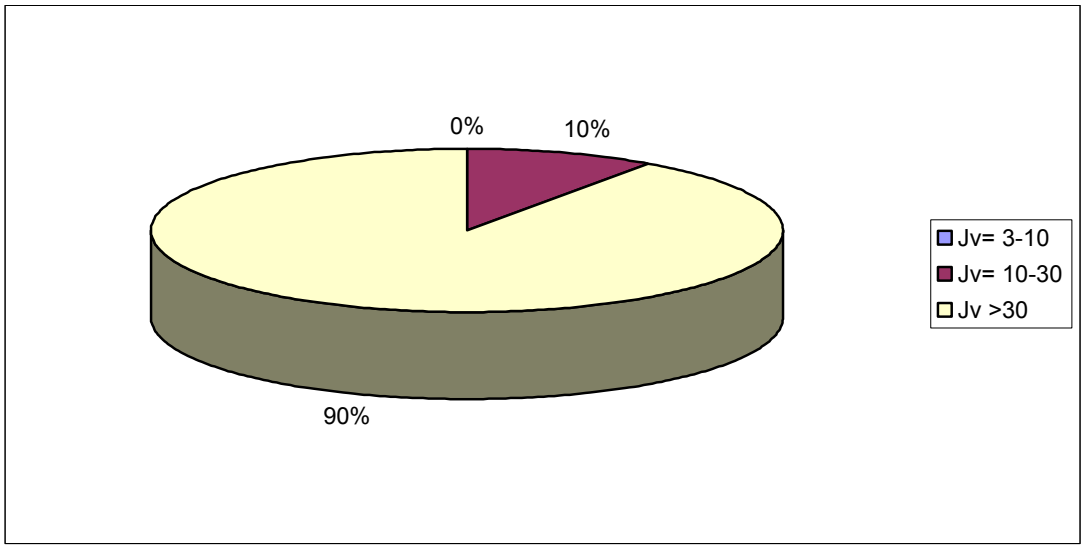

Figure 3.9. Percent detachment in each block size class.

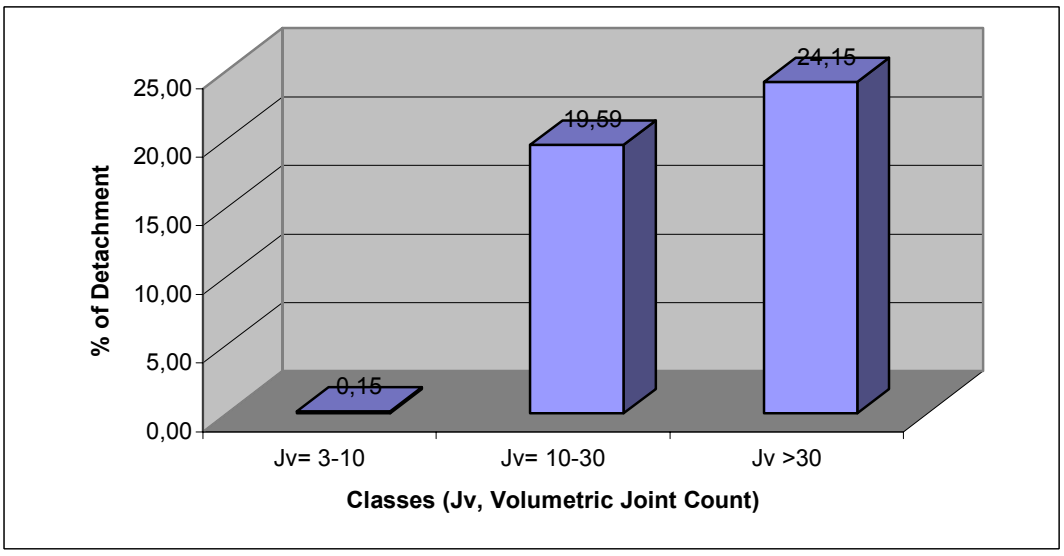

Figure 3.10. Detachment density in each block size class.

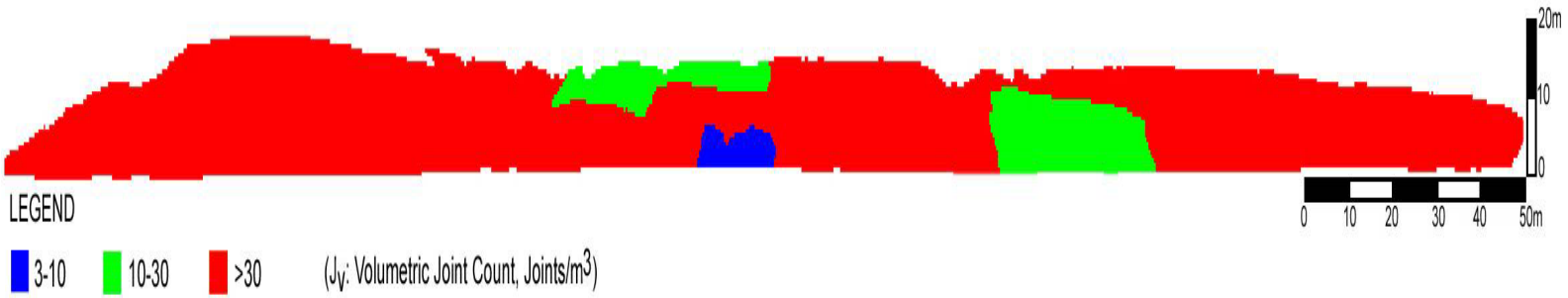

Figure 3.11. Zonation map of the cut slope for the block size layer.

3.1.5. Daylight Layer

During the field studies, it is observed that some of the instabilities were resulted from daylighting along the bedding plane, the freedom of a rock block to slide along a weakness plane. Because of shearing and folding, dip direction and dip amount of the bedding plane continuously change over the study area which makes it to display daylighting in some very local areas. The daylight layer was produced through field observations and measurements only along bedding plane. The daylighting of the joints is not considered since the persistence of the joint sets is very low. The daylight layer consists of two classes, zone with daylight and zone without daylight (Figures 3.12-3.14). In zones with daylight, 10% of the total detachment occur. The remaining 90% of detachments occur in zones without daylight (Figure 3.12). Conversely, detachment takes place in 53% of the class with daylight and in 22% of class without daylight (Figure 3.13)

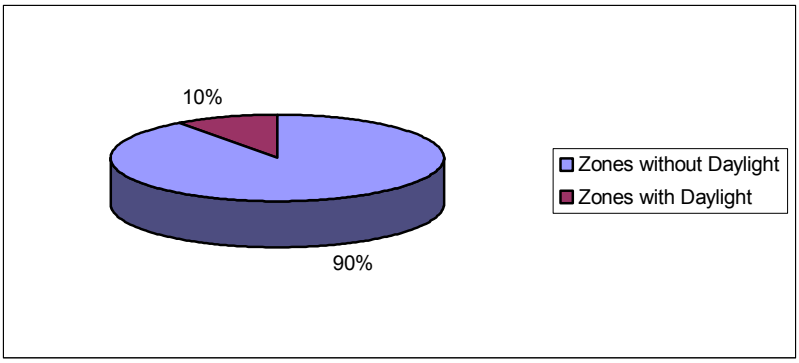

Figure 3.12. Percent detachment in daylight class.

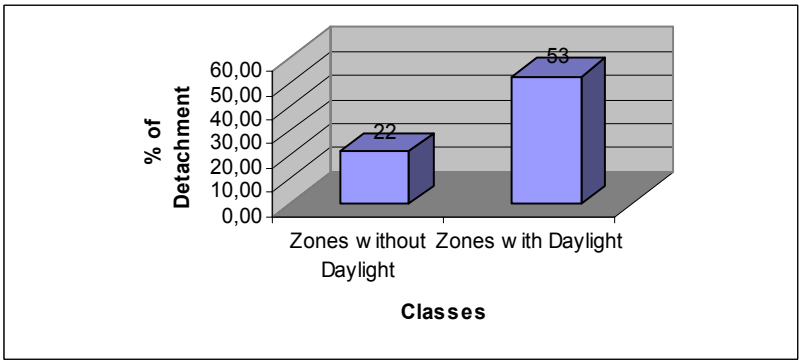

Figure 3.13. Detachment density in each daylight class.

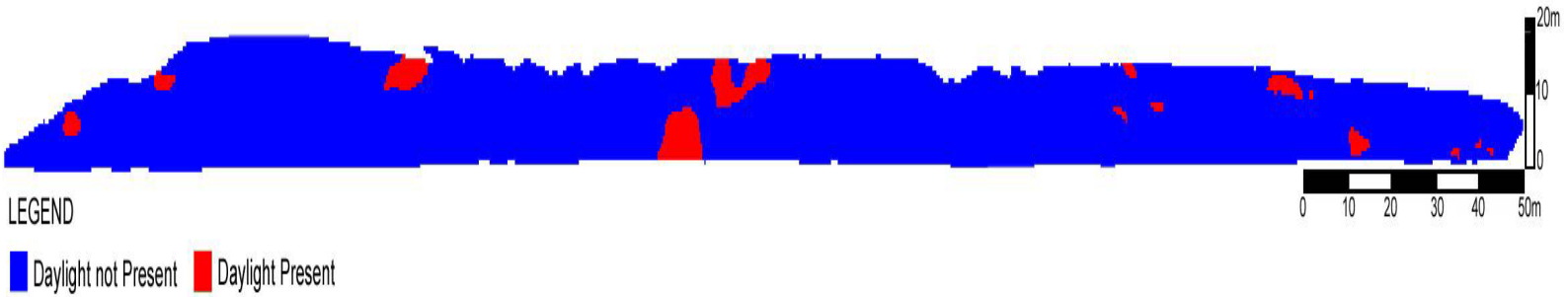

Figure 3.14. Zonation map of the cut slope for the daylight layer.

3.1.6. Shear Zone Layer

During the field investigation and scan-line survey, the observed shear zones (Figure 3.15) which may affect the stability were mapped to produce the shear zone layer. The orientation of shear zones is not important. However, the presence of shear zones results in crushed and loosened rock mass in the vicinity where it is present.

An example of the shear zones observed in the study area is given in Figure 3.15. This layer was divided into 2 classes that are zones with shear zones and zones without shear zones (Figures 3.16-3.18). 3% of the detachments takes place in the zones with shearing and the remaining 97% occurs in the zones without shearing (Figure 3.16). For the density of the detachments in each class, 34% of zones with shearing has detachments and in 23% of zones without shearing detachments occurs (Figure 3.17).

Figure 3.15. Some of the shear zones observed in the study area.

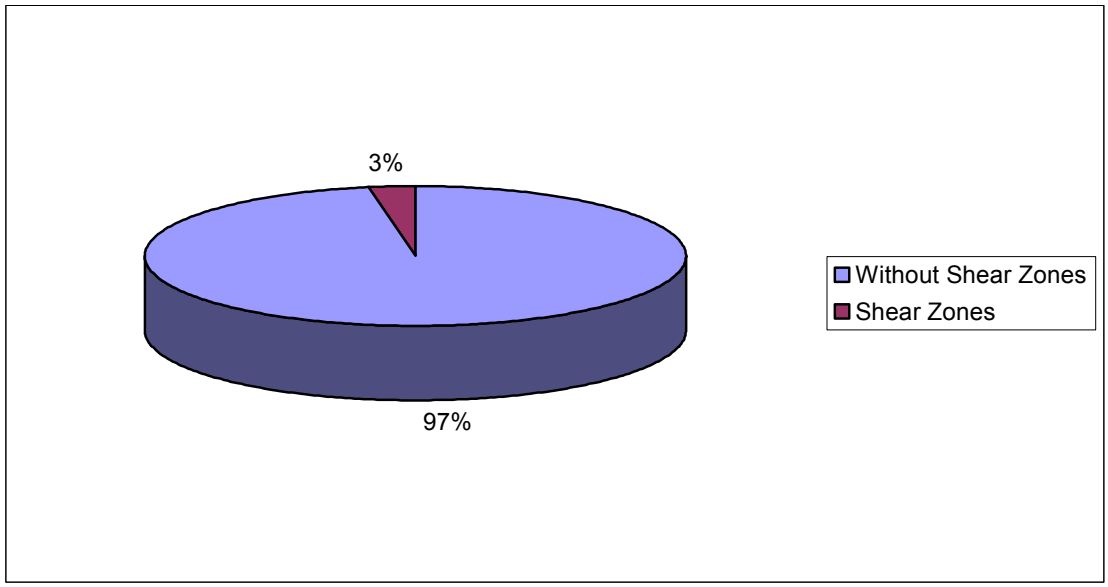

Figure 3.16. Percent detachment in the shear zones class.

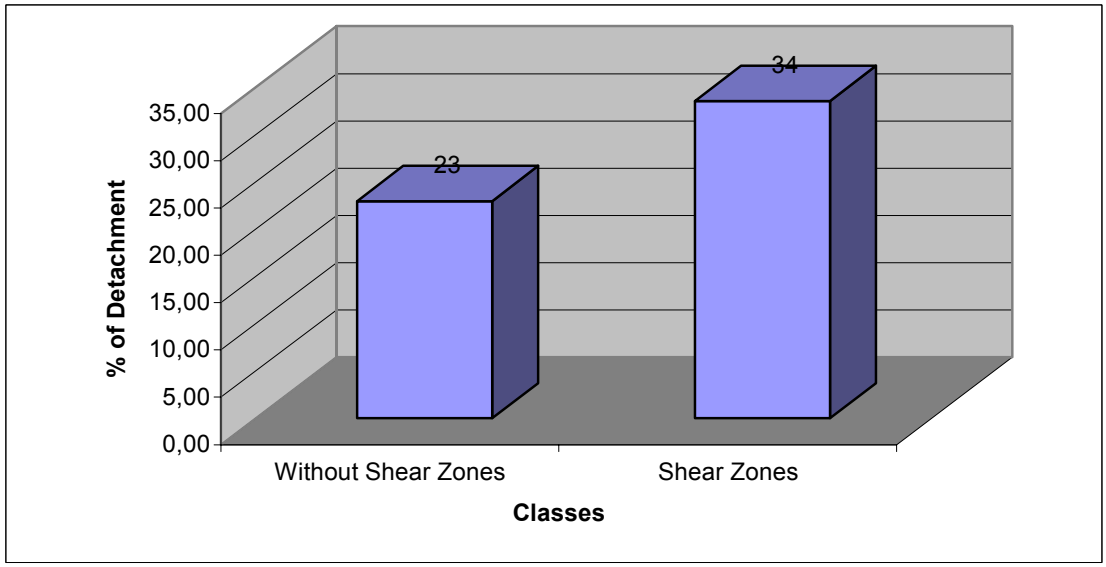

Figure 3.17. Detachment density in the shear zones class.

Figure 3.18. Zonation map of the cut slope for the shear zone layer.

3.2. Detachment susceptibility analyses

As already mentioned in the previous sections, two methodologies namely statistical index (W_i) (Van Westen, 1997) and weighting factor (Wf) (Çevik, 2002) were used to produce final detachment susceptibility map. The statistical index method is based on map crossing of a landslide map (or detachment map in this study) with a certain parameter map. The map crossing results in a cross-table, which can be used to calculate the density of landslides (detachments) per parameter class. A standardization of these density values can be obtained by relating them to the overall density in the entire area (Van Westen, 1997). As a result, W_i values for each class of each parameter map was obtained quantitatively by employing the following formula:

$$\ln Wi = \ln\left(\frac{Densclas}{Densmap}\right) = \ln\left(\frac{\frac{Npix(Si)}{Npix(Ni)}}{\frac{\sum Npix(Si)}{\sum Npix(Ni)}}\right)$$

where,

Wi : The weight given to a certain parameter class

Densclas : The landslide (detachment) density within the parameter class.

Densmap : The landslide (detachment) density within the entire map.

Npix(Si) : Number of pixels, which contain landslides (detachments), in a certain parameter class.

Npix(Ni) : Total number of pixels in a certain parameter class.

Obtained W_i values were assigned to each parameter class (Table 3.4), then all five layers were summed to obtain final susceptibility map. On the basis of the relationship between pixel value (W_i values) and cumulative pixel count (Figure 3.19), the final susceptibility map was divided into 4 zones (Figure 3.20).

Table 3.4. Statistical index (W_i) values for each parameter class.

Data Layers	Classes	W_i
Point Load Strength	A. 4-10 MPa	0,18
	B. 2-4 MPa	0,81
	C. 1-2 MPa	2,14
	D. <1 MPa	3,09
Weathering	A. Slightly Weathered	0,12
	B. Moderately Weathered	1,06
	C. Highly Weathered	3,16
Block size	A. J_v=3-10	0
	B. J_v=10-30	0,84
	C. J_v>30	1,04
Daylight	A. Present	2,27
	b. Not present	0,94
Shear Zone	A. Present	1,45
	B. Not present	0,99

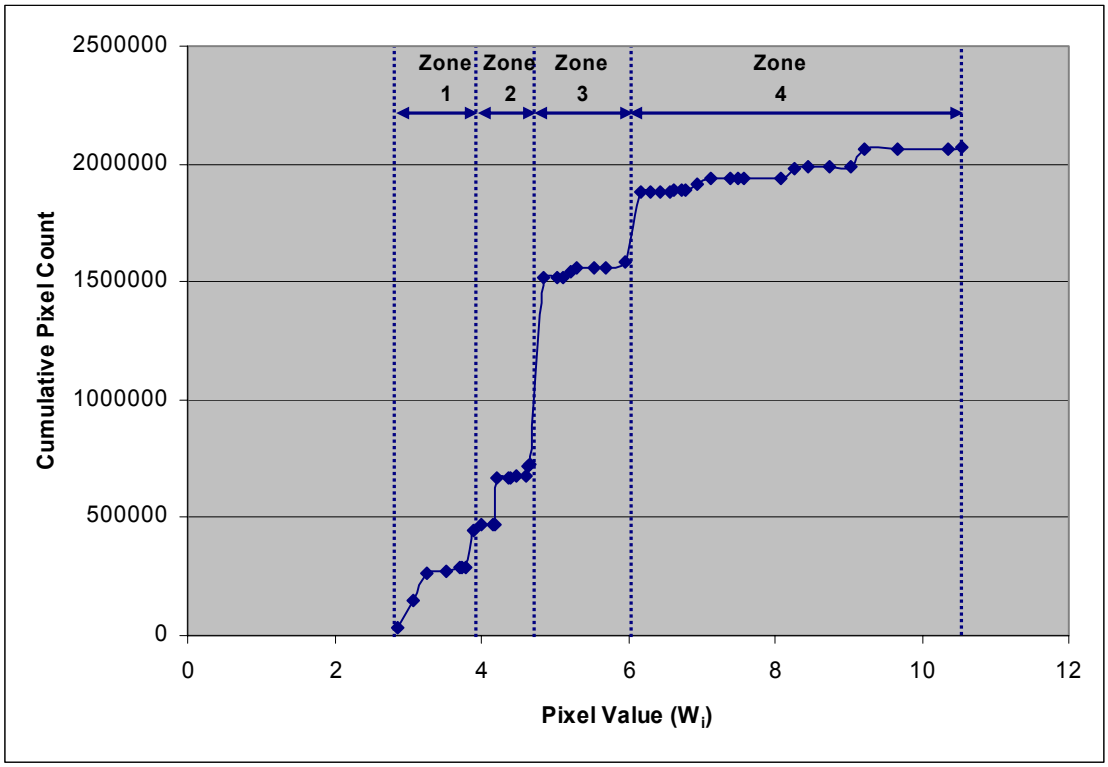

Figure 3.19. Cumulative pixel count for the range of pixel W_i values.

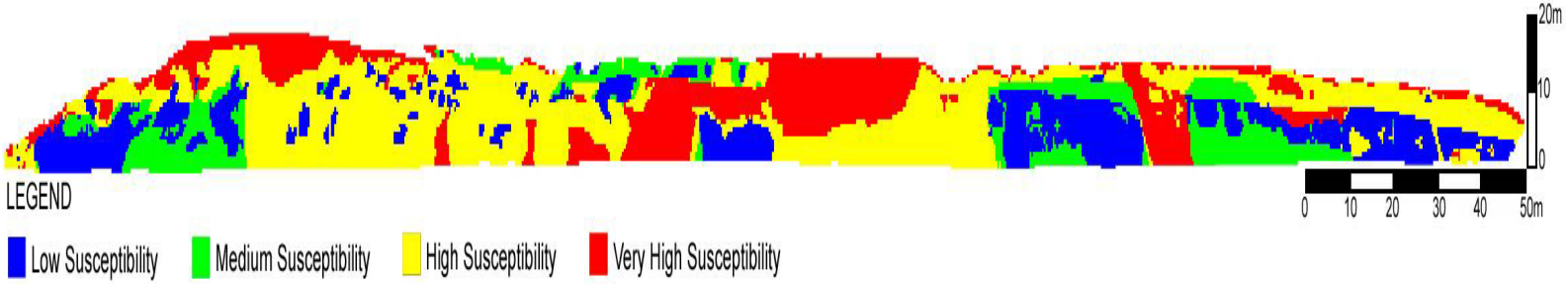

Figure 3.20. Detachment suscptibility map obtained by statistical index (W_i) method.

In the statistical index method, it is assumed that each parameter map (point load strength, weathering, block size, daylight and shear zones) has an equal effect on instability which may not be the case in reality. Therefore, introducing a weighting factor for each parameter map would be another perspective. In this thesis, this is done by solely statistical analysis rather than applying engineering judgment to partly eliminate the effect of subjectivity. Previously mentioned weighting factor method (Wf) is the basis for assigning weightings to each parameter map. To do this, first Wi values of each pixel were determined by statistical index method. Then, all pixel values within the detachment zones belonging to each layer were summed up. By using the maximum and minimum of all layers, the results were stretched (Çevik, 2002). The following formula is the basis for the determination of the weighting factors of each parameter map:

$$WF = \frac{\left(TW_i\_value\right) - \left(Min\_TW_i\_value\right)}{\left(Max\_TW_i\_value\right) - \left(Min\_TW_i\_value\right)} x100$$

Where,

WF: Weighting factor for each parameter map

TW_i_value:Total weighting index value of pixels within detachment zones for each parameter map

Min_TW_i_value: Minimum total weighting index value within selected parameter maps

Max_TW_i_value: Maximum total weighting index value within selected parameter maps.

By applying this formula, the weighting factor values ranging from 1 to 100 were determined (Table 3.5). For the analysis, each weighting value of each parameter class, determined by statistical index (W_i) method, is multiplied by

weighting factors of the related parameter map, and finally all parameter maps were summed up to yield the final susceptibility map. In the light of cumulative pixel count versus pixel value ($Wf*W_i$) (Figure 3.21), the final susceptibility map obtained by weighting factor method was then divided into 4 zones (Figure 3.22).

Table 3.5. Weighting factor (Wf) values for each parameter class.

Data Layers	Classes	W_i	Wf for each layer
Point Load Strength	A. 4-10 MPa B. 2-4 MPa C. 1-2 MPa D. <1 MPa	0,18 0,81 2,14 3,09	100
Weathering	A. Slightly Weathered B. Moderately Weathered C. Highly Weathered	0,12 1,06 3,16	56,65
Block size	A. J_v=3-10 B. J_v=10-30 C. J_v>30	0 0,84 1,04	1
Daylight	A. Present b. Not present	2,27 0,94	30,52
Shear Zone	A. Present	1,45	12,74
	B. Not present	0,99	

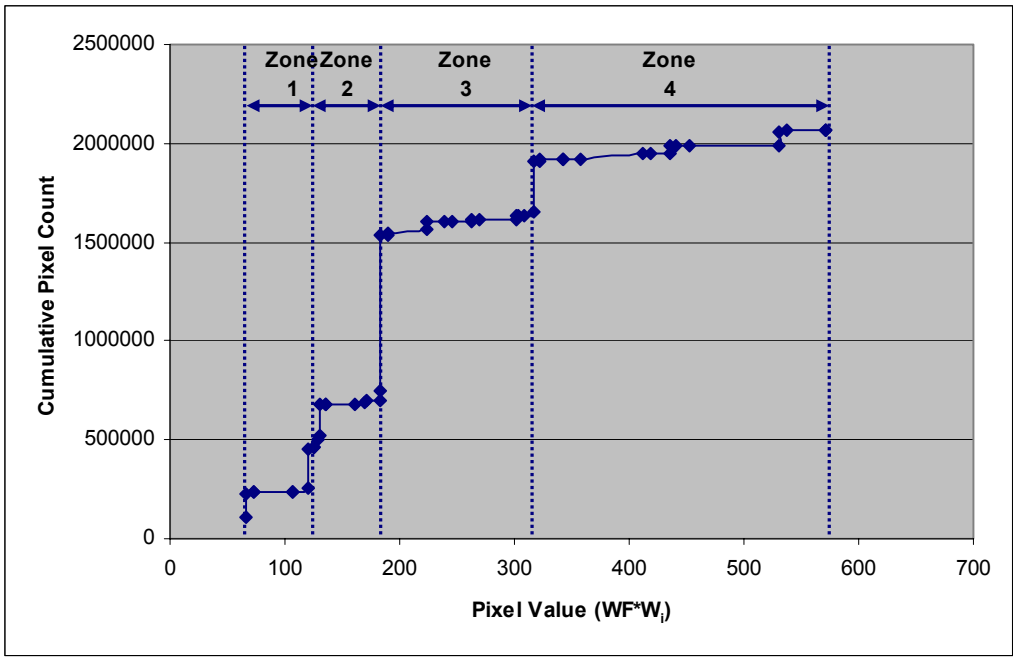

Figure 3.21. Cumulative pixel count for the range of pixel values ($Wf*W_i$).

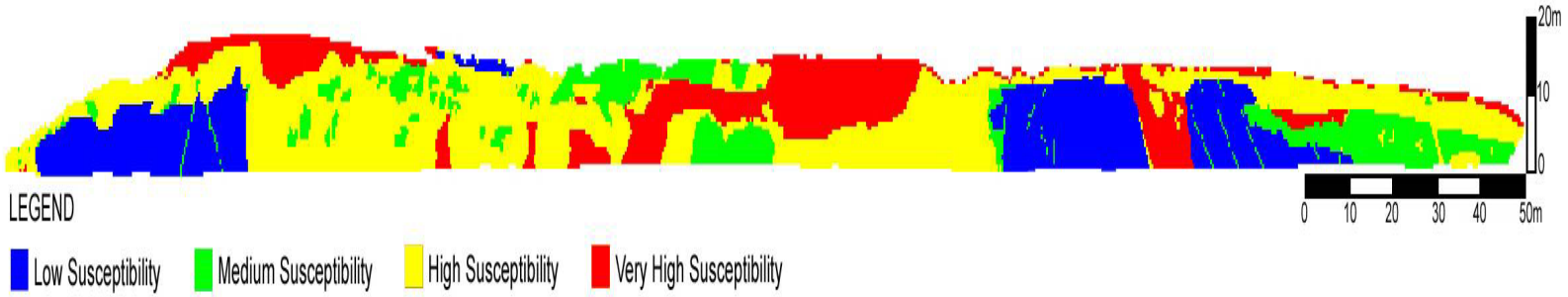

Figure 3.22. Detachment susceptibility map obtained by weighting factor (Wf) method.

Finally, further analyses were carried out in order to determine the degree of conformity between the susceptibility maps obtained by the statistical index (W_i) and weighting factor (Wf) methods. As a result, there is 75% match in the zones calculated by the two methods (Figure 3.23). Also matching and unmatching zones are shown in Figure 3.24.

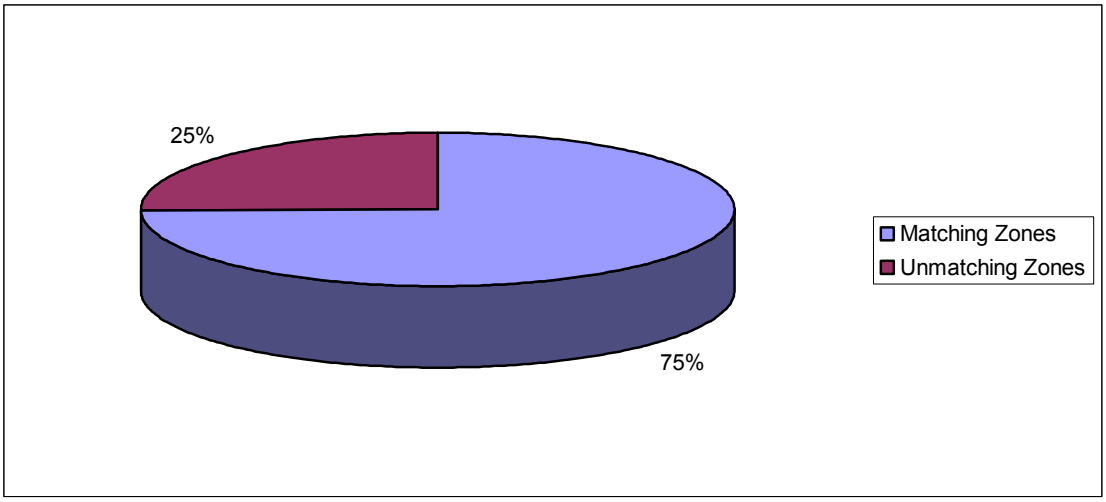

Figure 3.23. Percentage of match (overlap) in the two susceptibility maps.

Figure 3.24. Map showing matching and unmatching zones obtained by both methods.

3.3. Sensitivity analysis

The analysis in this section was carried out so as to test the role of each parameter layer on the final susceptibility zonation map. To do this, one of the parameter maps was taken out of the analysis each time and the analysis was carried out with the remaining four parameter maps. This procedure was performed for both statistical index (W_i) and weighting factor (Wf) methods. However, during the analysis using weighting factor methodology weighting factors for the analysis without point load strength layer and the block size layer needed to be rearranged because of the change in two parameters that are maximum and minimum total weighting index value within selected parameter maps, in the calculation of the weighting factors. For these two cases, the new values are given in Table 3.6

Table 3.6. Re-calculated weighting factor values for each parameter map

Without Point Load Strength layer	
Layers	Weighting Factor for each layer
Weathering layer	100,00
Block Size layer	1,00
Daylight layer	53,87
Shear Zone layer	22,49
Without Block Size layer	
Layers	Weighting Factor for each layer
Point Load Strength layer	100,00
Weathering layer	50,33
Daylight layer	20,38
Shear Zone layer	1,00

The resulting final susceptibility maps are illustrated in Figures 3.24 to 3.35.

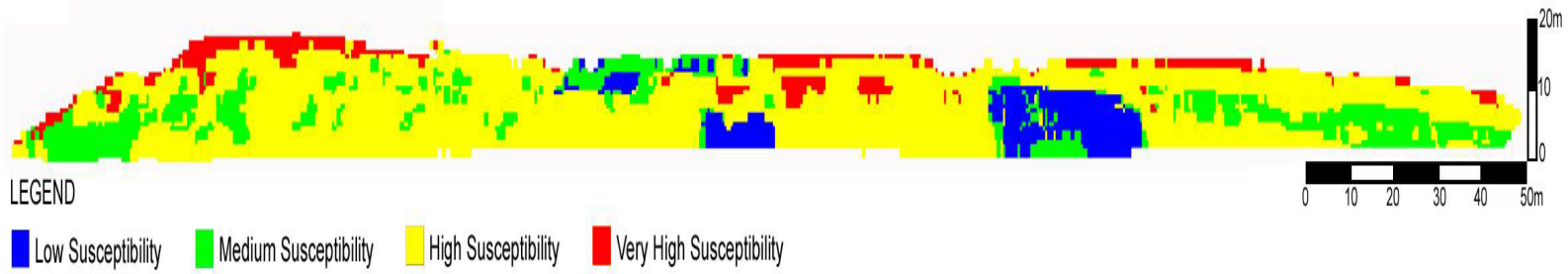

Figure 3.25. Detachment susceptibility map obtained from W_i method by excluding point load strength layer.

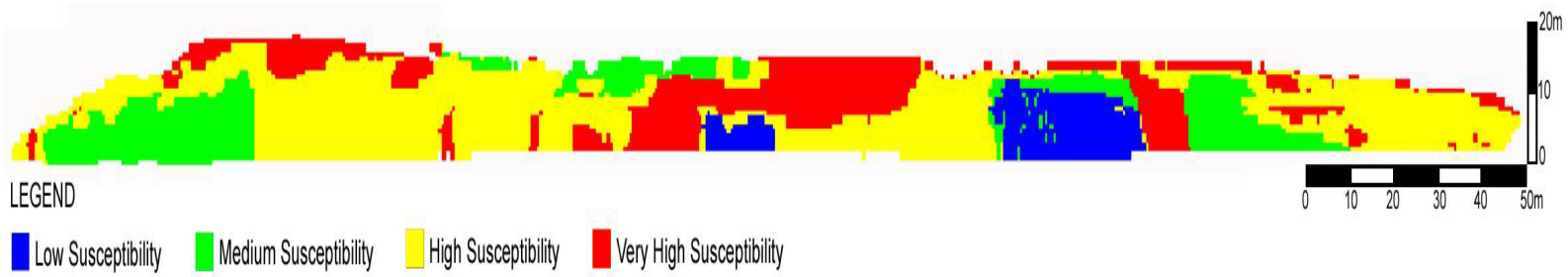

Figure 3.26. Detachment susceptibility map obtained from W_i method by excluding weathering layer.

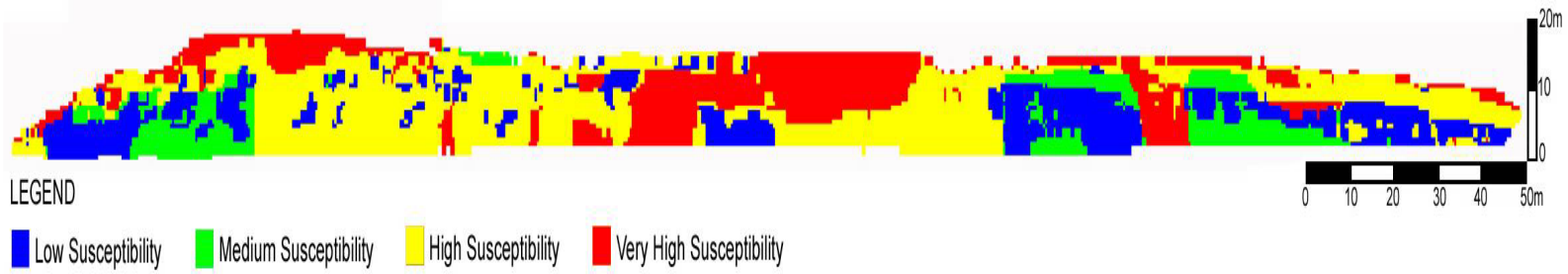

Figure 3.27. Detachment susceptibility map obtained from W_i method by excluding block size layer.

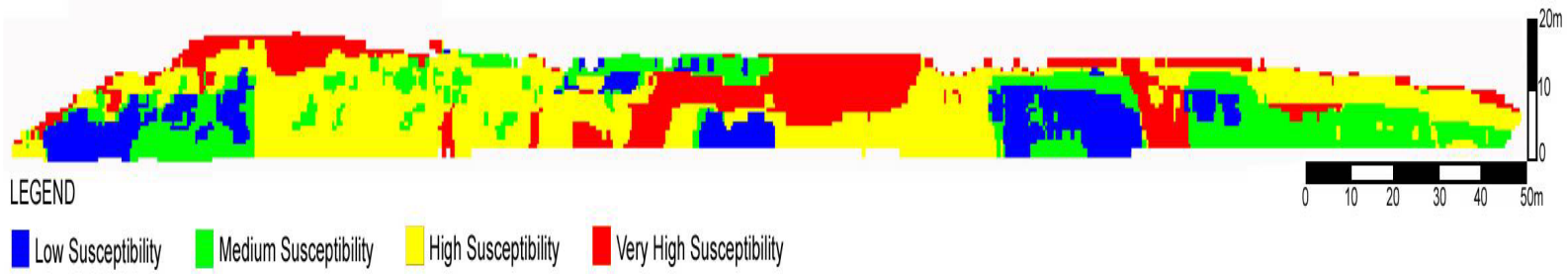

Figure 3.28. Detachment susceptibility map obtained from W_i method by excluding daylight layer.

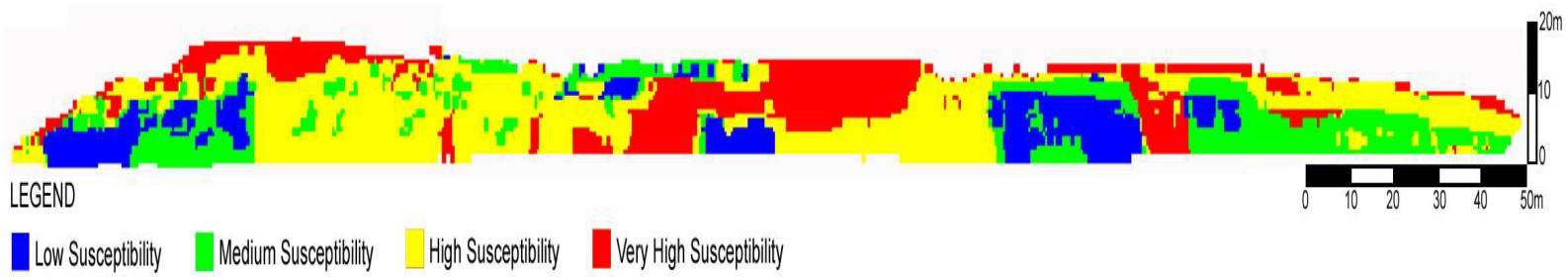

Figure 3.29. Detachment susceptibility map obtained from W_i method by excluding shear zone layer.

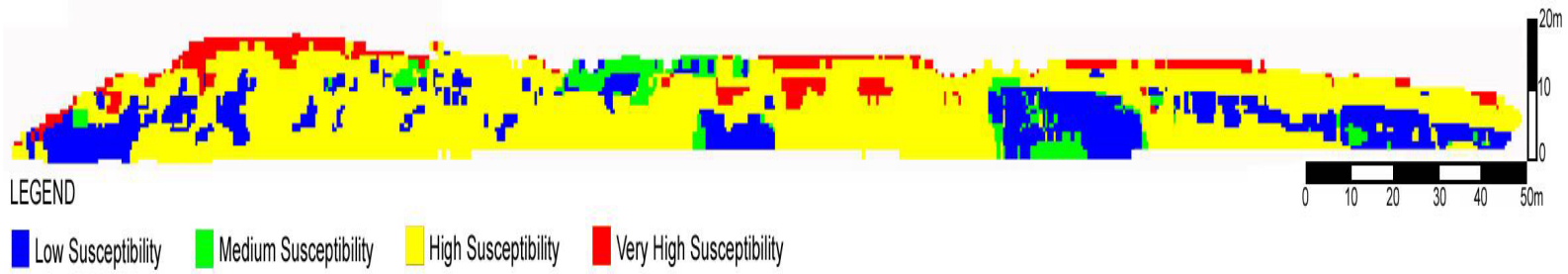

Figure 3.30. Detachment susceptibility map obtained from Wf method by excluding point load strength layer.

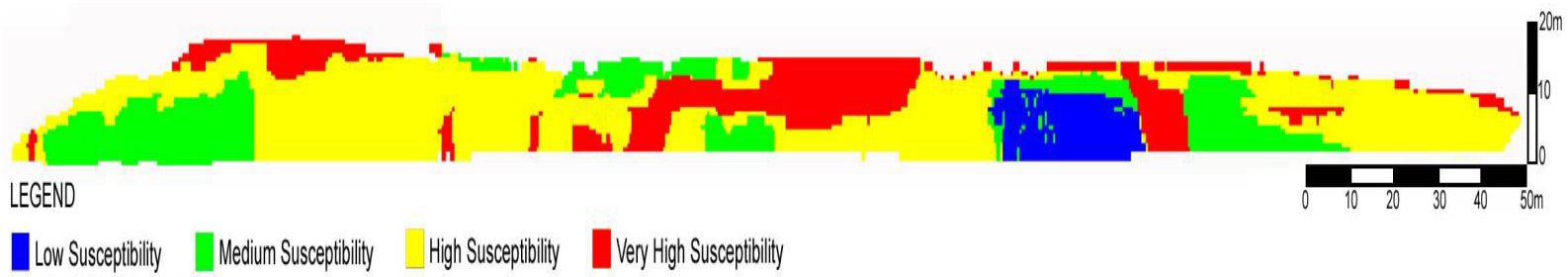

Figure 3.31. Detachment susceptibility map obtained from Wf method by excluding weathering layer.

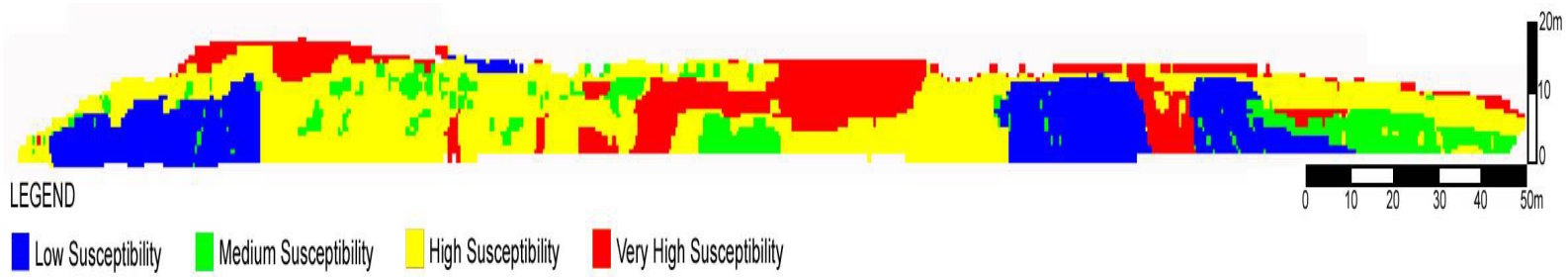

Figure 3.32. Detachment susceptibility map obtained from Wf method by excluding block size layer.

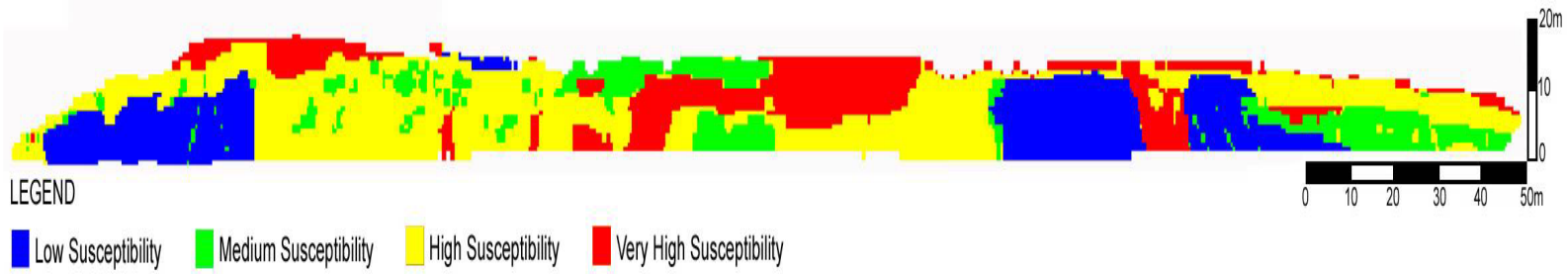

Figure 3.33. Detachment susceptibility map obtained from Wf method by excluding daylight layer.

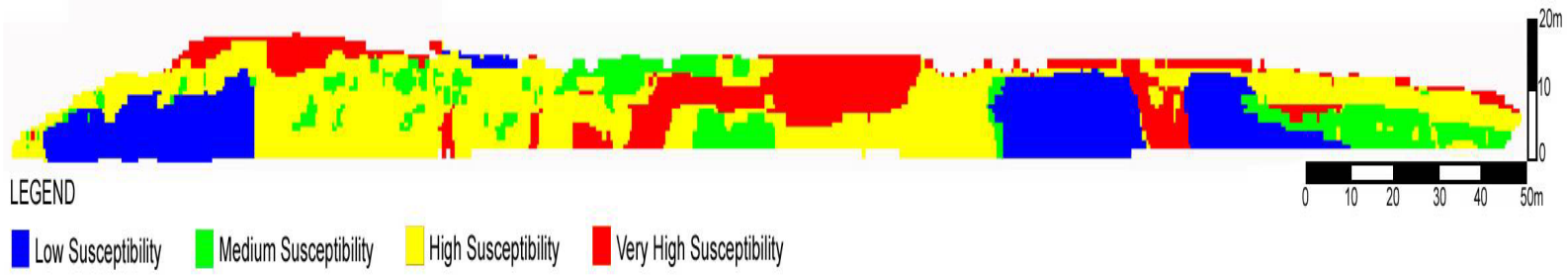

Figure 3.34. Detachment susceptibility map obtained from Wf method by excluding shear zone layer.

CHAPTER IV

SLOPE STABILITY ANALYSES

Slope stability analyses involve accurate determination of shear strength parameters and also geometry of the rock mass behind the slope face. Because of highly jointed and sheared nature of the limestone in the study area, some difficulties were faced during the determination of the shear strength parameters that will be discussed in the following sections. For the determination of the slope geometry, theodolite was used.

During the analyses, considering the low persistence of the joints and small block size of the limestone, possibility of discontinuity controlled failure was eliminated. So only the stability against mass failure was investigated throughout this chapter.

The strength of the jointed rock mass in the study area was estimated through the use of Hoek and Brown failure criterion-2002 (Hoek et al., 2002). So as to carry out the analyses, the study area was divided into six sections based on the rock mass characteristics (such as weathering and block size) and the variations in the intact rock strength (Figure 4.1). In these six sections, limit equilibrium analyses were carried out in order to determine unstable sections.

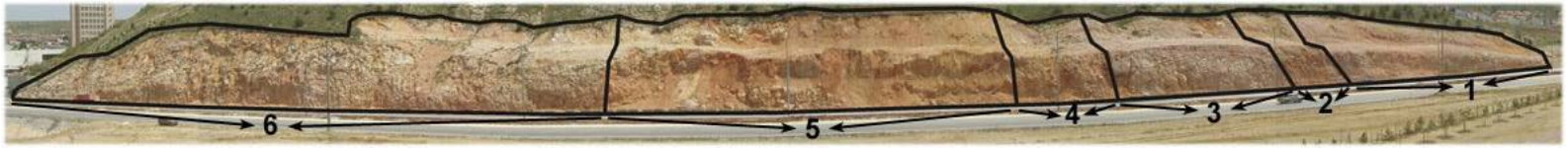

Figure 4.1. Division of the study are into six sections for the limit equilibrium analysis.

4.1. Determination of the strength of the rock mass

In order to use the Hoek-Brown criterion for the determination of the strength and deformability of jointed rock masses, three 'properties' of the rock mass have to be estimated. These are the uniaxial compressive strength (UCS) of the intact rock pieces, the value of the Hoek-Brown constant m_i for these intact rock pieces, and the value of the Geological Strength Index (GSI) for the rock mass (Hoek, 2000). In addition to these properties, the disturbance of the in-situ rock mass was also considered in the determination of the strength of the rock mass. By employing these three properties and including the effect of disturbance, the values of internal friction angle (Φ), cohesion (c), the uniaxial compressive strength of rock mass (σ_{cm}) and the deformation modulus (E) of the rock mass can be calculated. Since Hoek and Brown failure criterion displays non-linear or curved failure envelope, internal friction angle (Φ) and cohesion (c) values are defined instantaneous which varies according to the effective normal stress level along the failure surface. During the limit equilibrium analysis using Slide software, grid search method was used. With this method, the stabilities of exactly 28611 possible failure surfaces were analyzed through Hoek and Brown failure criterion and the most critical failure surface (surface with the minimum safety factor) was determined for each of the six sections. For the determination of the failure envelopes, Roclab software was utilized. The software requires the determination of the three properties (UCS, m_i and GSI) and the disturbance factor. The average uniaxial compressive strength (UCS) values of the intact rock for each of the six section were determined by the correlation with the point load strength values (Table 4.1).

Table 4.1. UCS values estimated from the point load strength index test for each section.

Section	**1**	**2**	**3**	**4**	**5**	**6**
UCS (MPa)	48,8	20,8	50,5	37	12	41,4

Due to the difficulties in obtaining suitable samples for triaxial testing, intact rock parameter m_i was estimated as 8 (micritic limestone) from the table given by Hoek (2000). On the other hand, 0.7 is preferred for the disturbance factor which corresponds to the mechanical excavations in slopes.

Before the discussion of the determination of the GSI values, a brief review and some explanations about the use of this methodology in this thesis have to be made. Hoek and Brown (1997) proposed a new classification called Geological Strength Index (GSI), instead of RMR, due to the limitations in the RMR System for very poor quality rock masses. The GSI System is based upon the visual impression of the rock mass structure (Sönmez and Ulusay, 2002). For this reason, some modifications to GSI system was made (Sönmez and Ulusay, 1999) in order to provide a more quantitative basis for the calculation of the GSI values. Also, the authors of GSI made some modifications on their system through the time (Hoek, 1998; Hoek et al., 1998, Hoek and Marinos, 2000; Hoek and Marinos, 2001). In this study, GSI values were calculated according to the quantitative method (Sönmez and Ulusay, 2002) (Figure 4.2), and then the obtained values are compared with the descriptive categories in chart proposed by Hoek and Brown (1997). During the calculations, the ranges of GSI values were determined rather than a single value which is also the procedure proposed by the originators of this system. This procedure was carried for each of the six sections (Table 4.2).

Since it is not possible to show all instantaneous internal friction angle (Φ_i) and cohesion (c_i) values of these slip surfaces only the values of the most critical slip surfaces for each section were shown in the analysis part. Therefore, rather than giving specific shear strength parameter values (Φ_i and c_i), the failure envelopes of the rock mass for each of the six section were tabulated in this section of the thesis (Figures 4.3 to 4.8).

Table 4.2. GSI values and related parameters in each section of the cut slope according to the methodology proposed by Sönmez and Ulusay (2002).

Section	**1**	**2**	**3**	**4**	**5**	**6**
Roughness Rating (R_r)	3	3	5	3	3	5
Weathering Rating (R_w)	5	3	5	3-5	1-3	3
Infilling Rating (R_f)	2-6	2-6	2-6	2	0-2	2-6
Volumetric Joint Count, J_v (joint/m^3)	30-70	70	30	30	40	60
Surface Condition Rating, SCR ($SCR=R_r+R_w+R_f$)	10-14	8-12	12-16	8-10	4-8	10-14
Structure Rating, SR ($SR=-17,5\ln(J_v)+79,8$)	5-20	5	20	20	15	8
GSI (Range of values)	31-44	27-35	40-49	31-36	19-29	32-41
GSI (Average value)	38	31	45	33	24	37

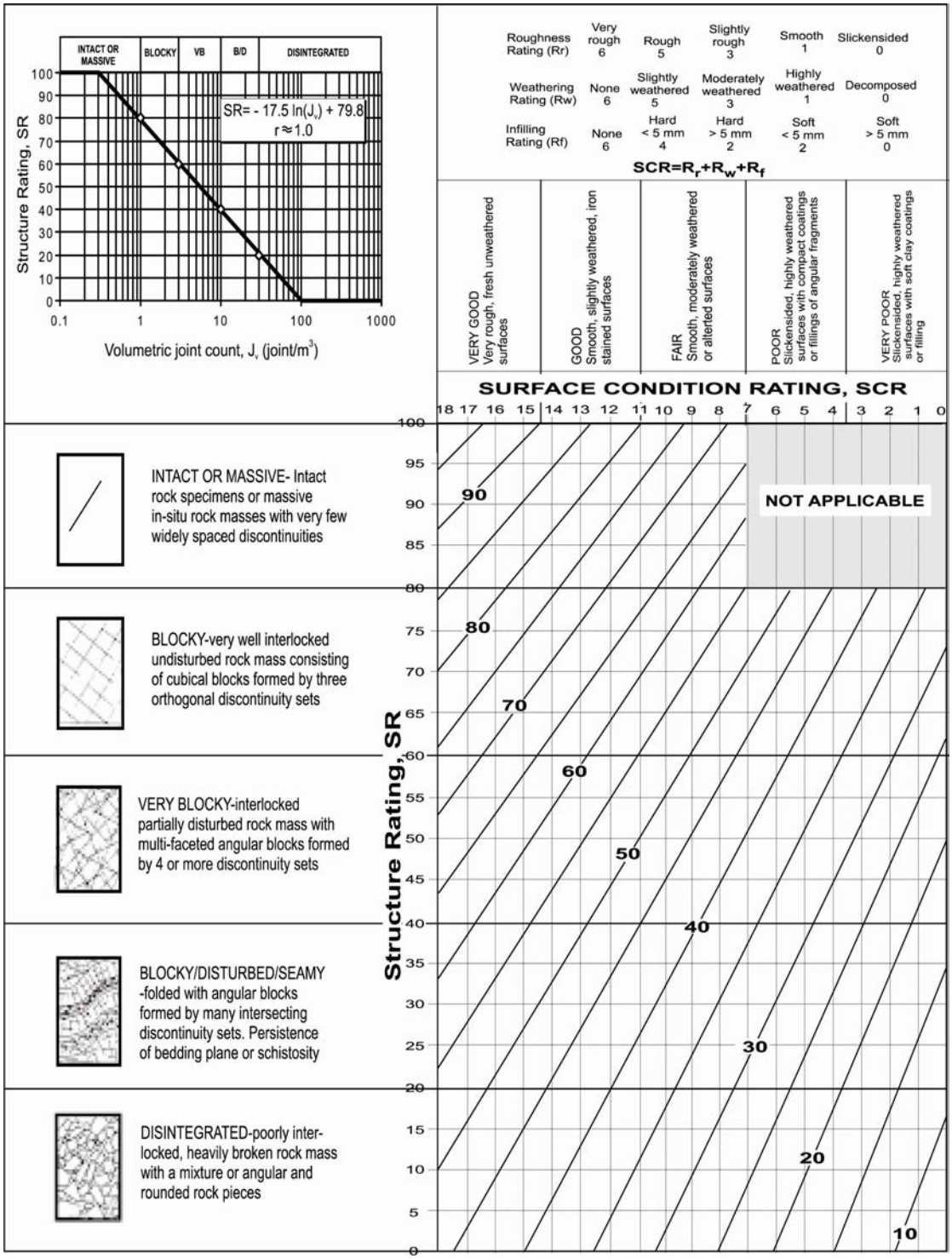

Figure 4.2. Quantitative GSI system proposed by Sönmez and Ulusay (2002).

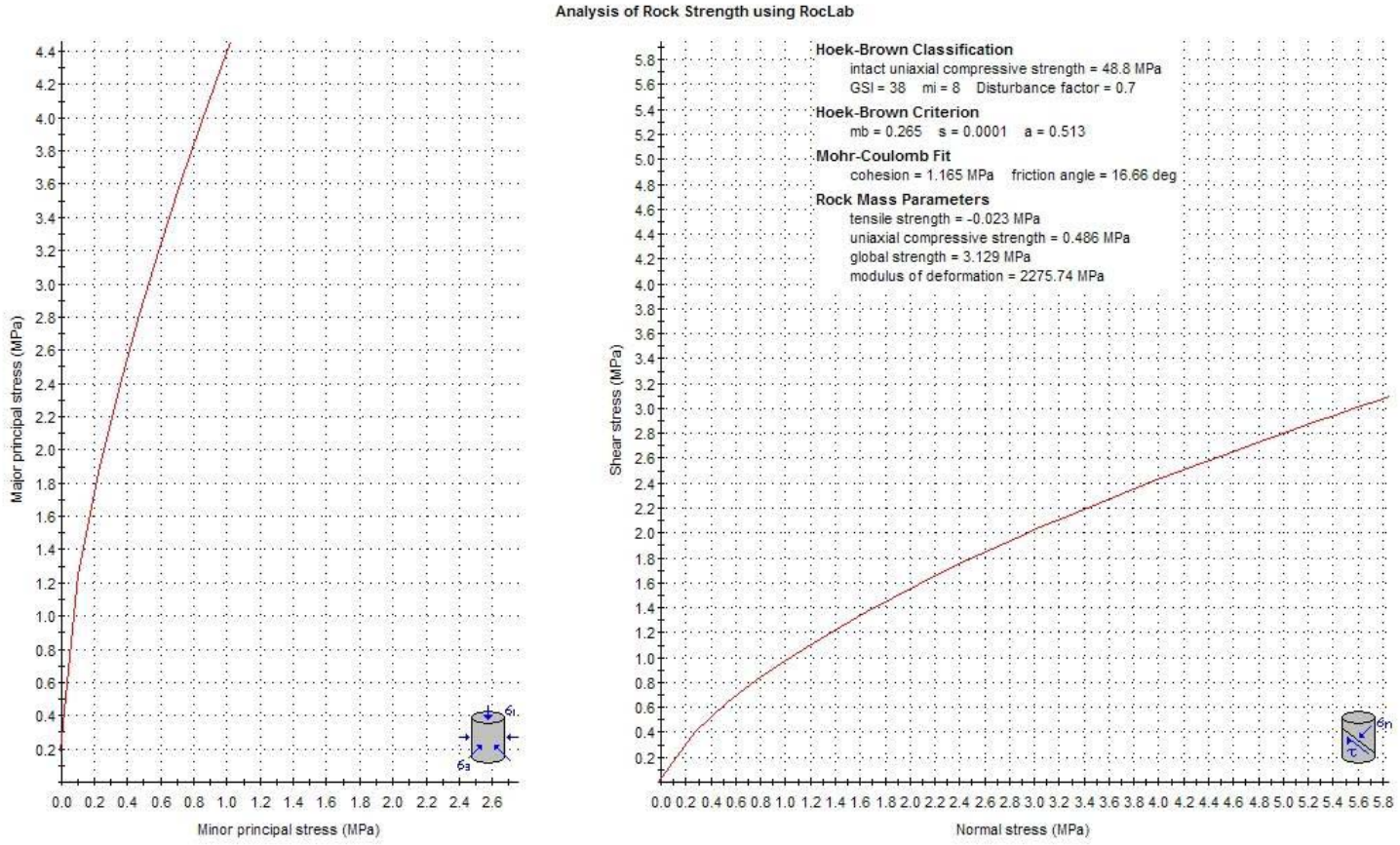

Figure 4.3. Determination of various rock mass parameters including cohesion (c) and internal friction angle (Φ) through RockLab software for section 1.

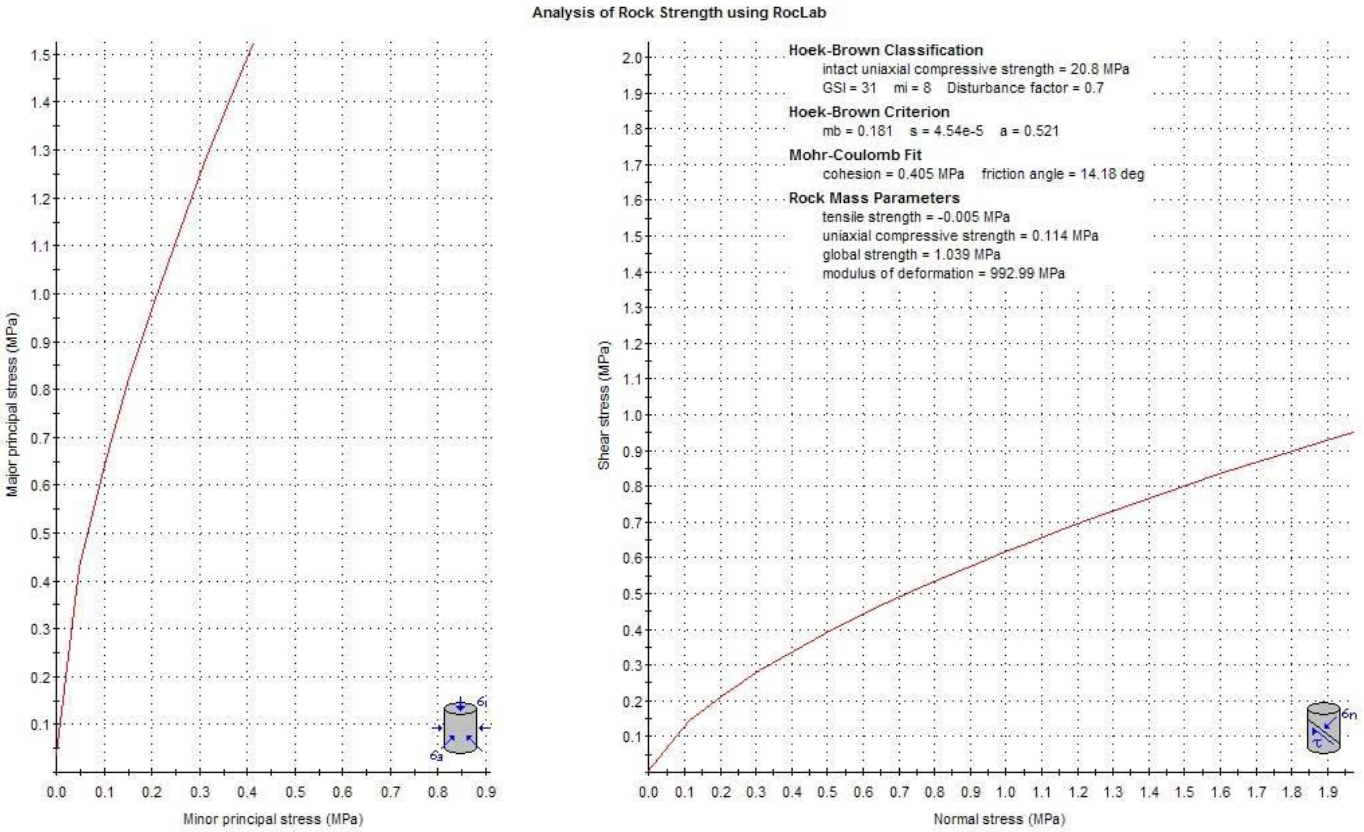

Figure 4.4. Determination of various rock mass parameters including cohesion (c) and internal friction angle (Φ) through RockLab software for section 2.

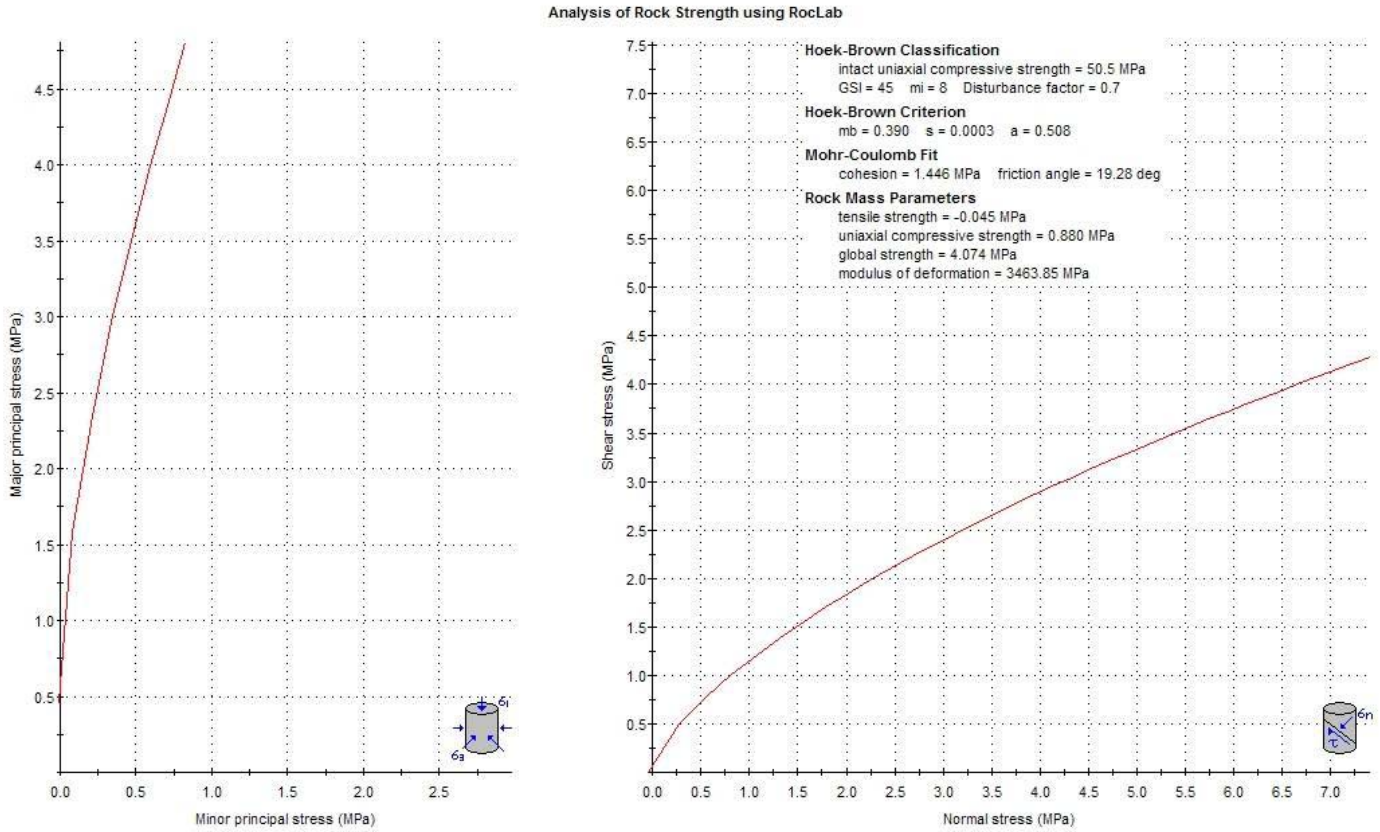

Figure 4.5. Determination of various rock mass parameters including cohesion (c) and internal friction angle (Φ) through RockLab software for section 3.

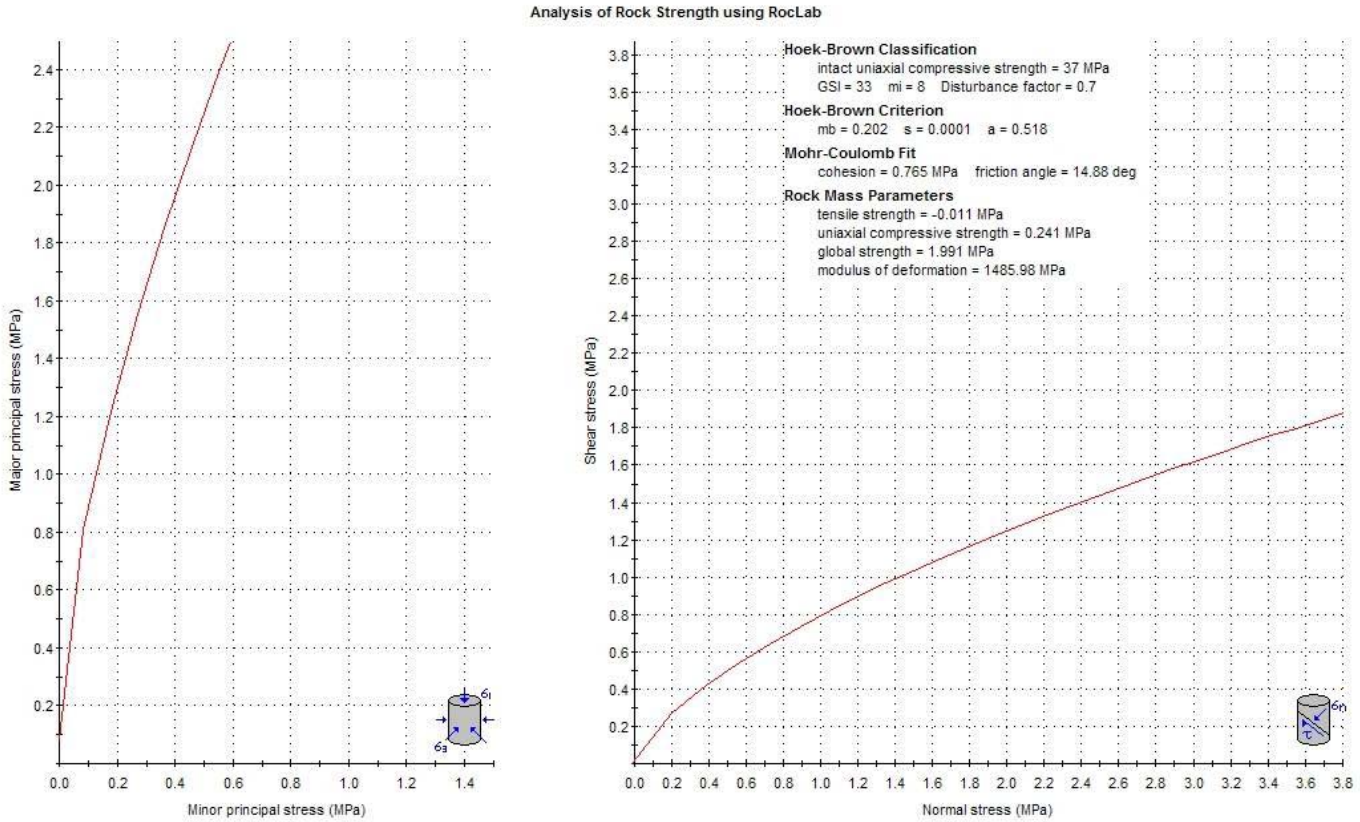

Figure 4.6. Determination of various rock mass parameters including cohesion (c) and internal friction angle (Φ) through RockLab software for section 4.

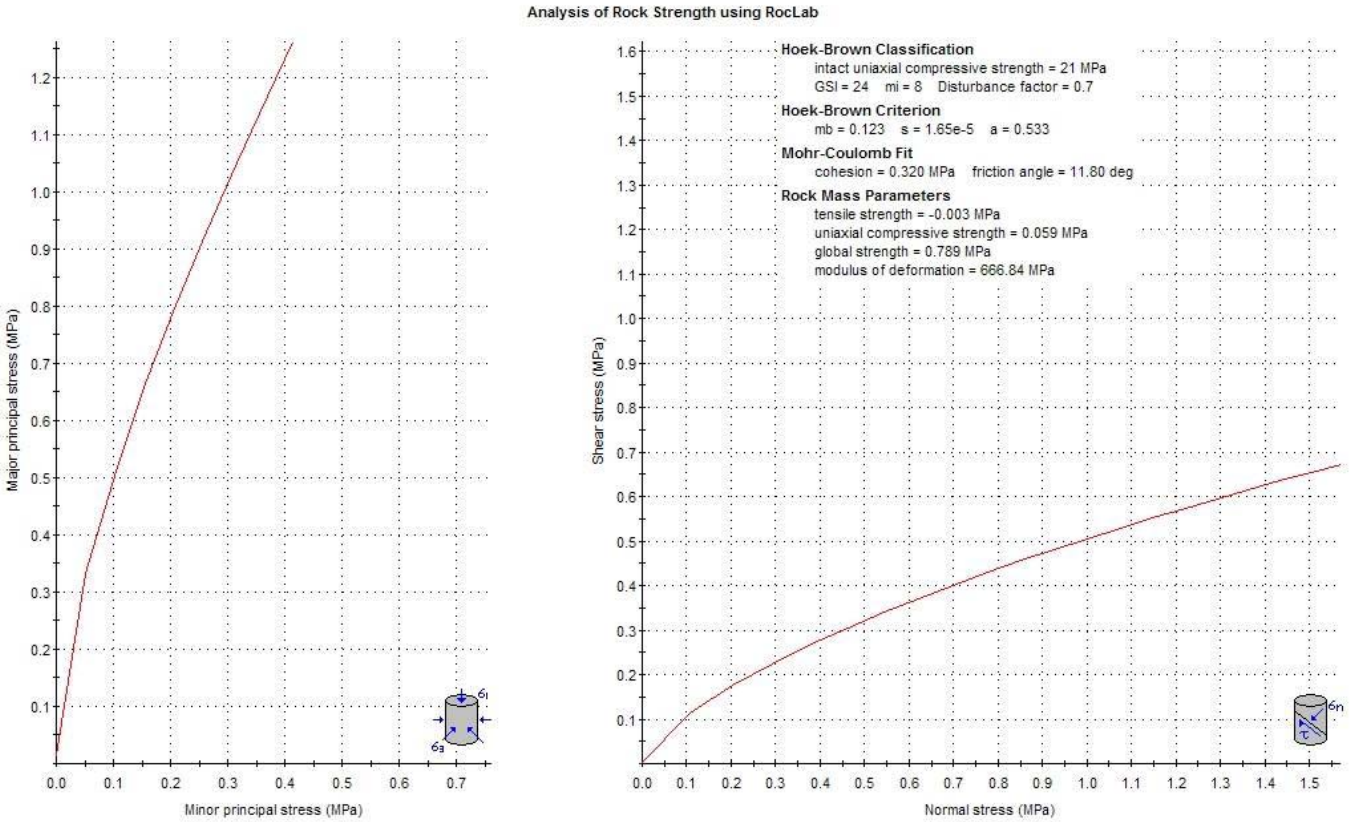

Figure 4.7. Determination of various rock mass parameters including cohesion (c) and internal friction angle (Φ) through RockLab software for section 5.

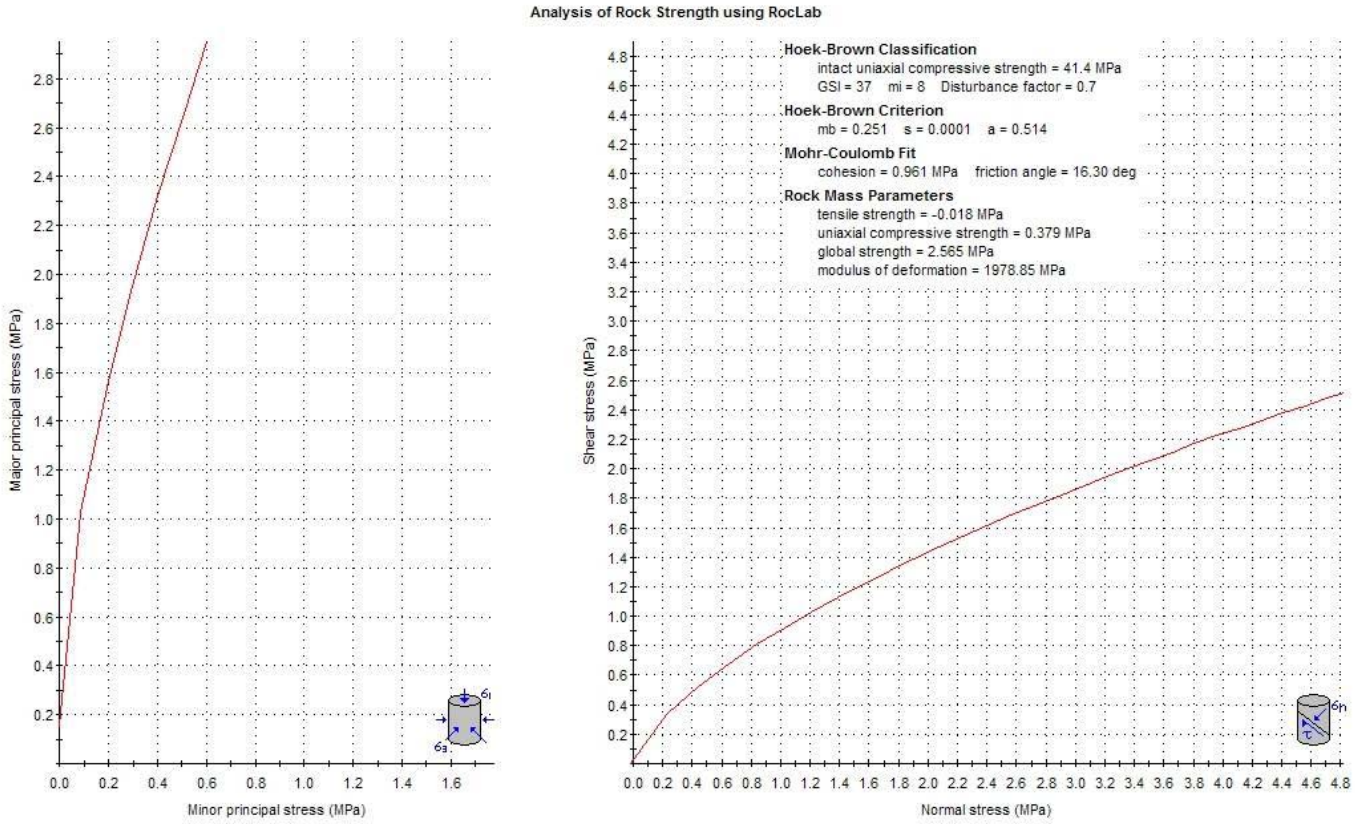

Figure 4.8. Determination of various rock mass parameters including cohesion (c) and internal friction angle (Φ) through RockLab software for section 6.

4.2. Limit equilibrium analysis

As a general rule, when designing slopes in rock, the initial approach should always be to search for potential failures controlled by adverse structural conditions. These may take the form of planar failures on outward dipping features, wedge failures on intersecting features, toppling failures on inward dipping failures or complex failure modes involving all of these processes. Only when the potential for structurally controlled failures has been eliminated should consideration be given to treating the rock mass as an isotropic material as required by the Hoek-Brown failure criterion (Hoek, 2000).

Since the possibility of structurally controlled failures was eliminated due to the previously discussed reasons, only the stability of the slope against mass failure is investigated in this section. Since the rock mass is deformed by folding and shearing, closely jointed in most of the study area and intersected mainly by three discontinuities (two joint sets and a bedding plane), it may display a homogenous character and circular failure is a possibility in such conditions. For this reason, the stability of the slope against circular mass failure along previously determined six sections was analyzed through Slide software (version 4.010) by Rocscience (2002b). During the analysis, 1/3 of the peak ground acceleration value (Marcuson and Franklin, 1983), which corresponds to 0.03 g, is used.

The analyses are carried out by using Bishop`s simplified method (Bishop, 1955; Anderson and Richards, 1992; Bromhead, 1992; Abramson et al., 1996) by dividing the rock mass into 30 slices. Dry slope case is assumed. The average instantaneous cohesion and friction angle values are depicted in Table 4.3. Also the instantaneous cohesion and friction angle values are given for each slice of the most critical failure surfaces of each section in Appendix D. The distribution of the factor of safety values and the location of the most critical

failure surfaces in all sections were illustrated in Figures 4.9 to 4.14. Finally, the results of the analyses are tabulated in Table 4.4 for each section.

Table 4.3. Average instantaneous shear strength parameters for each section

Section	1	2	3	4	5	6
Average instantenous cohesion (c_i) (kPa)	72,5	21,1	131	37,9	12,9	64,9
Average instantenous friction angle (Φ_i) (°)	58,6	54,1	58,4	57,7	43,5	55,2

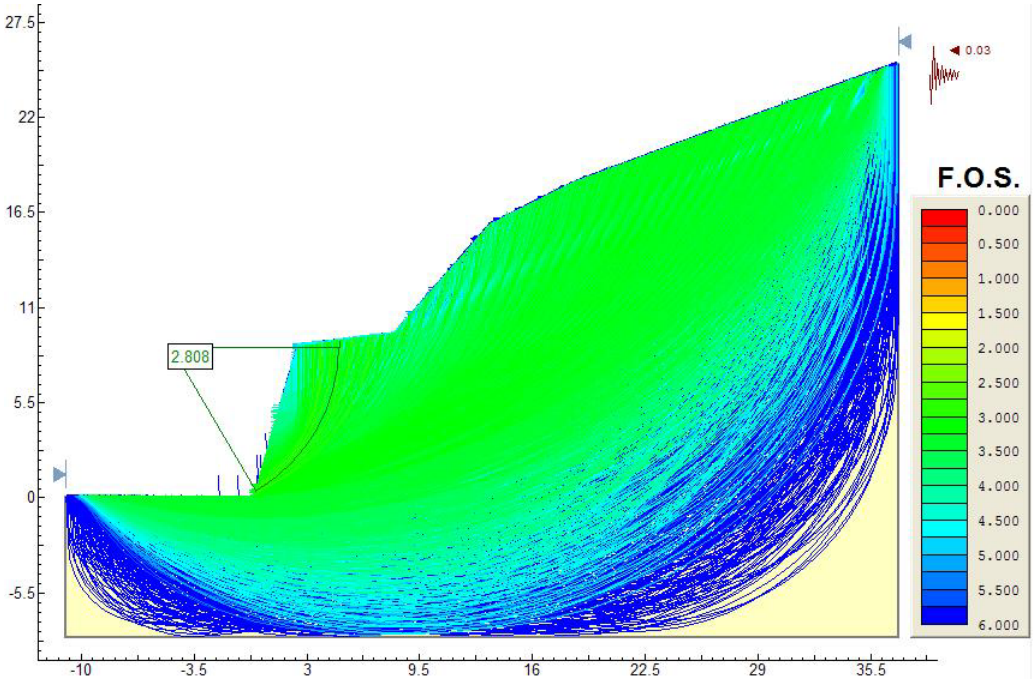

Figure 4.9. Stability analysis in section 1 against circular mass failure showing factor of safety distribution and the location of the most critical failure surface.

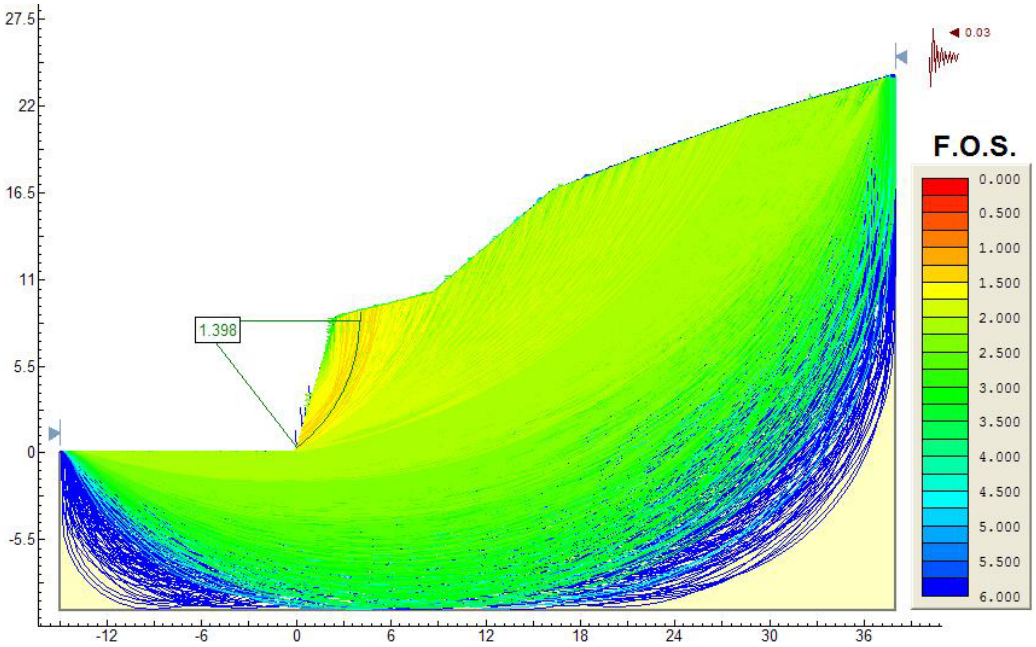

Figure 4.10. Stability analysis in section 2 against circular mass failure showing factor of safety distribution and the location of the most critical failure surface.

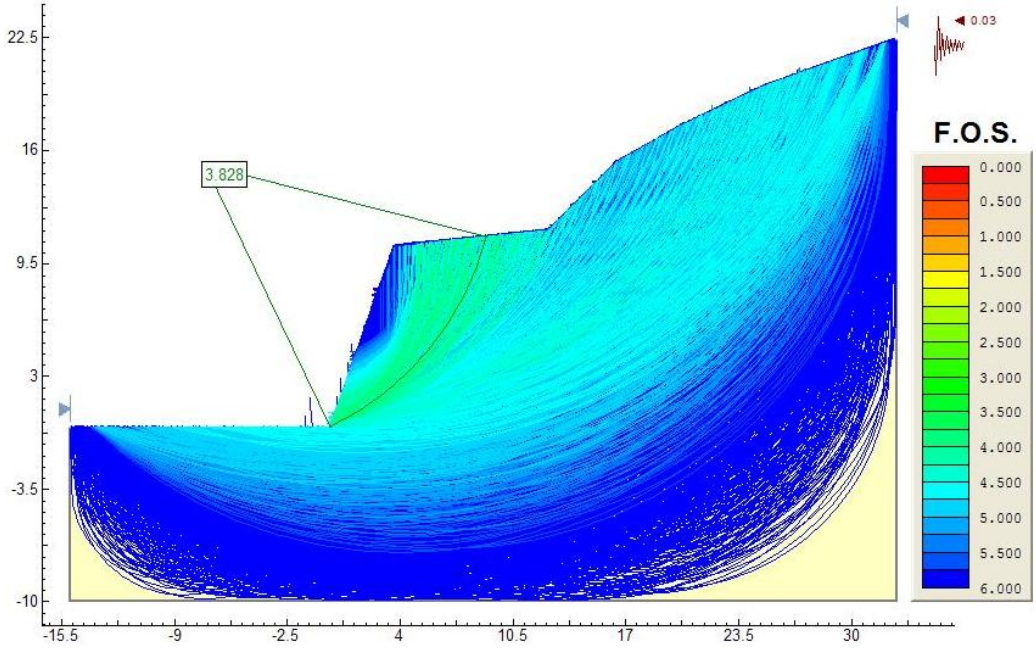

Figure 4.11. Stability analysis in section 3 against circular mass failure showing factor of safety distribution and the location of the most critical failure surface.

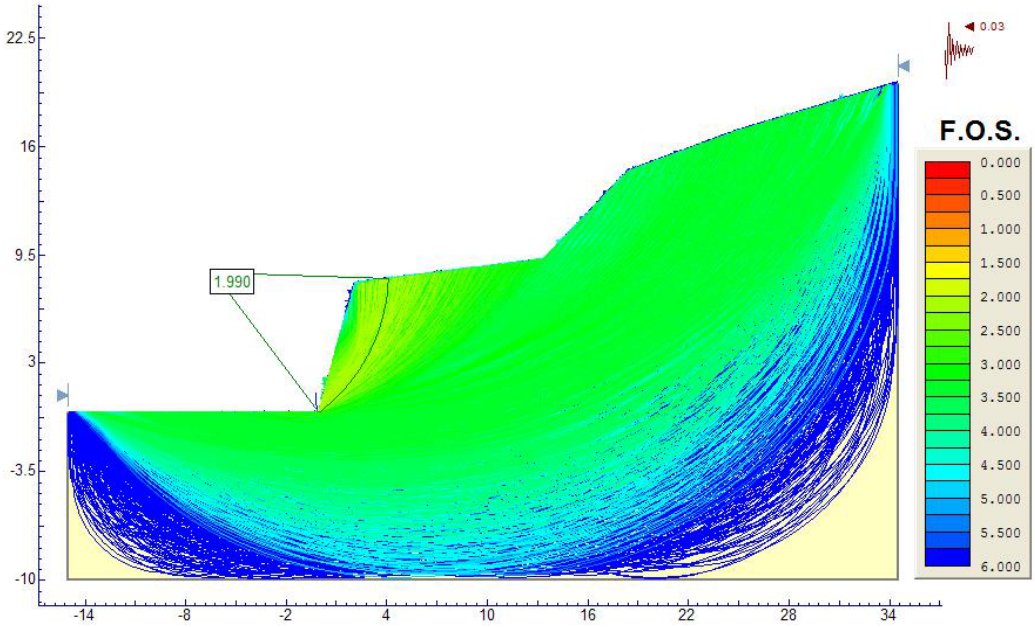

Figure 4.12. Stability analysis in section 4 against circular mass failure showing factor of safety distribution and the location of the most critical failure surface.

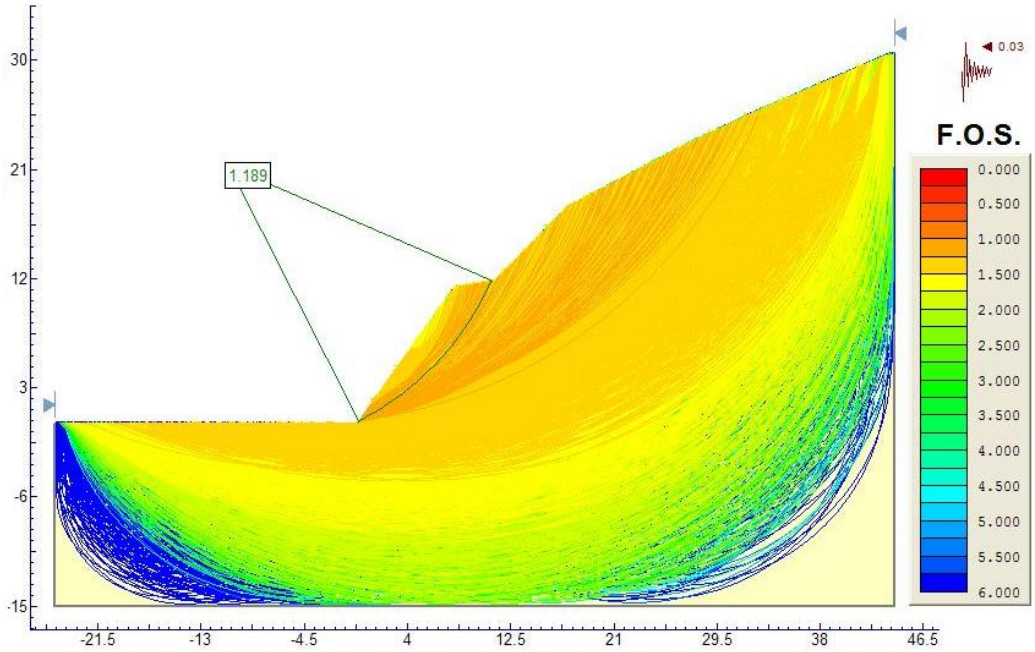

Figure 4.13. Stability analysis in section 5 against circular mass failure showing factor of safety distribution and the location of the most critical failure surface.

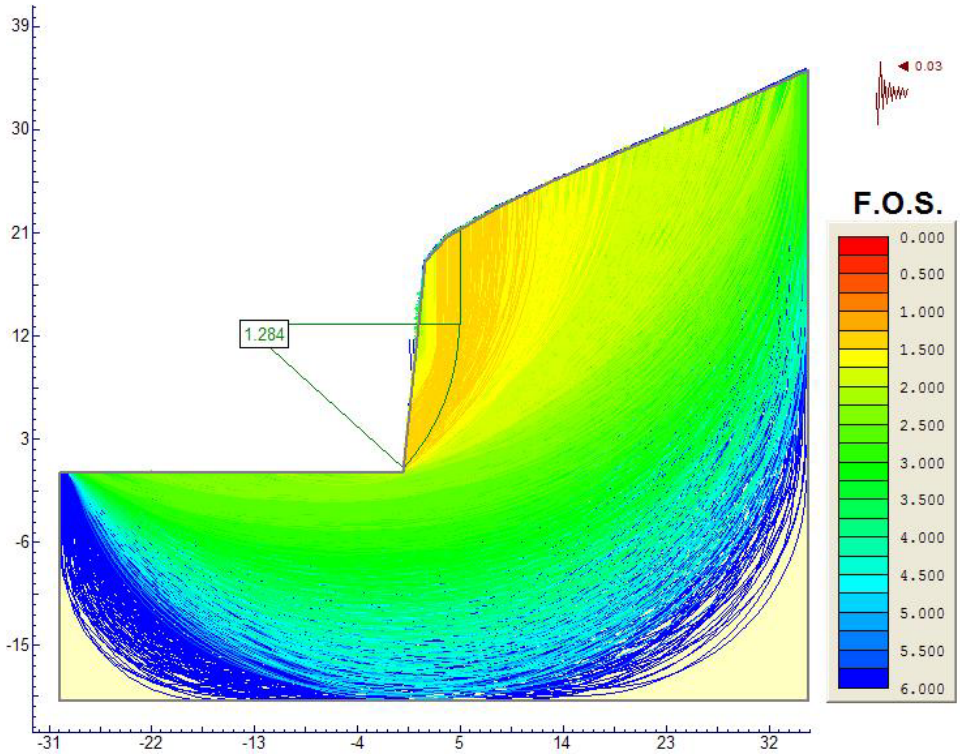

Figure 4.14. Stability analysis in section 6 against circular mass failure showing factor of safety distribution and the location of the most critical failure surface.

Table 4.4. Factor of safety against circular mass failure for each section.

Section	1	2	3	4	5	6
Factor of safety value	2,81	1,40	3,83	1,99	1,19	1,28

CHAPTER V

DISCUSSION AND RECOMMENDATIONS

In this section, the results of overlay and limit equilibrium analyses are discussed and some recommendations related to the stability of the slope are also made.

5.1. Overlay analysis

As discussed previously in this thesis, there are five parameter layers that are point load strength layer, weathering layer, block size layer, daylight layer and shear zone layer. Strength of the rock, weathering, fracture or joint spacing and the orientation of the discontinuities are widely used parameters in characterizing the rock masses, such as in the case of Bieniawski's Rock Mass Rating System (Bieniawski, 1989). Using the point load strength values is the most practical way to characterize the strength of the rock throughout the study area. However, some locations were beyond our reach to carry out this test. Therefore, the strength values of these zones were assigned by correlating or approximating from the accessible locations that display similar rock structure. Since there are mainly two joint sets and a bedding plane in the study area instead of using discontinuity spacing values, block size, which is capable of integrating the spacing values of these three discontinuity sets, is used. Also during the field studies, some detachments were observed due to the local deformations and daylight of the bedding plane. So the daylight layer was prepared by visual observations in order to include the effect of these local deformations or variations in the orientation along the bedding plane.

Throughout the field investigations, it is also noticed that the shear zones in the study area have resulted in crushed and loosened rock mass where it is present so this parameter is needed to be included in the analysis as a factor contributing instability. In the analysis, no buffer zones were used for this layer because the effect of shearing is totally confined to the shear zone.

At the end of the analysis using both methodologies (statistical index and weighting factor), a total of twelve susceptibility maps were obtained. Two of them are obtained by including all of the five parameter layers and the remaining is obtained by removing one of the parameter layers at each time. The accuracy of these twelve layers in estimating the detachments is given in Table 5.1. As a result of the analysis the susceptibility map determined by statistical index (W_i) method without including block size layer came out to be the most accurate one in estimating the detachments. The values indicate that 94.7% of the total detachments in the study area fall into high and very high susceptibility zone obtained by this susceptibility map. The closest value to this one is 94.2%, which is obtained by using weighting factor method and excluding block size layer. However, the boundary between low and medium susceptibility zones is not clear in this one as in the map obtained by statistical index method. When we compare all of the values which represent the accuracy of high and very high susceptibility zones in estimating the detachments, it is seen that these values are ranging from 88.3% (without daylight layer) to 94.7% (without block size layer) which can be accepted as high degree of accuracy. After the determination of the final susceptibility maps, the accuracy was also checked by comparing the results with the current situation in the study area. Generally all of the maps were quite good at estimating the existing situation in the study area. Although some differences can be observed at some locations, there are no radical deviations among the maps. As a result of the field investigations, the susceptibility map obtained by using statistical index method and excluding the block size layer is selected as the most accurate one in representing the present state of the study area.

Table 5.1. Results of overlay analysis for each susceptibility map.

WF method					**Wi method**				
without Block size					**without Block size**				
Suscept. Zones	Low	Med.	High	V. high	Suscept. Zones	Low	Med.	High	V. high
% of total detacment	3,5	2,2	43,9	50,3	% of total detacment	2,0	3,3	33,6	61,1
Density of detachment (%)	3,7	4,3	22,5	56,0	Density of detachment (%)	2,1	6,8	18,4	57,3
without Daylight					**without Daylight**				
Suscept. Zones	Low	Med.	High	V. high	Suscept. Zones	Low	Med.	High	V. high
% of total detacment	3,8	7,9	38,1	50,2	% of total detacment	1,0	10,8	36,1	52,2
Density of detachment (%)	4,0	12,7	20,8	56,3	Density of detachment (%)	1,5	11,2	20,1	56,0
without Point Load					**without Point Load**				
Suscept. Zones	Low	Med.	High	V. high	Suscept. Zones	Low	Med.	High	V. high
% of total detacment	1,9	6,7	67,9	23,6	% of total detacment	0,6	7,2	68,6	23,6
Density of detachment (%)	2,0	29,3	24,1	73,6	Density of detachment (%)	1,7	9,4	23,9	73,6
without Shear Zone					**without Shear Zone**				
Suscept. Zones	Low	Med.	High	V. high	Suscept. Zones	Low	Med.	High	V. high
% of total detacment	4,0	5,4	41,6	48,9	% of total detacment	0,8	8,2	33,7	57,3
Density of detachment (%)	4,1	9,3	22,2	56,0	Density of detachment (%)	1,4	9,0	18,9	56,5
without Weathering					**without Weathering**				
Suscept. Zones	Low	Med.	High	V. high	Suscept. Zones	Low	Med.	High	V. high
% of total detacment	1,2	6,6	43,3	48,9	% of total detacment	1,2	6,4	37,9	54,4
Density of detachment (%)	4,4	7,2	19,4	55,1	Density of detachment (%)	3,5	7,8	17,9	53,8
with all layers					**with all layers**				
Suscept. Zones	Low	Med.	High	V. high	Suscept. Zones	Low	Med.	High	V. high
% of total detacment	3,5	5,8	41,7	48,9	% of total detacment	2,0	6,9	33,7	57,4
Density of detachment (%)	3,7	9,7	22,2	55,9	Density of detachment (%)	2,1	11,9	19,0	56,5

According to the weighting factor method and susceptibility analysis, the block size came out to be the least effective parameter (almost no effect) in this stability analysis. In reality, it is one of the most important parameters when dealing with this kind of small scale detachments. The smaller the block size, the easier the rock to move or detach in case of heavy rainfalls, water pressure in the joints, freezing and thawing or by root growth. However, the block size proved to be an unnecessary layer because most of the study area is dominated by very small size blocks (about 87% of the study area) and the remaining part is mostly located in small size blocks where the extent of medium block size is negligible. So there are no radical differences in most of the zones in terms of

block size, such as the difference between large and small block size zones. Also, although 90% of the detachments took place in very small size blocks zone, the vast area occupied by this zone resulted in a low density of detachments. On the other hand, although the point load strength and the weathering are two different layers, they're greatly interrelated with each other. The point load strength or the strength of intact rock is dependent on the composition of the intact rock and in some parts of the study area, there is chert present in the rock which may have positive effect in terms of the strength. However, the weathering is a more effective parameter than these variations in the composition for this study. The weathering has the prime responsibility for the decrease in the rock strength. So, although weighting factors for the point load strength layer and the weathering are 100 and 56.65, respectively, some of this 100 value is greatly dependent on the weathering layer. Therefore, in reality the weathering is probably a more operative parameter in the detachments. However, the weighting factor value of the point load strength layer can be assumed to be reasonable since it integrates both weathering and composition as its constitutional inputs.

For the both methodologies, the main drawback of the statistical index method is assigning equal weights to each layer which may generally not be the case in reality, in that case assigning weighting factor seems to be a more logical way of modeling the effect of each factor contributing instability. However, the formula used in this thesis for the determination of the weighting factors seems to bear some inconsistencies. For example, during the analysis including all layers, the weighting factor of shear zone layer was determined as 12.74%. However, after removing the block size layer and carrying out the analysis with the remaining four layers, the weighting factor values of all layers, except point load strength layer, decreases significantly and results in a weighting factor value of 1% for the shear zone layer. For another example, assume that we have again five parameters that has very similar effect on the stability in the reality, like 18%, 19%, 20%, 21% and 22%. After applying the

formula by weighting factor method we amplify 22% to 100% and 18% to 1% which results in very contradictory situation with reality. On the other hand, since there is a significant difference between the importance or the effect of the parameter layers used in this study, this drawback of the weighting factor method didn't affected the results much.

5.2. Limit equilibrium analysis

Factor of safety concept has evolved in order to determine the conservatism that should be explicitly incorporated into a design. Typical factor of safety values used in the geotechnical engineering practice in transportation projects lies between 1.25 and 1.5 for slopes with no potential impact on permanent structures (Turner and Schuster, 1996). However, the acceptable factor of safety value for long term dynamic design condition is given as 1.1 according to the General Directorate of Highways of Turkey (KGM, 1995). Considering the importance of the highway, a value of 1.25 is accepted as the lowest factor of safety in this study.

According to the results of the limit equilibrium analysis, except the section 5, all the other sections have factor of safety values higher that the accepted limiting value. Therefore, no mass failure is expected for these sections (sections 1, 2, 3, 4, and 6). However, the section 5 has a factor of safety lower than 1.25 under dynamic conditions. Although the properties of the rock mass are expected to become better towards the inner side of the slope, the calculated factor of safety (1.19) for long term stability should be increased.

5.3. Remedial measures

There are various support techniques in the literature (Turner and Schuster, 1996) to improve the stability of a slope. Among these, rock bolting, slope flattening, toe support, shotcrete, and wire mesh are very frequenly applied techniques in engineering practice. Rock bolting is not suitable for the cut slope due to the highly fractured nature of the rock mass. Slope flattening also not practical because there are high buildings at the back of the cut slope. Wire mesh and shotcrete may be applied only for preventing small individual rock fragments from detaching. However, the toe support in the form of retaining wall with or without anchor may significantly increase the factor of safety. The application of the toe support should be carried out to an extent that satisfies the acceptable factor of safety value of 1.25. The result of the limit equilibrium analysis for the section 5 is shown in Figure 5.1. It indicates that the toe support should be capable of exerting 30 kN/m^2 pressure in order to overcome the long term instability. The position of the toe support should begin from the toe of the slope and extend up approximately about 1.9 m along the slope face (Figure 5.1).

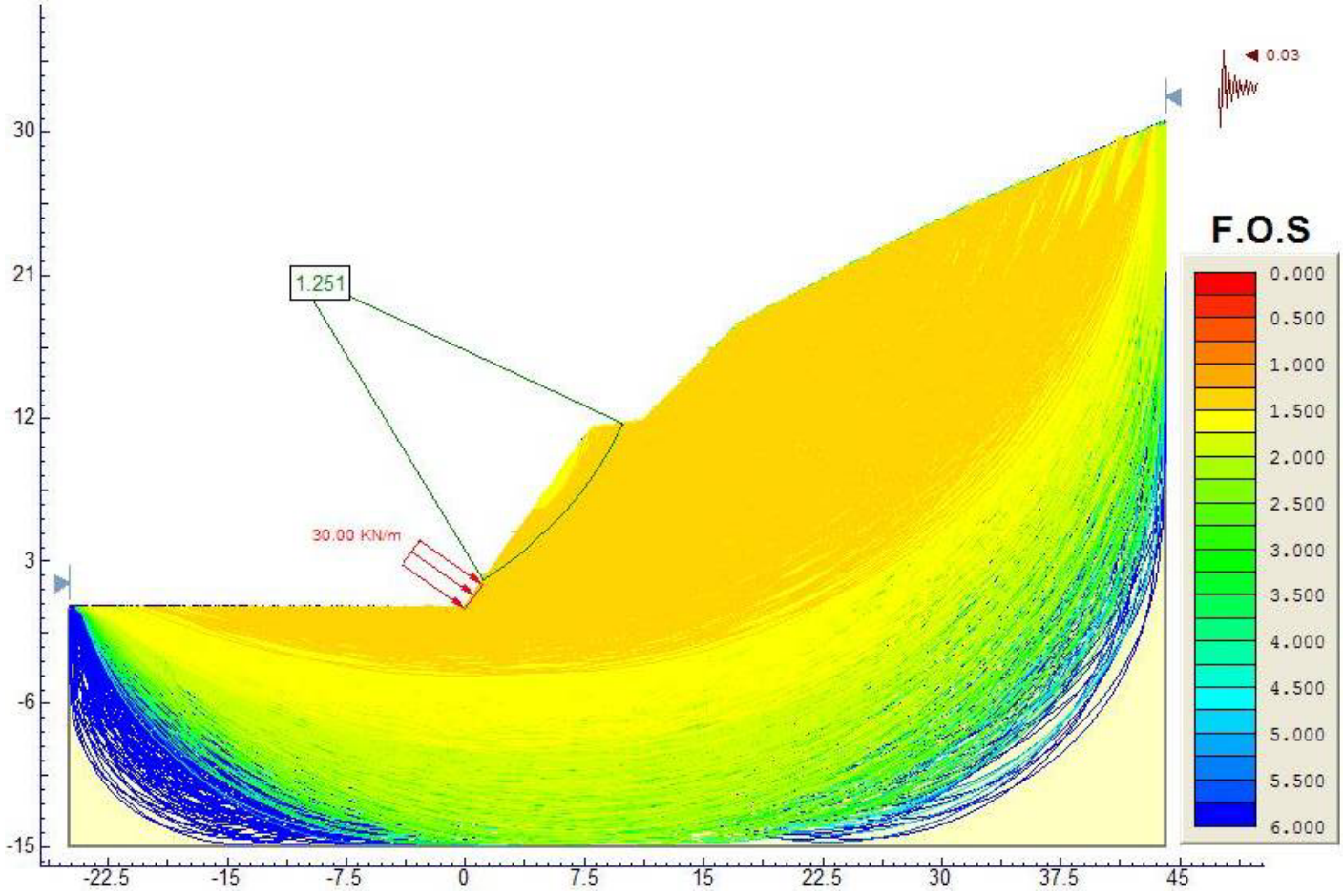

Figure 5.1. Application of an external load near the toe of the slope in section 5.

According to the results of overlay analysis, small scale instabilities in the study area take place in the form of rock falls, sloughing, raveling or detachment of degraded, highly weathered soil like rock. In the bench, average slope angle and bench width is about 45° and 5 meters, respectively. When considering these values, detachment that takes place in the slope face above the bench bear no threat against the traffic safety. Also the accumulation of loose detached and eroded particles in the toe of the slope (Figure 5.2) is very useful in decreasing the bouncing or rolling of detached rock pieces.

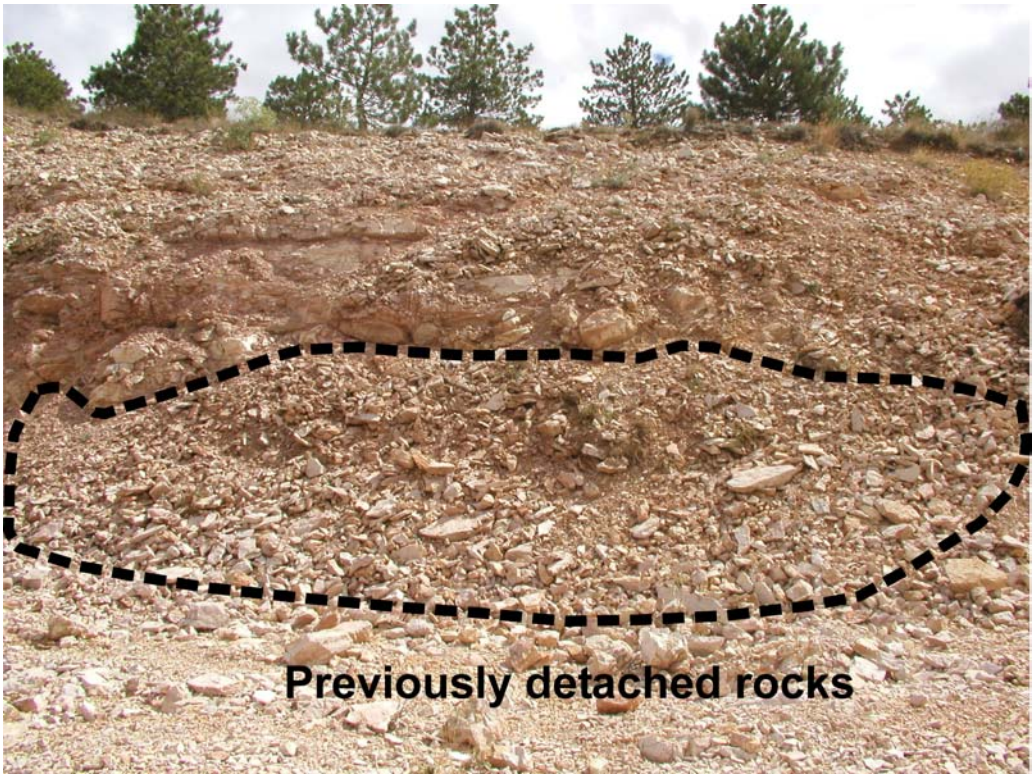

Figure 5.2. Accumulation of loose rocks acts as a remedial measure by absorbing the energy of detached pieces of rock.

This is the case for the entire bench, so no remedial measures are needed in the bench except periodic control and removal of the excess accumulated materials which may cause instabilities in the slope face below after long periods of accumulation.

For the slope face the expected detachments are being in the form of raveling type of rock falls or loosening of weathered soil like rock (sloughing). For the entire slope face rock falls or detachments can be observed because of the very small block size of the limestone, traffic vibration, and due to the uncertainties related to the effect of rainfall, freeze-thaw process or the variation of pore pressure for each single rock block/piece (or any other kind of processes can not be estimated with ease). However, in low and medium susceptibility zones, the detachments are expected to be restricted into a fall of few rock pieces which will be very small scale and local. On the other hand for the high and very high susceptibility zones, both detachment of highly degraded rock material and fall of more intact rock blocks expected consistently and more large scale than the ones in low and medium susceptibility zones (although not comparable to mass failure) (Figure 5.3 and 5.4).

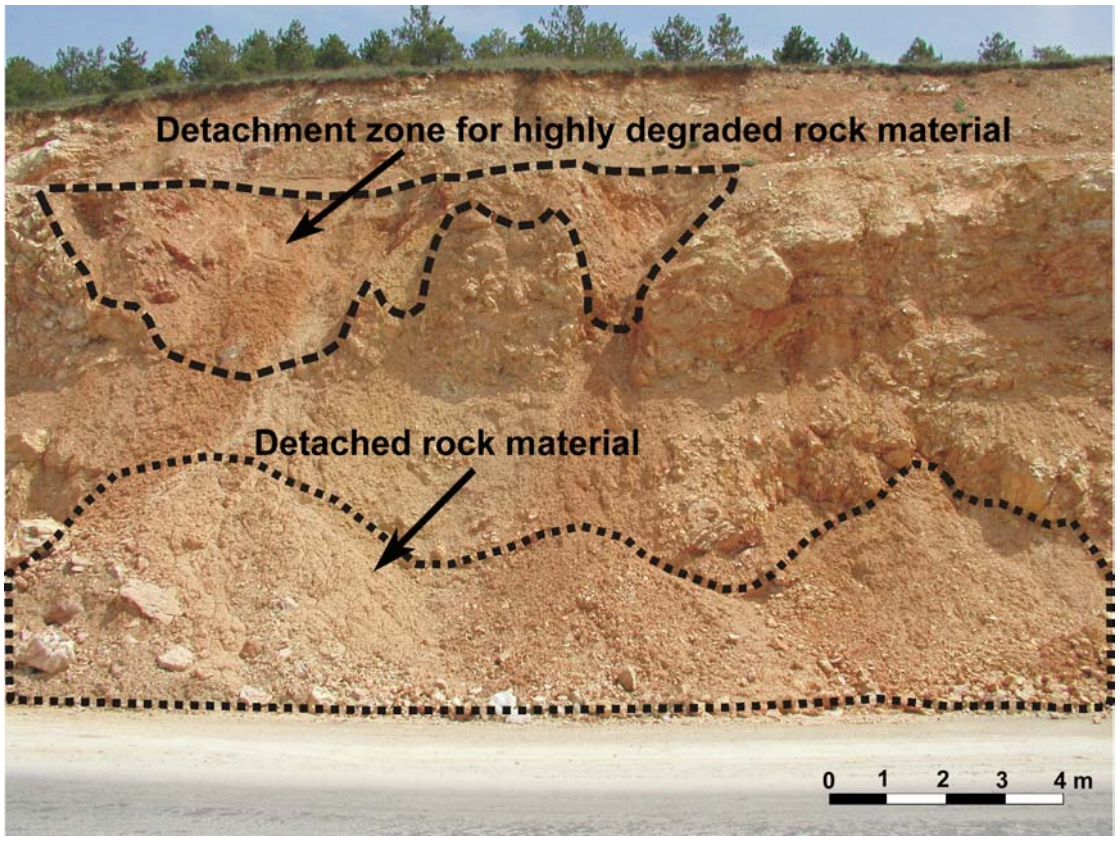

Figure 5.3. Large scale detachments in highly degraded material.

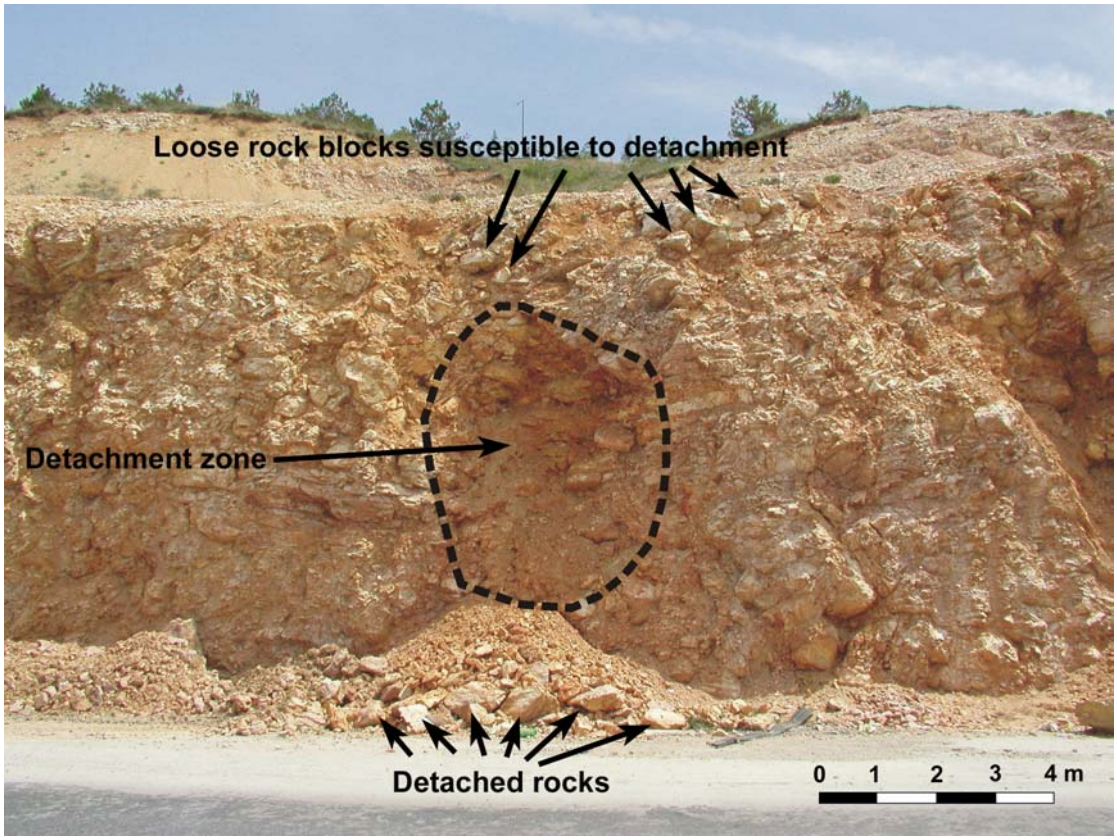

Figure 5.4. Large scale detachments, incorporating a number of rock blocks.

The study area is divided into three figures for better visualization/presentation from Figures 5.5 to 5.7. The remedial measures are recommended on these figures based on the susceptibility map obtained by excluding block size layer utilizing statistical index method and limit equilibrium analysis. Figures 5.5 and 5.6 include slope above bench. Because of the previously discussed reasons no remediation or recommendations are made for the slope above the bench so the recommendations are restricted to the slope below bench. For section A in Figure 5.5, the most of the area fall into low to medium susceptibility zone, only a very small part is found in very high susceptibility. So considering these conditions and also the low average height and reasonable distance of the slope to the road at that section, catch/barrier fences or concrete barriers (as the ones also present in the study area) are

thought to be sufficient. However, section B (Figure 5.5) falls into very high susceptibility zone and when compared with section A, average height is greater at this location, which is an important parameter in case of bouncing or rolling of the rock blocks. So, since the block size is very small (J_v>30) in this section, using wire mesh with shotcrete is suggested. For section C (Figure 5.5), although the area falls into low susceptibility zone again the application of catch/barrier fences or concrete barriers would be useful for restricting the fall of individual and very local pieces of rock. On the other hand, the most of the section D (Figure 5.6) fall into high to very high susceptibility zone, again wire mesh with shotcrete is suggested for this section since most of the area is dominated by degraded soil like rock material and very small block size rocks (J_v>30). Considering the results of limit equilibrium analysis, application of toe support along section E (Figure 5.6), to increase the factor of safety value to the acceptable limits, is suggested. Finally, section F (Figure 5.7) is found mostly in low, high and very high susceptibility zones. This zone has the greater average height (18.5 m at the highest point) and also the closest part of the slope to the road. As a result of all these conditions, wire mesh with shotcrete (considering very small size blocks) for all of this section is advised. Although significant portion of this section is in low susceptibility, the presence of the high to very high susceptibility zones standing above results in containment of this zone in this remediation.

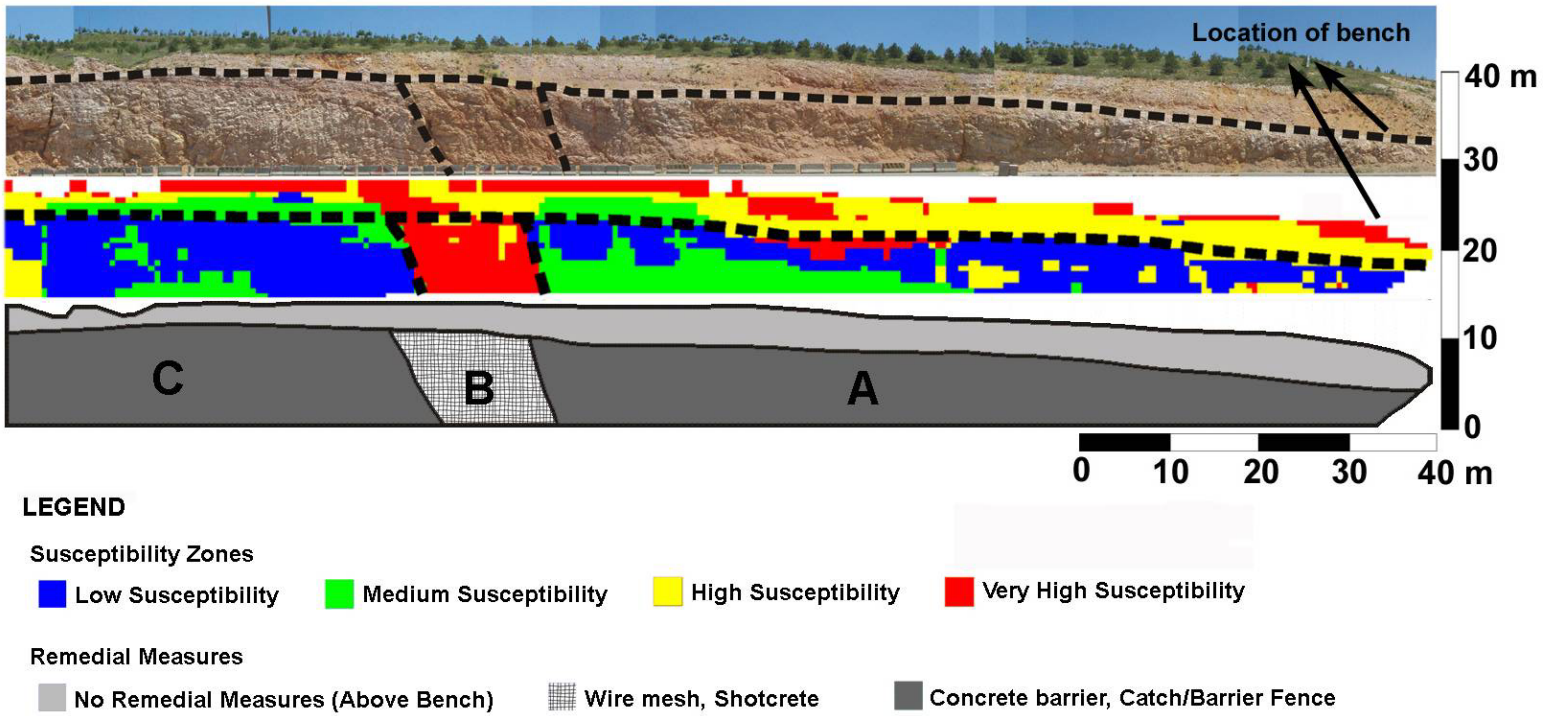

Figure 5.5. The location of different remedial measures for the first part of the slope in conjunction with susceptibility zonation map.

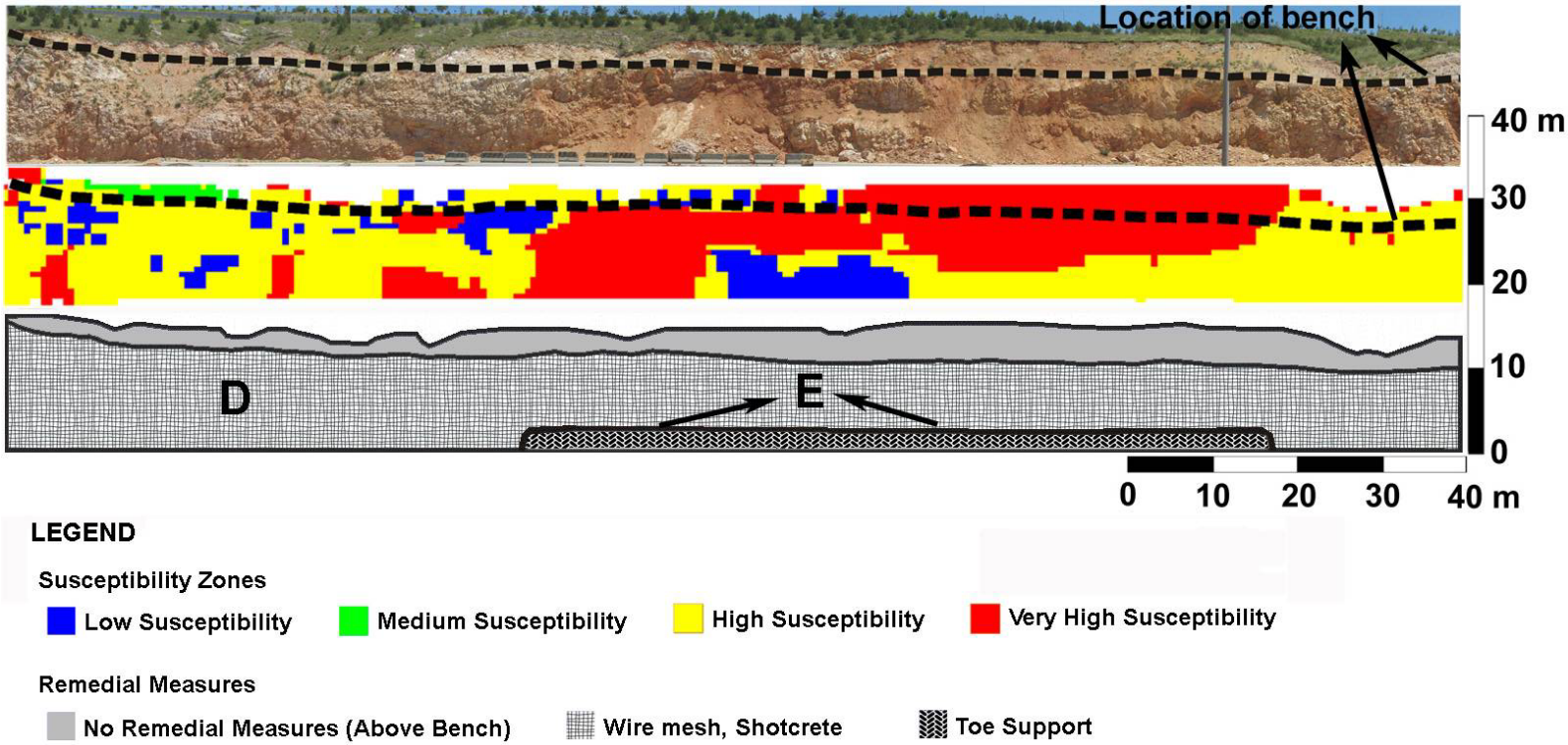

Figure 5.6. The location of different remedial measures for the second part of the slope in conjunction with susceptibility zonation map.

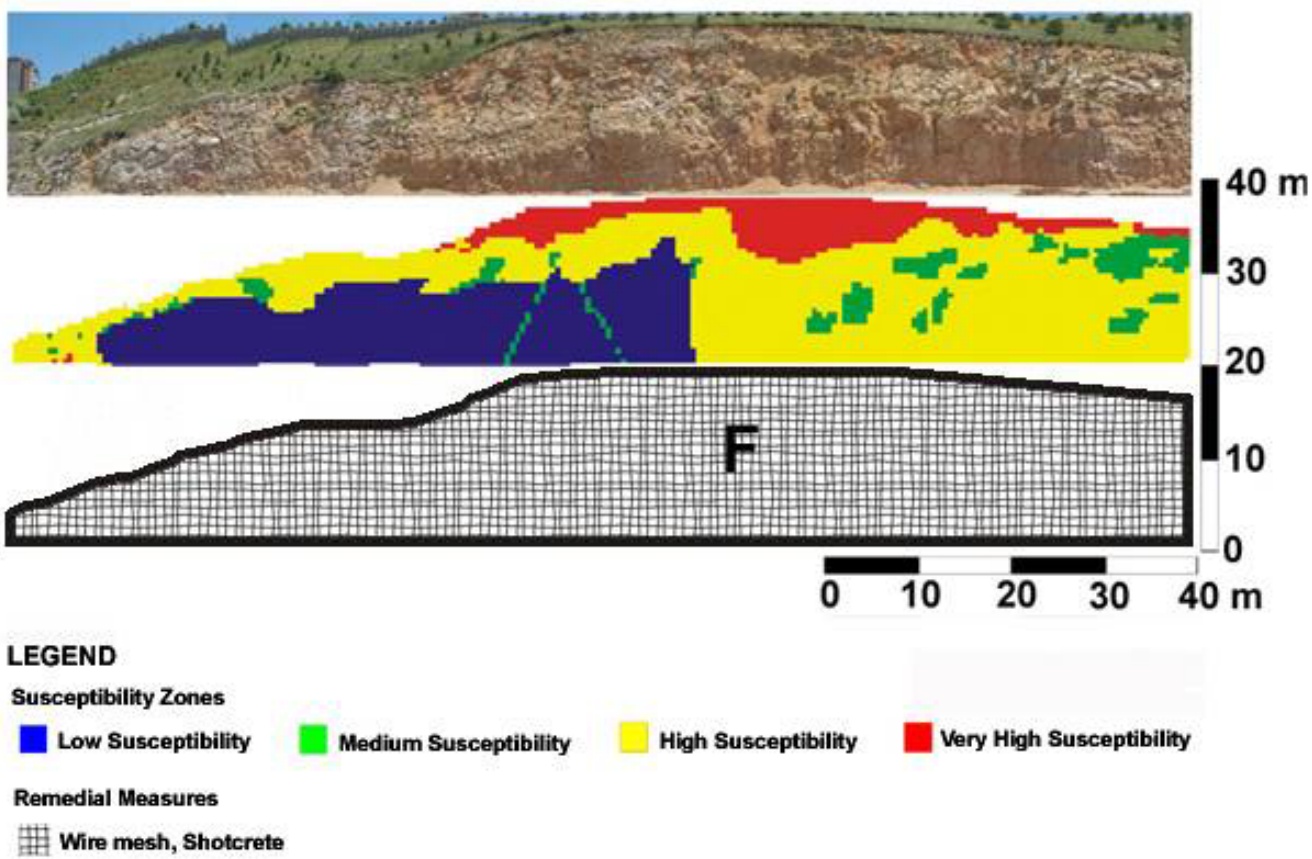

Figure 5.7. The location of different remedial measures for the third part of the slope in conjunction with susceptibility zonation map.

CHAPTER VI

CONCLUSIONS

The study area was investigated in detail throughout the application of various techniques. It is clear that limestone is the only unit prevailing in the study area. Its complex and variable structure make it harder to study, add some degree of uncertainity in some parts of the data acquisition and the analysis.

The limestone is white to beige, clayey and/or biomicritic, thin to medium bedded. It contains chert nodules and bands. It is slightly to highly weathered. It is highly fractured and sheared. In addition to shear zones, it has mainly three discontinuity sets (two joint sets and bedding plane). It has moderate unit weight, medium porosity, moderate velocity and uniaxial compressive strength, and very high to high slake durability.

The overlay analyses and field check reveal that detachment susceptibility map without block size layer gives the best result. As a result of overlay analyses, weathering and decrease in intact rock strength are found to be the key factors affecting the distribution of the detachments in the study area. The analyses indicate some risky zones where detachments are likely to occur in the future. The suitable remediations are recommended for these zones which include catch/barrier fences, concrete barrier blocks and application of wire mesh with shotcrete.

Due to the very small block size and very low persistence of the joint sets of the limestone, the possibility of discontinuity controlled failure was eliminated. On the other hand, although the results of the limit equilibrium analyses show

that no mass failure is expected in the study area, in one of the section location (section 5), the factor of safety value is below acceptable limits. This problem can be overcome by the application of toe support.

As a conclusion there are some risky zones in the study area which may fail in the coming years, this depends primarily on the climatic conditions. Heavy rains, harsh weather condition, freeze-thaw action, increase in pore pressure in joints, erosion and etc. may greatly affect the stability by triggering an increase in the driving factors against stability.

REFERENCES

Abrahamson, N., A., Silva, W.J., 1997, “Empirical response spectral attenuation relations for shaloow crustal earthquakes”, Seismological Research Letters, 68 (1), pp. 94-127.

Abramson, L.W., Lee, T.S., Sharma, S., Boyce, G.M., 1996, “Slope stability and stabilization methods”, John Wiley & Sons Inc., 628 p.

Akyürek, B., Duru, M., Sütçü, Y.F., Papak, İ., Şaroğlu, F., Pehlivan N., Gönenç, O., Granit, S., Yaşar, T., 1996, “Ankara İlinin Çevre Jeolojisi ve Doğal Kaynaklar Projesi”, MTA Jeolojik Etüdler Dairesi, Ankara.

Anderson, M.G., Richards, K.S., 1992, “Slope stability”, John Wiley & Sons, 648 p.

Anon, 1979, “Description of rock masses for engineering purposes”, Geological Society Engineering Group Working Party Report. Quarterly Journal of Engineering Geology, 10, pp. 355-388.

Atkinson, P.M., Massari, R., 1998, “Generalized linear modelling of landslide susceptibility in the Central Apennines, Italy”, Comput. Geosci., 24, pp. 373–385.

Bieniawski, Z.T., 1989, “Engineering rock mass classification”, Mc Graw Hill, New York, 237 p.

Bishop, A.W.,1955, “The use of the slip circle in the stability analysis of slopes”, Geotechnique, 5, pp. 7-17.

Boore, D., M., Joyner, W., B., Fumal, T. E., 1997, “Equations for estimating horizontal response spectra and peak acceleration from western North American earthquakes: A summary of recent work”, Seismological Research Letters, 68(1), pp. 128-153.

Bromhead, E.N., 1992, “The stability of slopes”, Chapman & Hall, London, 411 p.

BSI (British Standard Institution), 1981, “Code of Practice for Site Investigations”, BS 5930, British Standard Institution, London, 147 p.

Campbell, W.K., 1988, “Predicting strong ground motion in Utah”, In: Hays, W.W., Gori, P.L. (Eds.), Evaluation of Regional and Urban Earthquake Hazard Risks in Utah. USGS Professional Paper, pp. L1– L31.

Carrara, A., Cardinali, M., Guzzetti, F., Reichenbach, P., 1995, “GIS technology in mapping landslide hazard”, In Carrara A, Guzzetti F (eds) Geographical information systems in assessing natural Hazards, Kluwer, pp. 135–175.

Çevik, E., 2002, “GIS Based Landslide Susceptibility Mapping For The Segment (KM 60- KM 83) of NG Pipeline, Norh of Hendek”, M.Sc. Thesis, METU, Turkey, Ankara, 77p.

Çevik, E., Topal, T., 2003, “GIS-based landslide susceptibility mapping for a problematic segment of the natural gas pipeline, Hendek (Turkey)”, Environmental Geology, 44, pp. 949-962.

Dai, F.C., Lee, C.F., Li, J., Xu, Z.W., 2001, “Assessment of landslide susceptibility on the natural terrain of Lantau Island, Hong Kong”, Environmental Geology, 40, pp. 381–391.

DMİ, 2002, Devlet Meteoroloji İşleri Genel Müdürlüğü, http://www.meteor.gov.tr/webler/iklim/iklimmaster.htm, (Connected in: 12.08.2002).

DMİ, 2004, Devlet Meteoroloji İşleri Genel Müdürlüğü - Ankara Meteoroloji Bölge Müdürlüğü, http://ankara.meteor.gov.tr/ankara.htm, (Connected in: 22.10.2004).

Fookes, P.G., Hawkins, A.B., 1988, “Limestone weathering: its engineering significance and a proposed classification scheme”, Quarterly Journal of Engineering Geology, 1988, 21, pp. 7-31.

Franklin, J.A., Dusseault, M.B., 1989, “Rock Engineering”, McGraw-Hill, 600 p.

Fukushima, Y., Tanaka, T., 1990, “A new attenuation relation for peak horizontal ground acceleration of strong ground motion in Japan”, Bull. Seismol. Soc. Am., 80, pp. 757– 783.

Goodman, R.E., 1989, “Introduction to rock mechanics”, Second Edition, John Wiley and Sons, 592 p.

Gülkan, P., Yücemen, S., Koçyiğit, A., Doyuran, V., Başöz, N., 1993, “En Son Verilere Göre Hazırlanan Türkiye Deprem Bölgeleri Haritası”, ODTÜ Deprem Mühendisliği Araştırma Merkezi, Rapor No. 93-01 (unpublished).

Hawkes, I., Mellor, M., 1970, “Uniaxial testing in rock mechanics laboratories”. Engineering Geology, 4, pp. 177-285.

Hoek, E., 1998; Reliability of Hoek-Brown estimates of rock mass properties and their impact on design, International Journal of Rock Mechanics and Mining Sciences 1998, 35, pp. 63-68.

Hoek, E., 2000, “Rock Engineering”, Course Notes, http://www.rocscience.com, 299 p.

Hoek, E., Bray, J.W., 1977, “Rock slope engineering”, The Institution of Mining and Metallurgy, London, 402 p.

Hoek, E., Brown, E.T., 1997, “Practical estimates of rock mass strength”, International Journal of Rock Mechanics and Mining Sciences, 34 (8), pp. 1165-1186.

Hoek, E., Carranza-Torres, C. and Corkum, B., 2002, “Hoek-Brown criterion – 2002 edition”, Proc. North American Rock Mechanics Society meeting in Toronto in July 2002, 1, pp. 267-273.

Hoek, E., Marinos, P., 2000, “A geologically friendly tool for rock mass strength estimation”, Proceedings of the International Conference on Geotechnical and Geological Engineering (GeoEng2000), Melbourne, Australia, Technamic Publishing Co. Inc., pp. 1422-1440.

Hoek, E., Marinos, P., 2001, “Estimating the geotechnical properties of heterogeneous rock masses such as flysch”, Bulletin of Engineering Geolology and the Environment, 60, pp. 85-92.

Hoek, E., Marinos, P., Benissi, M., 1998, “Applicability of the geological strength index (GSI) classification for very weak and sheared rock masses: the case of the Athens schist formation. Bulletin of Engineering Geology and the Environment, 57, pp. 151-160.

ISRM (International Society for Rock Mechanics), 1981, “Rock characterization, testing and monitoring – ISRM Suggested Methods”, Pergamon Press, Oxford, Brown, E.T.(ed), 211 p.

ISRM (International Society for Rock Mechanics), 1985, “Point load test, suggested method for determining point load strength”, International Journal of Rock Mechanics, Mining Science and Geomechanics Abstracts, 22, pp. 51-60.

Joyner, W.B., Boore, D.M., 1988, “Measurement, characterization, and prediction of strong ground motion”, Earthquake Engineering and Soil Dynamics: 2. Recent Advances in Ground Motion Evalution, ASCE, New York, pp. 43– 102.

Kandilli Observatory, Sayısal Grafik San. Ve Tic. Ltd. Şti., 2004, Türkiye Deprem Sitesi - Deprem Haritası, http://www.sayisalgrafik.com.tr/deprem/tr_frames.htm, (Connected in: 20.10.2004).

KGM, 1995, “Zemin araştırma işine ait teknik şartname”, Karayolları Genel Müdürlüğü, 43 p.

Luzi, L., Pergalani, F.,1996, “Applications of statistical and GIS techniques to slope instability zonation (1:50.000 Fabriano geological map sheet)”, Soil Dynamics and Earthquake Engineering, 15, pp. 83-94.

Marcuson, W.F., Franklin, A.G., 1983, “Analysis and remedial measures to improve the stability of existing dams”, Seismic Design of Embankments and Caverns, T.R.Howard eds., ASCE, New York, pp. 43– 102..

Microimages, 2000, “TNT-MIPS, Scientific Sofware-The Map and Image Processing System”, Version 6.2, Microimages Inc., USA.

Norbury, D.R., 1986, “The point load test. Site Investigation Practice: Assessing BS 5930”, Special Publication No.2, pp. 325-329.

Priest, S.D., 1993, “Discontinuity analysis for rock engineering”, Chapman & Hall, London, 473 p.

Rocscience, 1999, “Dips, Scientific Software- Data Interpretation Package Using Stereographic Projection”, Version 5.04, Rocscience Inc., Canada, 90p.

Rocscience, 2002a, “Roclab, Scientifc Software, , Rock Mass Strength Analysis using the Generalized Hoek-Brown failure criterion”, Version 1.004, Rocscience Inc., Canada, 27p.

Rocscience, 2002b, “Slide, Scientific Software-2D limit equilibrium slope stability for soil and rock slopes”, Version 4.010, Rocscience Inc., Canada, 196p.

Rowbotham, D.N., Dudycha, D., 1998, “GIS modelling of slope stability in Phewa Tal watershed, Nepal”, Geomorhology, 26, pp. 151-170.

Sabetta, F., Pugliese, A., 1987, “Attenuation of peak horizontal acceleration and velocity from Italian strong motion records”, Bull. Seismol. Soc. Am. 77, pp. 1491– 1513.

Sadigh, K., Chang, C., Y., Egan, J., A., Makdisi, F., Youngs, R., 1997, “Attenuation relationships for shallow crustal earthquakes based on California strong motion data. Seismological Research Letters”, 68(1), pp. 180-189.

Sarıaslan, M.M., Yurdakul, M.E., Osmançelebioğlu, R., Basa, F., Erkal, T., Keçer, M., Şentürk, K., Mutlu, G., Aktimur, H.T., 1998, “Ankara İlinin Çevre Jeolojisi ve Doğal Kaynakları”, MTA, Derleme No:10069, Ankara, 416p.

Soeters, R., Van Westen, C.J., 1996, “Slope instability recognition analysis and zonation”, In Turner K.T., Schuster R.L. (eds) Landslide: investigation and mitigation. Special Report 47. Transportation Research Board, National Research Council, Washington, pp. 129–177.

Sönmez, H., Ulusay. R., 1999, “Modifications to the geological strength index (GSI) and their applicability to stability of slopes”, International Journal of Rock Mechanics and Mining Sciences, 36, pp. 743-760.

Sönmez, H., Ulusay, R., 2002, “A discussion on the Hoek-Brown failure criterion and suggested modifications to the criterion verified by slope stability case studies”, Yerbilimleri, 26, pp. 77-99.

Teoman, M.B., Topal, T., and Işık, N.S., 2004, “Assessment of slope stability in Ankara clay: a case study along E90 highway”, Environmental Geology, 45, 7, pp. 963-977.

Topal, T., 2000, “Nokta yükleme deneyi ile ilgili uygulamada karşılaşılan problemler”, Jeoloji Mühendisliği, 24, pp. 73-86.

Turner, K.A., Schuster, R.L., 1996, “Landslides: Investigation and mitigation”, National Academy Press, 672 p.

U.S. Army Corps of Engineers, 1994, “Rock Foundations”, Engineer Manual, Washington, 120 p.

Ulusay, R., Sönmez, H., 2002, “Kaya kütlelerinin mühendislik özellikleri”, TMMOB Jeoloji Mühendisleri Odası, 243 p.

Ulusay, R., Tuncay, E., Sönmez, H., Gökçeoğlu, C., 2004, “An attenuation relationship based on Turkish strong motion data and iso-acceleration map of Turkey”, Engineering Geology, 74, pp. 265-291.

Van Westen, C.J., 1993, “Application of geographic information systems to landslide hazard zonation”, ITC Publication 15, Enschede: ITC, Netherlands.

Van Westen, C.J., 1997, Statistical Landslide Hazard Analysis. ILWIS 2.1 for Windows Application Guide, ITC Publication, Enschede, pp. 73-84.

Van Westen, C.J., Terlien, T.J., 1996, “An approach towards deterministic landslide hazard analysis in GIS. A case study from Manizales (Colombia)”, Earth Surf Proc Landforms, 21, pp. 853–868.

Wu, W., Siddle, R.C., 1995, “A distributed slope stability model for steep forested basins.” Water Resour. Res., 31, pp. 2097–2110.

Yin, K.L., Yan, T.Z.,1988, “Statistical prediction model for slope instability of metamorphosed rocks” In Bonnard C (ed) Proc. 5th Int. Symp. on Landslides, Lausanne, Balkema, Rotterdam, pp. 1269–1272.

APPENDIX A

TEST DATA FOR THE DETERMINATION OF POROSITY, DRY AND SATURATED UNIT WEIGHTS

Table A.1. Porosity, dry and saturated unit weight values for each sample location.

Sample No:	Porosity (%)	Dry Unit Weight (kN/m^3)	Saturated Unit Weight (kN/m^3)
1	9,2	24,1	25,0
2	9,0	24,1	25,0
3	5,9	24,9	25,5
4	4,5	25,2	25,7
5	9,2	24,1	25,0
6	7,7	24,4	25,1
7	10,4	23,7	24,8
8	7,9	24,4	25,2
9	6,8	24,8	25,4
10	6,2	24,9	25,5
11	7,1	24,5	25,2
12	9,9	23,8	24,8
13	8,3	24,4	25,2
14	6,0	25,1	25,6
15	8,3	24,3	25,1
16	8,6	24,1	25,0
17	6,3	25,0	25,6
18	4,9	25,2	25,7
19	12,6	23,3	24,6
20	7,8	24,5	25,2
21	9,1	24,2	25,1
22	9,5	24,0	24,9
23	7,0	24,3	25,0
24	7,1	24,7	25,4
25	6,3	24,9	25,5
26	12,3	23,3	24,5
27	7,7	24,6	25,3
28	6,1	24,9	25,5
29	8,2	24,3	25,1
30	11,5	23,3	24,5
31	9,9	23,9	24,9
32	7,7	24,5	25,3
33	5,2	25,2	25,7
34	12,3	23,1	24,3
35	7,3	24,6	25,3
36	6,1	24,9	25,5

Figure A.1. Sample locations for the porosity, dry and saturated unit weight test.

APPENDIX B

POINT LOAD STRENGTH INDEX TEST DATA

Table B.1. Point load and corresponding uniaxial compressive strength values in details, from location 1 to 7.

Sample Locations	1	2	3	4	5	6	7
Point Load Strength Values (MPa) For 6 samples	3,10	1,79	1,90	2,71	2,31	3,66	4,91
	3,41	2,53	2,47	2,77	3,25	4,14	5,40
	3,73	3,40	3,68	3,55	3,64	4,51	5,69
	4,16	3,89	3,76	4,28	4,16	4,75	5,85
	4,27	4,08	3,87	4,80	4,44	4,98	5,95
	4,39	4,23	4,02	4,90	5,31	5,86	6,00
Average Point Load Strength Values at Each Location (MPa)	3,84	3,32	3,28	3,83	3,85	4,65	5,63
Corresponding Uniaxial Compressive Strength values at Each Location (MPa)	38,5	33,2	32,9	38,4	38,6	46,6	56,4

Table B.2. Point load and corresponding uniaxial compressive strength values in details, from location 8 to 14.

Sample Locations	8	9	10	11	12	13	14
Point Load Strength Values (MPa) For 6 samples	3,52	0,89	2,65	2,90	0,82	2,18	1,65
	3,78	0,95	2,96	3,48	1,36	2,32	1,66
	3,79	1,13	4,23	3,78	2,32	3,44	1,80
	3,89	1,51	4,90	4,32	2,55	4,27	3,40
	4,37	2,29	5,40	4,60	2,77	4,32	4,12
	5,12	3,63	6,19	5,03	3,37	4,82	5,53
Average Point Load Strength Values at Each Location (MPa)	4,08	1,73	4,39	4,02	2,20	3,56	3,03
Corresponding Uniaxial Compressive Strength values at Each Location (MPa)	40,8	17,3	43,9	40,2	22,0	35,6	30,3

Table B.3. Point load and corresponding uniaxial compressive strength values in details, from location 15 to 21.

Sample Locations	15	16	17	18	19	20	21
Point Load Strength Values (MPa) For 6 samples	2,53	3,72	1,39	2,54	0,90	2,65	2,60
	2,56	3,74	2,19	3,50	1,18	2,77	3,15
	2,63	3,88	2,24	3,64	2,12	2,92	3,28
	3,67	4,04	2,52	3,74	2,16	3,19	4,29
	4,56	4,56	3,73	3,88	2,42	3,37	4,62
	5,23	4,65	4,05	3,95	2,47	3,41	5,33
Average Point Load Strength Values at Each Location (MPa)	3,53	4,10	2,69	3,54	1,87	3,05	3,88
Corresponding Uniaxial Compressive Strength values at Each Location (MPa)	35,3	41,0	26,9	35,5	18,8	30,5	38,8

Table B.4. Point load and corresponding uniaxial compressive strength values in details, from location 22 to 28.

Sample Locations	22	23	24	25	26	27	28
Point Load Strength Values (MPa) For 6 samples	0,84	1,81	1,59	1,86	2,96	3,29	3,25
	1,32	1,99	2,86	2,02	2,97	3,36	3,37
	1,36	2,11	3,04	3,11	3,12	4,48	3,40
	1,86	2,58	3,52	3,86	5,00	4,60	3,64
	2,22	3,78	4,44	4,98	5,54	4,81	4,65
	3,23	4,64	4,56	5,58	5,80	5,17	5,16
Average Point Load Strength Values at Each Location (MPa)	1,81	2,82	3,34	3,57	4,23	4,29	3,91
Corresponding Uniaxial Compressive Strength values at Each Location (MPa)	18,1	28,2	33,4	35,7	42,4	42,9	39,2

Figure B.1. Sample locations for the point load strength index test.

APPENDIX C

SCHMIDT HAMMER REBOUND HARDNESS TEST DATA

Table C.1. Schmidt Hammer and corresponding uniaxial compressive strength values in details, from location 1 to 7.

Sample Locations	1	2	3	4	5	6	7
Schmidt Hammer Value for 10 measurements	14	14	35	46	22	26	18
	18	14	36	48	22	28	22
	20	16	38	48	25	28	22
	20	16	46	50	26	28	24
	21	18	46	52	26	30	26
	22	20	47	52	28	30	26
	23	20	48	54	32	30	28
	23	21	48	56	38	32	28
	24	23	49	56	40	32	30
	26	24	52	60	40	36	32
Average Schmidt Hammer Value	21,1	18,6	44,5	52,2	29,9	30,0	25,6
Dry Unit Weight(kN/m^3)	24,1	24,1	24,9	25,2	24,1	24,4	23,7
Corresponding Uniaxial Compressive Strength values at Each Location (MPa)	24,0	22,0	80,0	125,0	37,0	38,0	29,0

Table C.2. Schmidt Hammer and corresponding uniaxial compressive strength values in details, from location 8 to 14.

Sample Locations	8	9	10	11	12	13	14
Schmidt Hammer Value for 10 measurements	15	14	42	32	18	17	26
	16	15	44	33	18	17	28
	18	16	46	34	18	20	28
	20	16	46	36	18	24	30
	20	16	48	36	18	28	32
	22	18	48	38	18	28	34
	26	20	48	44	20	30	35
	26	22	49	46	22	32	36
	26	25	50	46	22	32	37
	33	26	50	48	28	32	38
Average Schmidt Hammer Value	22,2	18,8	47,1	39,3	20,0	26,0	32,4
Dry Unit Weight(kN/m^3)	24,4	24,8	24,9	24,5	23,8	24,4	25,1
Corresponding Uniaxial Compressive Strength values at Each Location (MPa)	24,0	22,0	95,0	60,0	23,0	30,0	44,0

Table C.3. Schmidt Hammer and corresponding uniaxial compressive strength values in details, from location 15 to 21.

Sample Locations	15	16	17	18	19	20	21
Schmidt Hammer Value for 10 measurements	20	19	22	34	18	18	18
	22	19	24	34	19	22	18
	25	20	28	34	20	22	22
	26	20	30	35	21	24	24
	28	22	30	35	22	24	26
	28	23	34	42	24	26	30
	28	26	36	42	28	26	31
	30	26	36	42	30	28	36
	33	27	39	44	34	30	36
	38	28	40	44	34	32	38
Average Schmidt Hammer Value	27,8	23,0	31,9	38,6	25,0	25,2	27,9
Dry Unit Weight(kN/m^3)	24,3	24,1	25,0	25,2	23,3	24,5	24,2
Corresponding Uniaxial Compressive Strength values at Each Location (MPa)	33,0	26,0	42,0	60,0	27,0	29,0	34,0

Table C.4. Schmidt Hammer and corresponding uniaxial compressive strength values in details, from location 22 to 28.

Sample Locations	22	23	24	25	26	27	28
Schmidt Hammer Value for 10 measurements	22	24	24	24	30	43	32
	24	26	24	34	32	44	32
	25	28	24	34	35	44	34
	26	30	25	34	36	47	36
	27	32	28	36	36	48	40
	29	34	32	40	36	48	40
	32	34	32	40	36	48	42
	35	34	34	42	38	49	43
	36	40	34	46	38	50	44
	36	40	40	46	40	50	46
Average Schmidt Hammer Value	29,2	32,2	29,7	37,6	35,7	47,1	38,9
Dry Unit Weight(kN/m^3)	24,0	24,3	24,7	24,9	23,3	24,6	24,9
Corresponding Uniaxial Compressive Strength values at Each Location (MPa)	36,0	41,0	38,0	58,0	47,0	90,0	60,0

Table C.5. Schmidt Hammer and corresponding uniaxial compressive strength values in details, from location 29 to 36.

Sample Locations	29	30	31	32	33	34	35	36
Schmidt Hammer Value for 10 measurements	24	28	12	48	14	17	25	20
	24	30	14	48	16	18	26	20
	25	30	14	48	18	20	30	22
	26	31	14	48	20	20	34	24
	28	32	16	48	24	22	34	24
	33	32	18	50	24	22	38	26
	34	34	19	51	25	26	38	28
	35	36	21	51	26	28	45	32
	36	36	24	51	28	29	46	32
	37	38	24	52	28	30	48	34
Average Schmidt Hammer Value	30,2	32,7	17,6	49,5	22,3	23,2	36,4	26,2
Dry Unit Weight(kN/m^3)	24,3	23,3	23,9	24,5	25,2	23,1	24,6	24,895
Corresponding Uniaxial Compressive Strength values at Each Location (MPa)	37,0	40,0	20,0	105,0	26,0	26,0	53,0	30

Figure C.1. Sample locations for the Schmidt rebound hardness test.

APPENDIX D

DETAILED INSTANTANEOUS COHESION (c_i) AND FRICTION ANGLE (Φ_i) VALUES FOR EACH SECTION

Instantaneous cohesion (c_i) and friction angle (Φ_i) values for each slice of each section are gıven in Figures D.1 to D.12

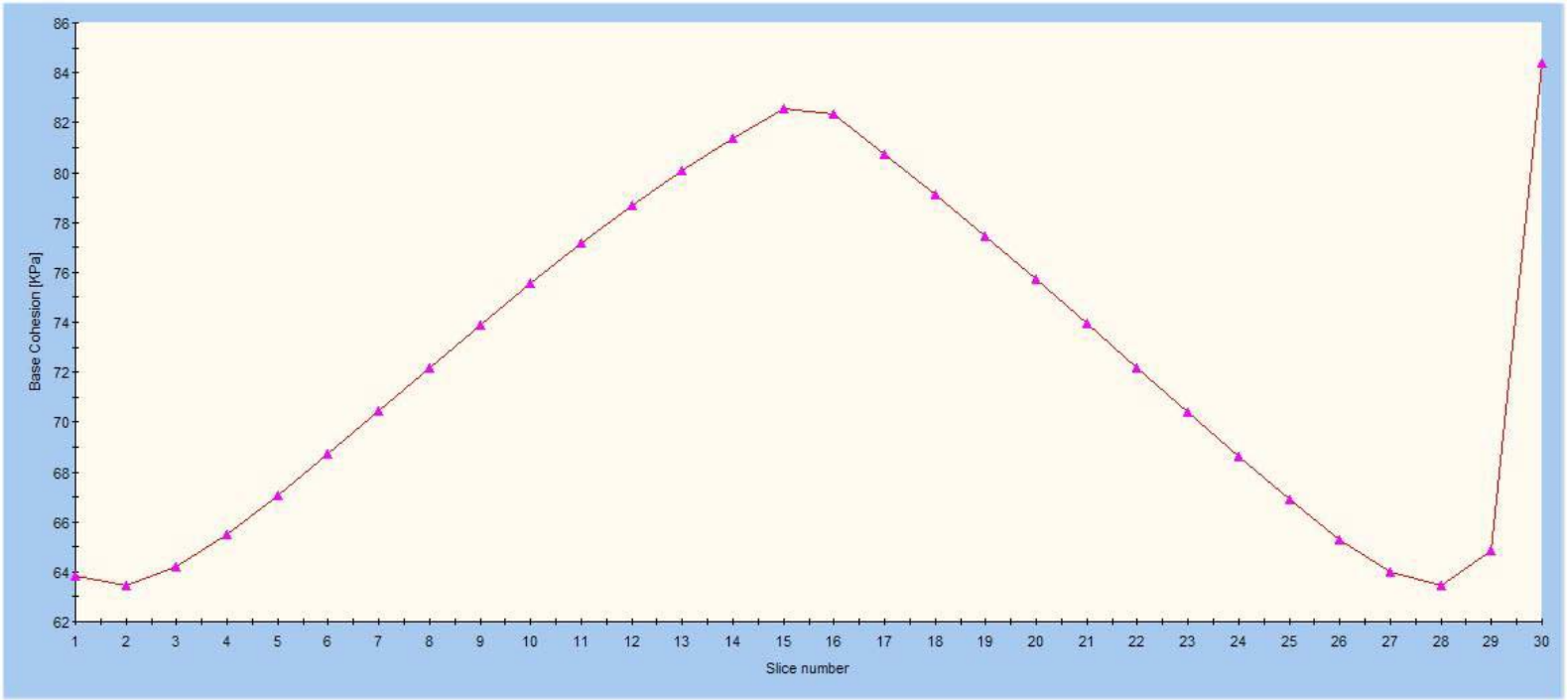

Figure D.1. Instantaneous cohesion (c_i) for each slice of the most critical failure surface in section 1.

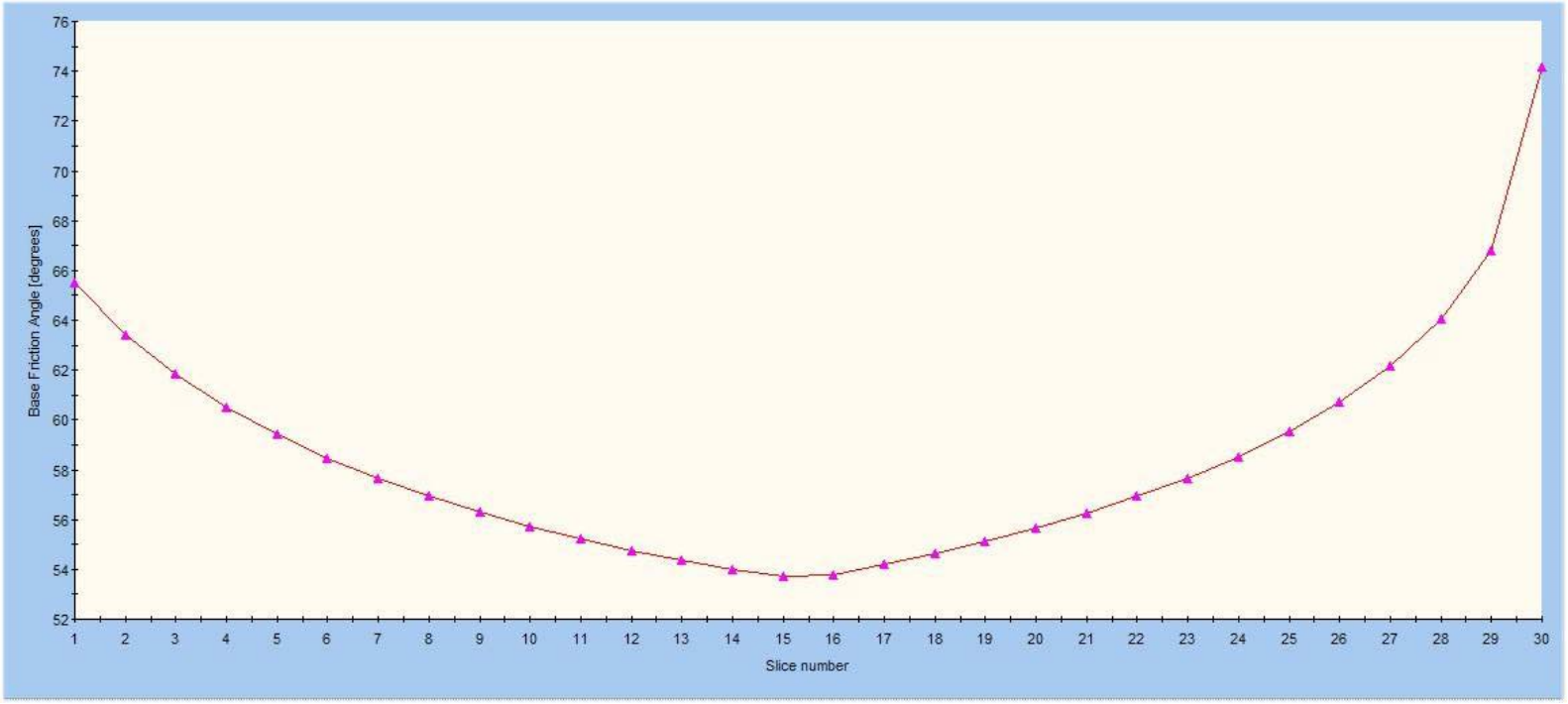

Figure D.2. Instantaneous friction angle (Φ_i) for each slice of the most critical failure surface in section 1.

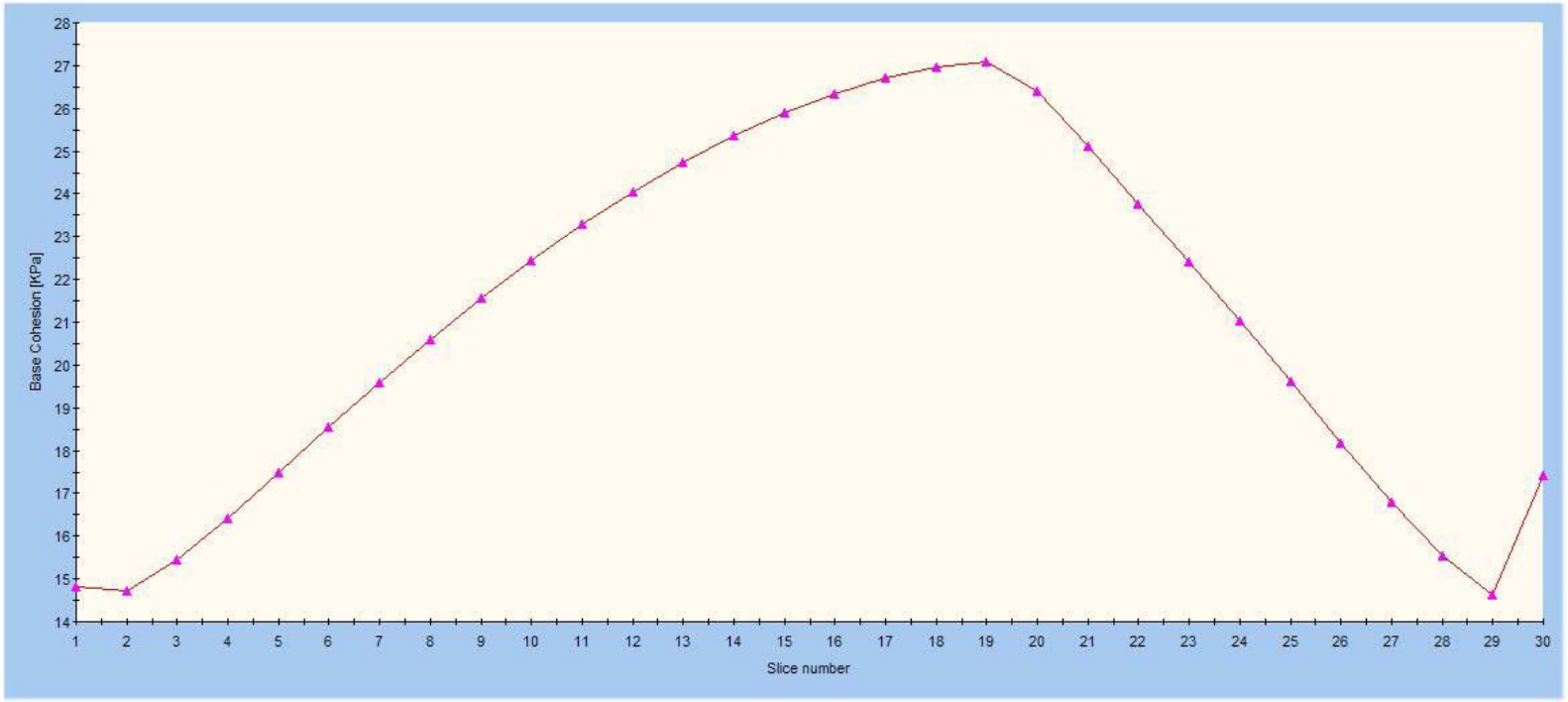

Figure D.3. Instantaneous cohesion (c_i) for each slice of the most critical failure surface in section 2.

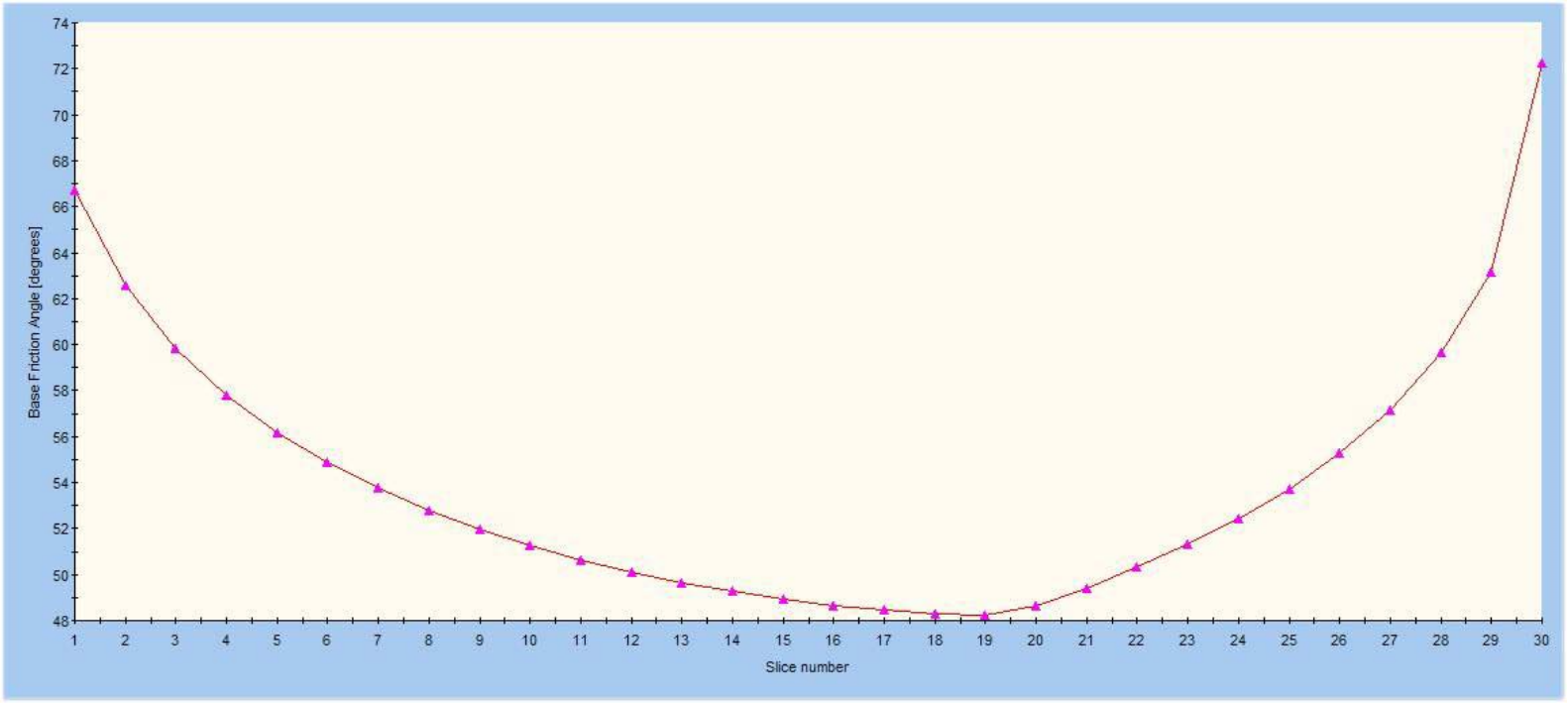

Figure D.4. Instantaneous friction angle (Φ_i) for each slice of the most critical failure surface in section 2.

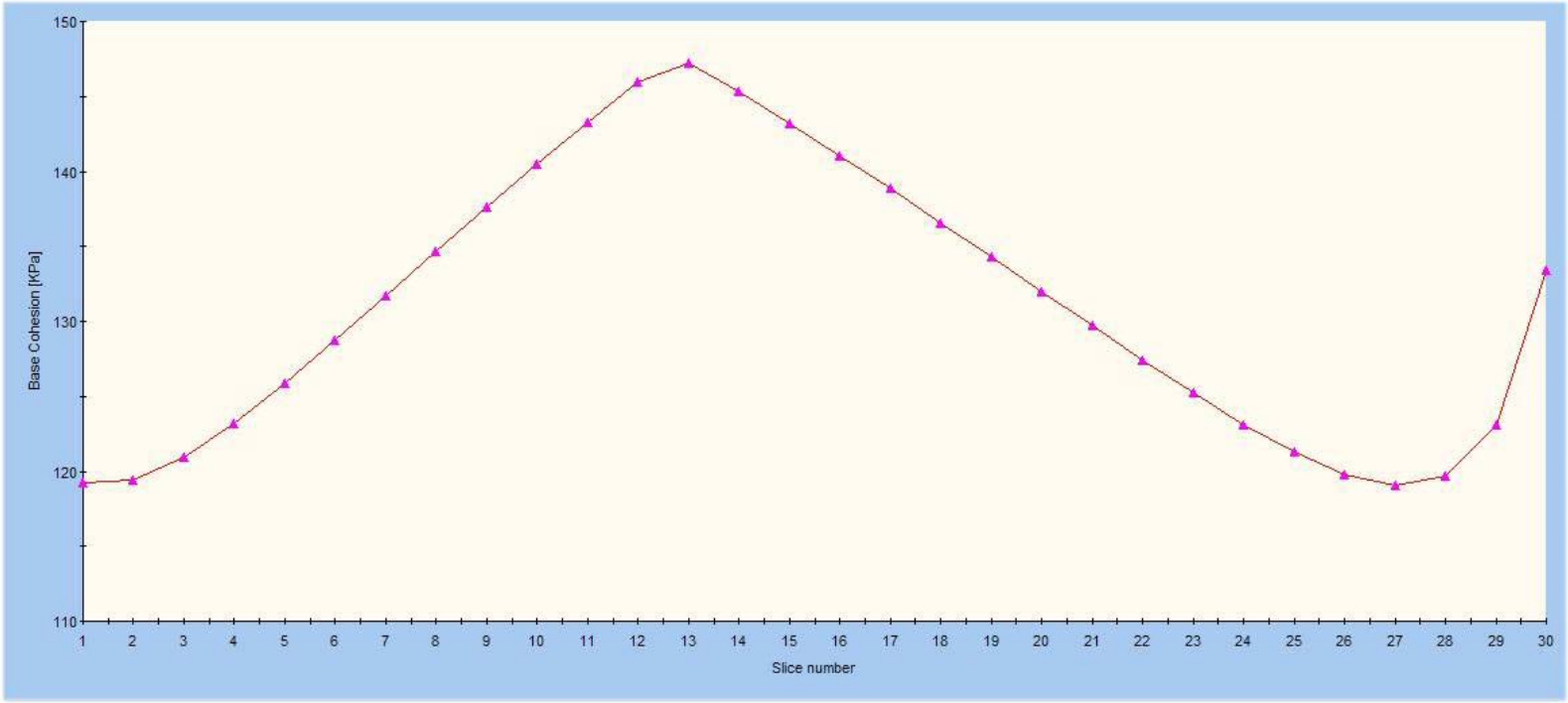

Figure D.5. Instantaneous cohesion (c_i) for each slice of the most critical failure surface in section 3.

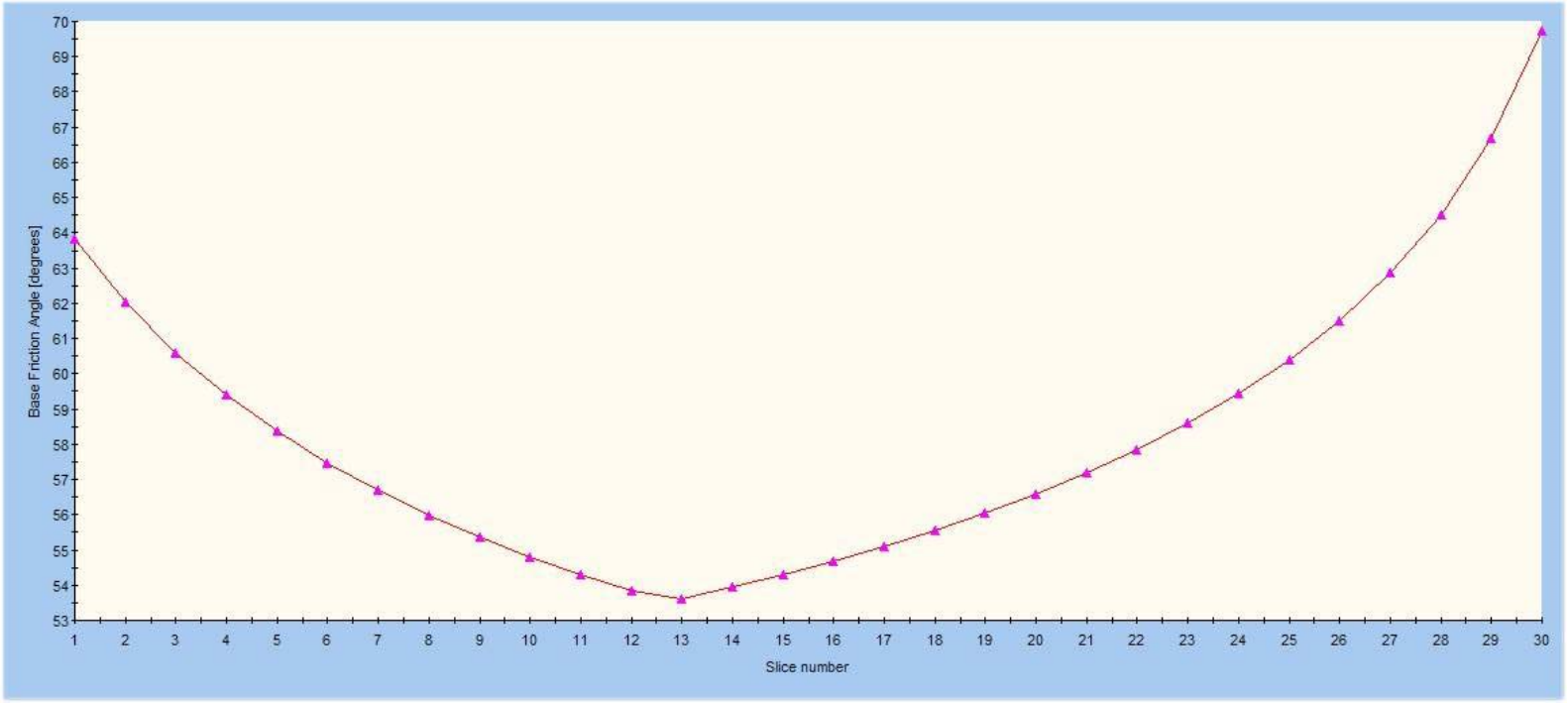

Figure D.6. Instantaneous friction angle (Φ_i) for each slice of the most critical failure surface in section 3.

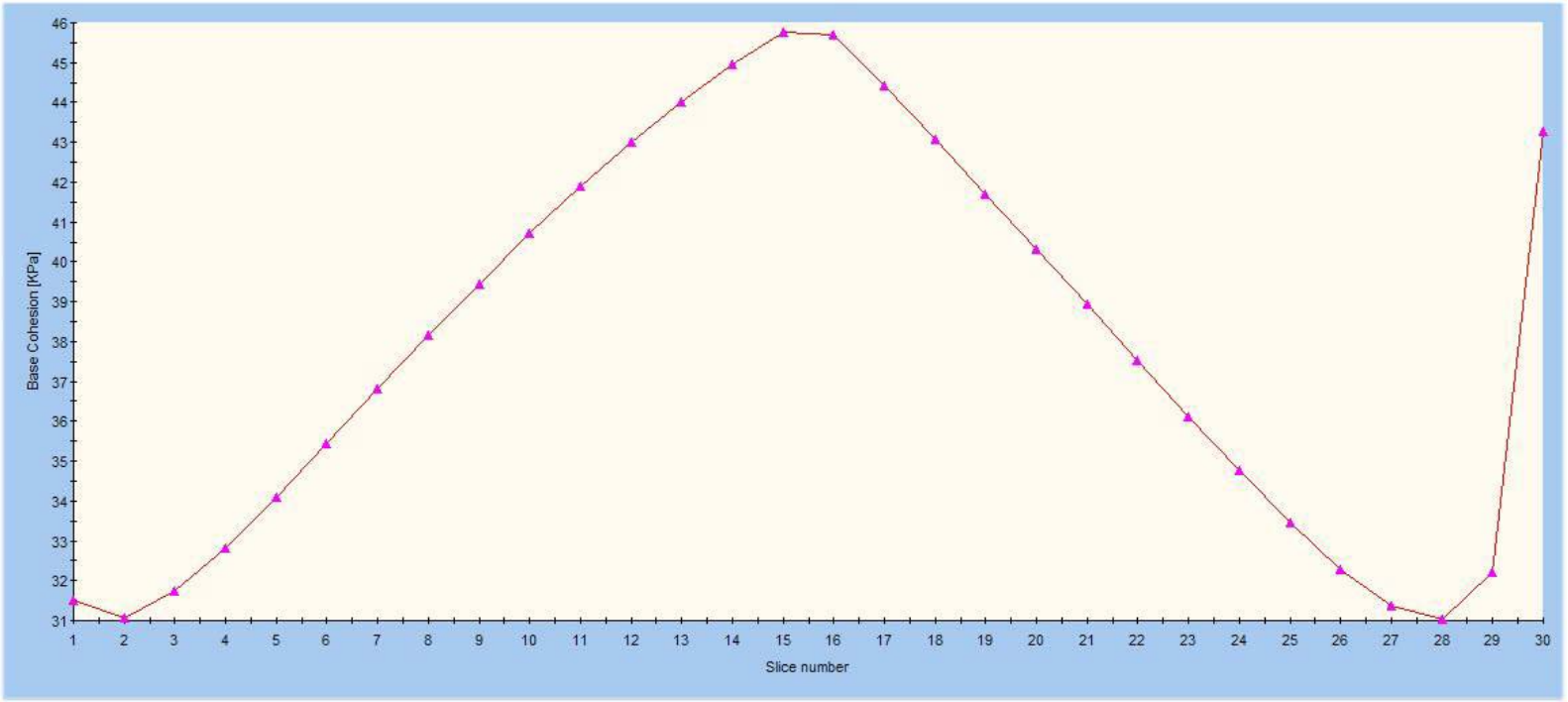

Figure D.7. Instantaneous cohesion (c_i) for each slice of the most critical failure surface in section 4.

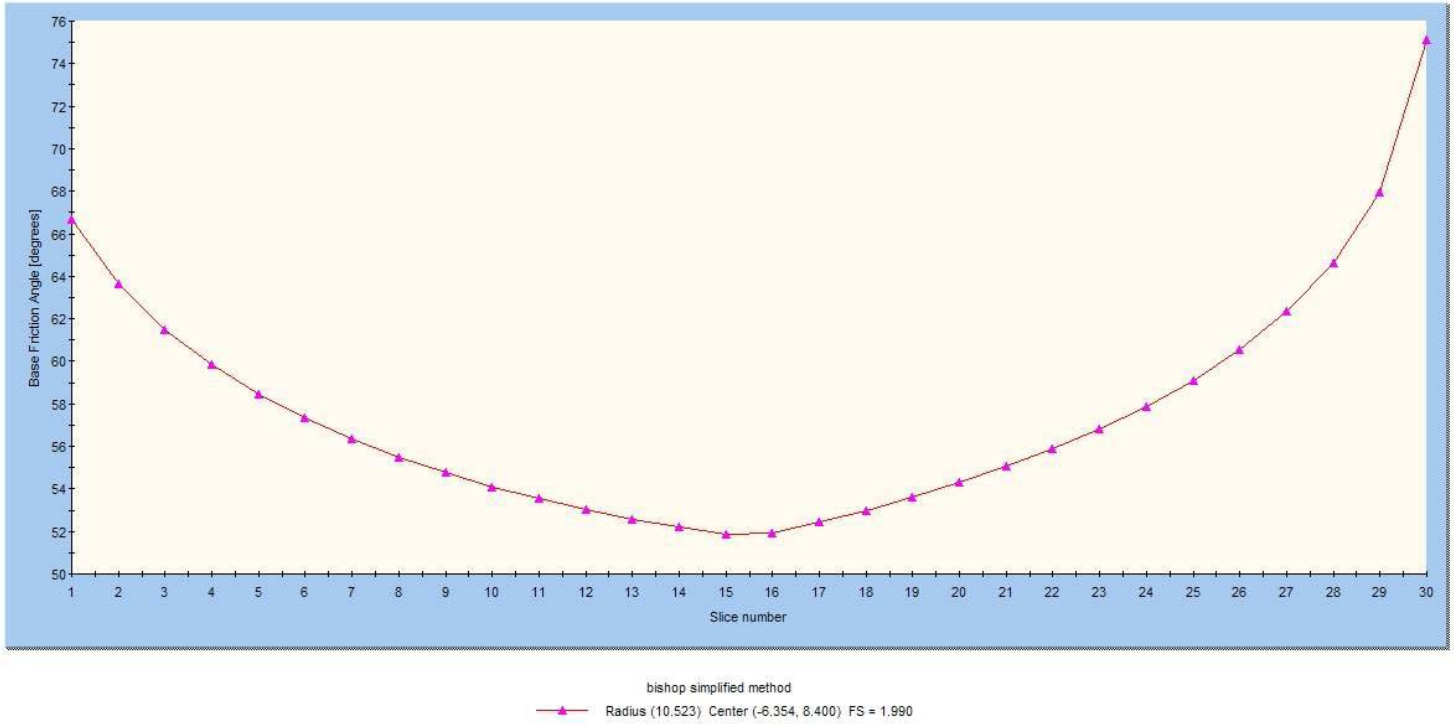

Figure D.8. Instantaneous friction angle (Φ_i) for each slice of the most critical failure surface in section 4.

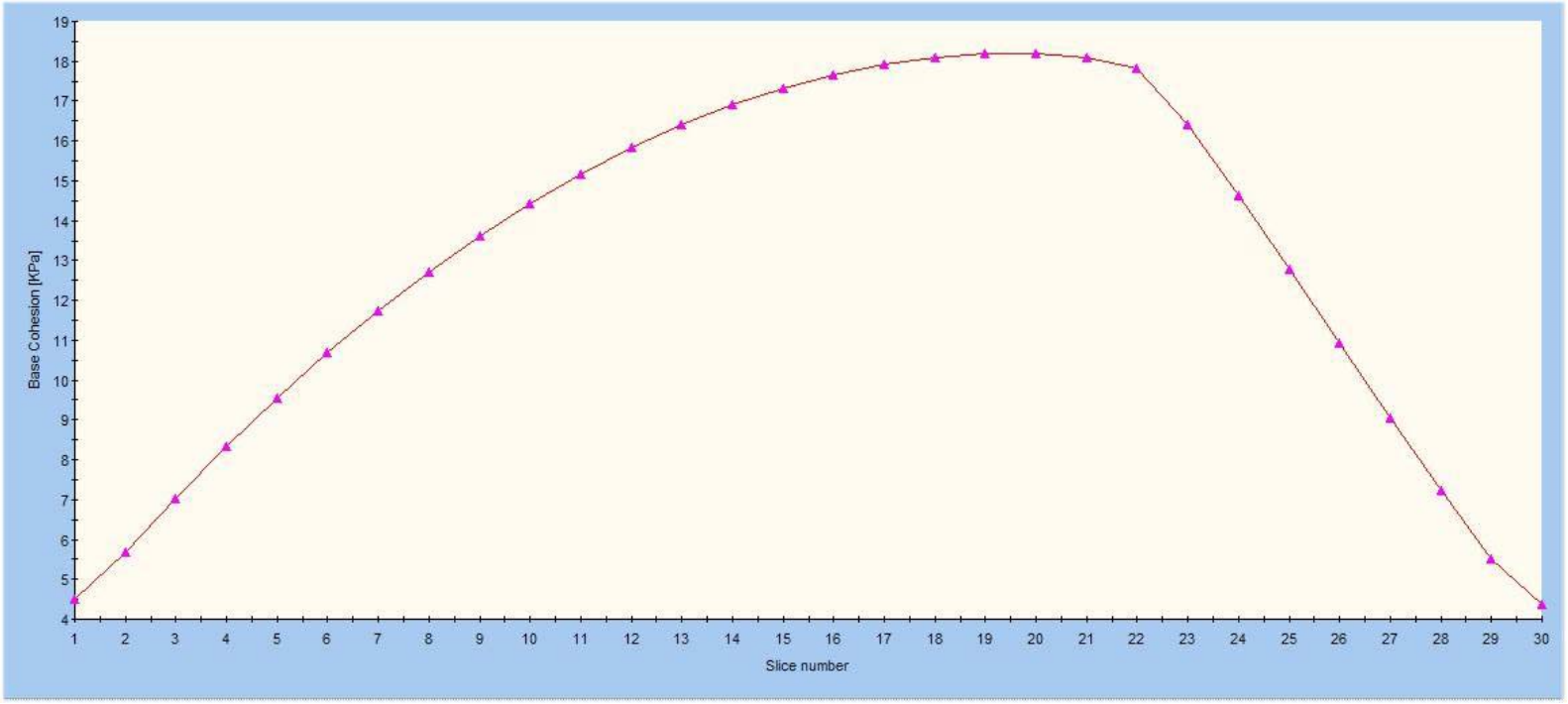

Figure D.9. Instantaneous cohesion (c_i) for each slice of the most critical failure surface in section 5.

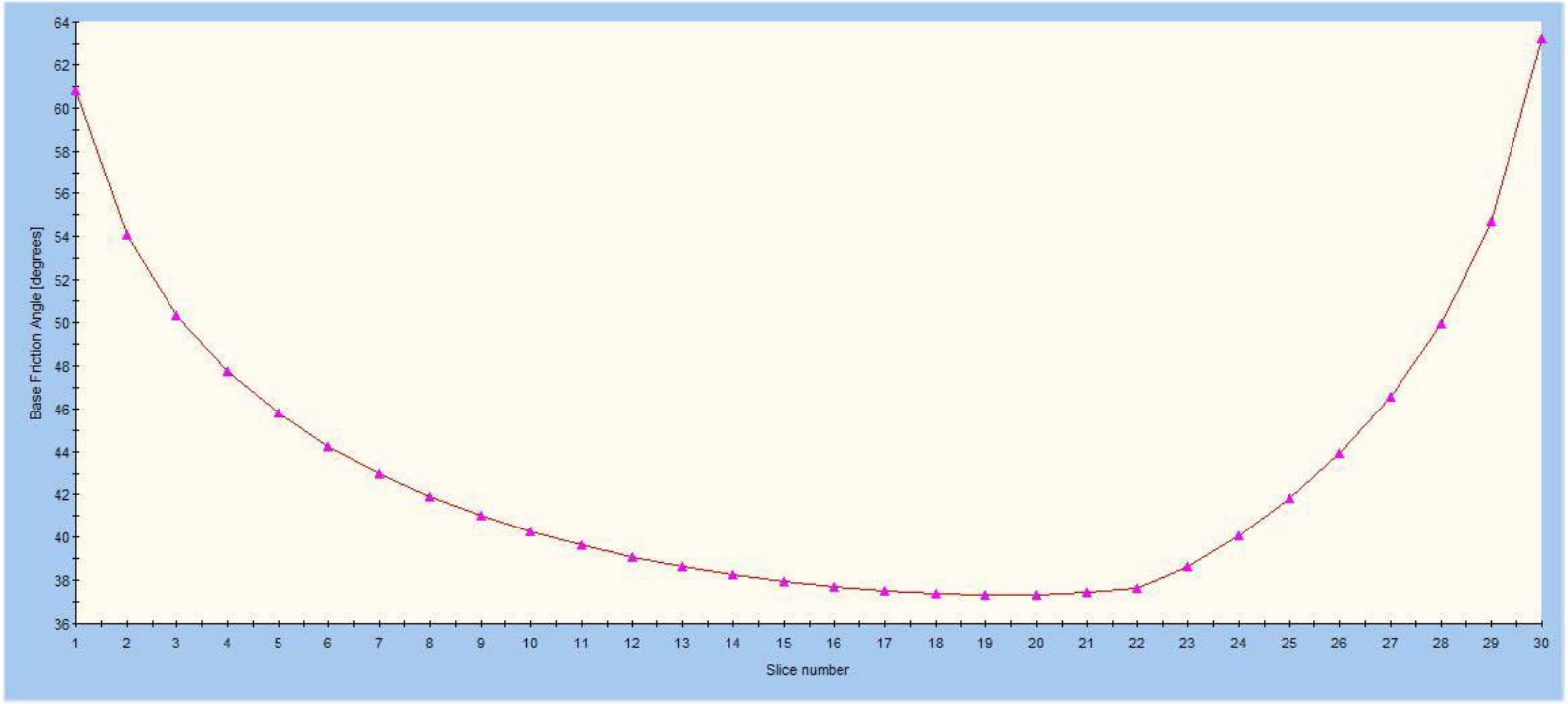

Figure D.10. Instantaneous friction angle (Φ_i) for each slice of the most critical failure surface in section 5.

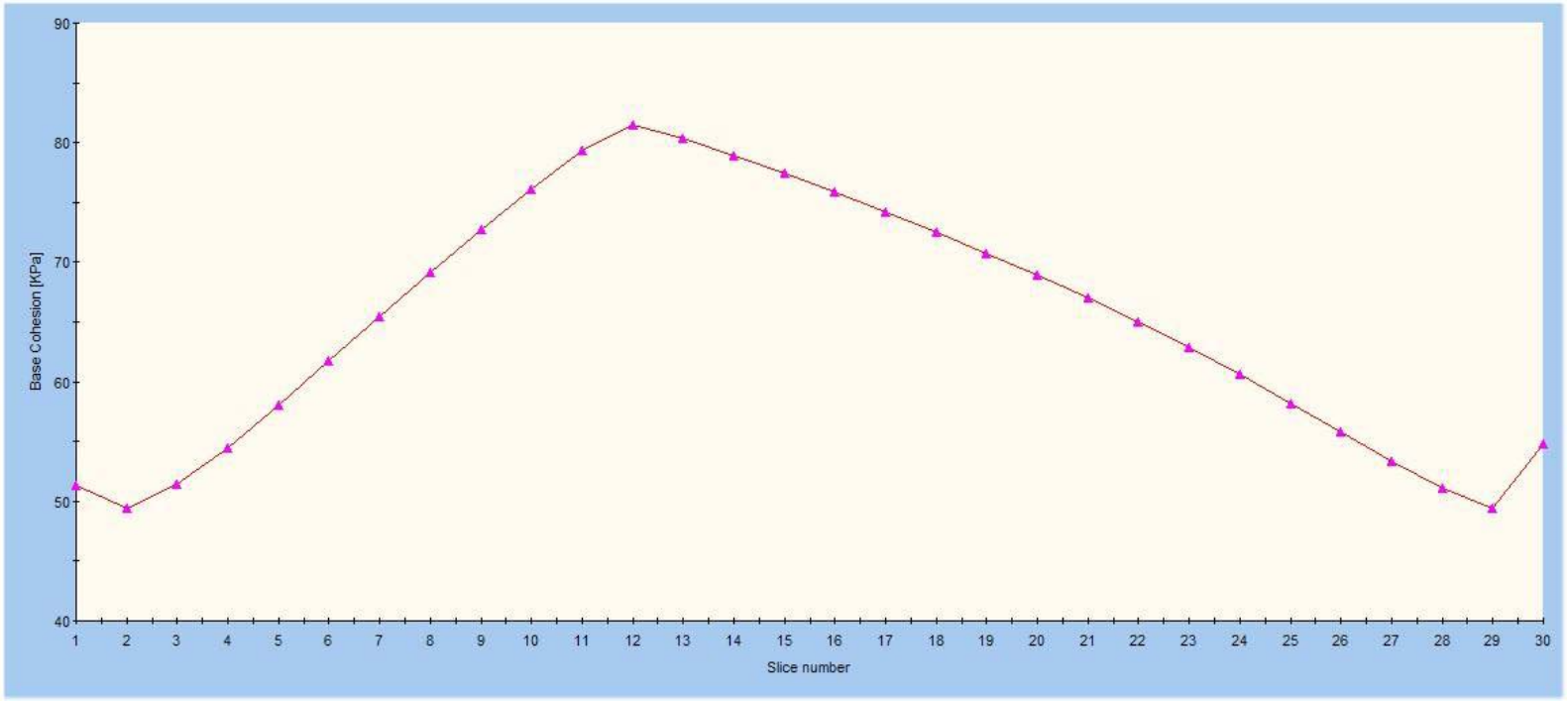

Figure D.11. Instantaneous cohesion (c_i) for each slice of the most critical failure surface in section 6.

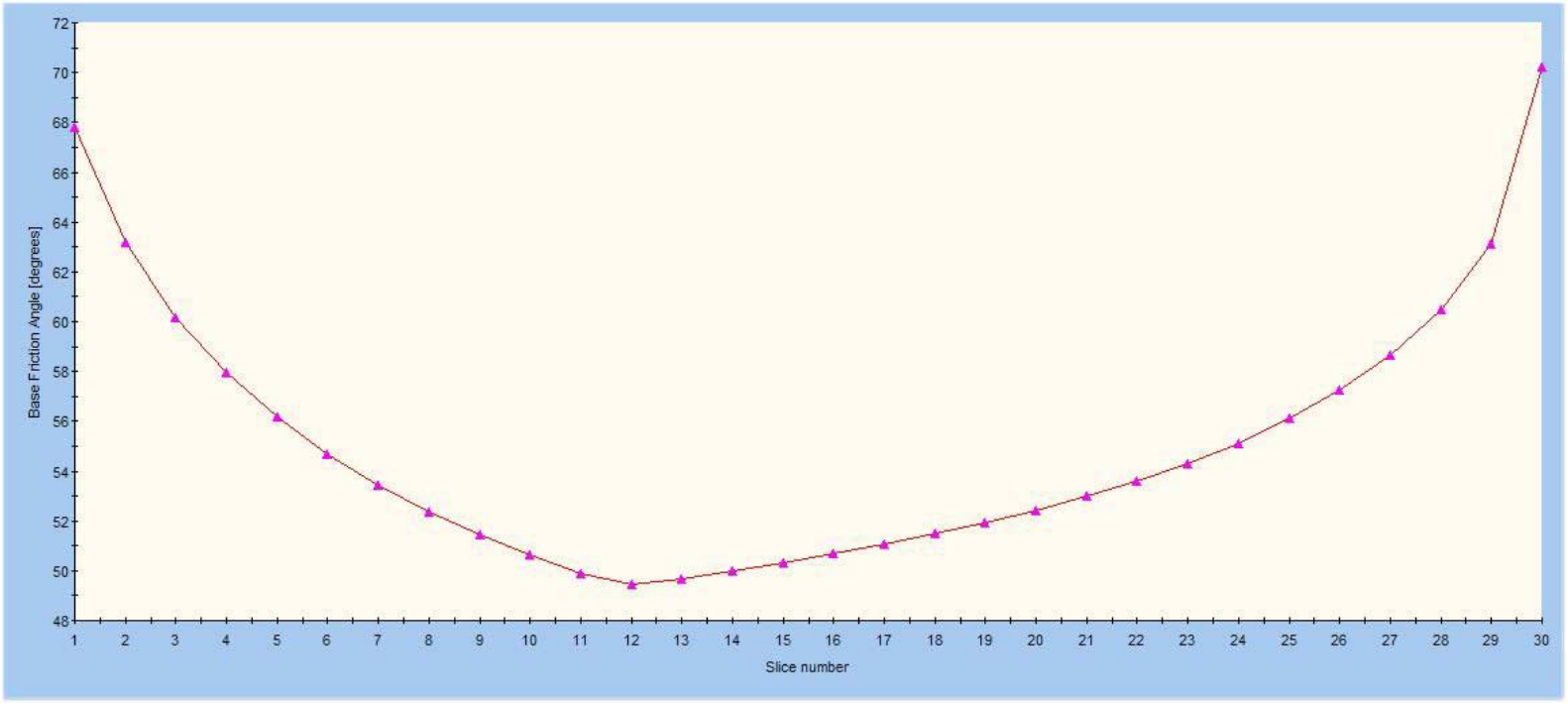

Figure D.12. Instantaneous friction angle (Φ_i) for each slice of the most critical failure surface in section 6